Occurrence and formation of sediment-storm bedforms in a coastal bay, southeast Brazil

ALEX C. BASTOS[1], BETINA C.R. LIMA[1], EDUARDO SIEGLE[2], DAPHNNE MOSCON[3], ALEXANDRE PASOLINI[4]

1. Laboratório Oceanografia Geológica, Universidade Federal Espírito Santo, Vitória-ES, Brazil
email: ac.bastos@terra.com.br, berlima@gmail.com

2. Instituto Oceanográfico, Universidade de São Paulo, Praça do Oceanográfico 191, São Paulo SP 05508120, Brazil
email: esiegle@io.usp.br

3. Laboratório Geologia Marinha, Universidade Federal Fluminense, Niterói-RJ, Brazil
email: daphnnemoraes@yahoo.com.br

4. CEPEMAR Consultoria Ambiental, Vitória-ES, Brazil
email: alexandre.pasolini@cepemar.com

Keywords: sediment transport, storm deposits, benthic boundary layers

ABSTRACT

Side-scan sonar survey has revealed the occurrence of sediment storm bedforms within Espírito Santo Bay, southeast Brazil. These bedforms are characterized by alternating bands of coarse and fine sands occurring between water depths of 5 to 8 m. A detailed investigation of the coarse sand areas showed the occurrence of wave-generated ripples with heights ranging from 0.10 to 0.20 m and wavelengths between 0.80 to 1.4 m. The ripples are slightly asymmetric with straight to sinuous crests. Hydrodynamic data and sediment transport estimations have shown that tidal currents alone are not capable of transporting sediments and that sediment movement occurs only in the presence of waves. A major storm event was observed during the deployment period. During this period of high wave energy, sediment transport calculations show that cross-shore transport was predominant and that coarse to very coarse sands are mobile as bedload. Results from the wave refraction model can explain the spatial distribution of these sediment storm bedforms within Espírito Santo Bay. The formation and maintenance of these sediment bedforms are probably related to storm-generated near bed currents and fine sediments resuspension that are advected by currents and deposited during lower energy conditions.

Introduction

Shelf seabed morphology and associated morphological changes are the consequence of combined effects of sediment erodibility, transportation and depositional processes. Sedimentary features (e.g., bedforms), found on the seabed, develop as a result of physical and geological processes and can be explained by temporal and spatial variations of sediment input and along-shore/cross-shore sediment transport. Overall, physical processes are induced by tidal currents, wave resuspension and wind- and wave-generated near bed currents. Storm-associated bedforms have been described elsewhere as tabular sand patches (Kenyon, 1970), rippled scour depression (Cacchione et al., 1984; Thieler et al., 2001; Green et al., 2004) and hummocky megaripples (Swift et al., 1983; Amos et al., 1996). The term tabular sand patches were used by Kenyon (1970) to describe patches of fine sands (symmetric or asymmetric) over a coarse lag deposit in tidally dominated shelves. Rippled scour depressions were described initially by Cacchione et al. (1984) as elongated shore-normal features, explained by non-uniform downwelling-bottom flows induced by storm. Swift et al. (1983) described a hummocky megaripple as with no well-defined orientation and asymmetry. In general, all these bedforms are characterized by sharp boundaries between rippled coarse sands and fine sand beds, with a subtle relief (<1 m). It seems to be a consensus that the rippled coarse sand (shell hash) bed is mobilized only during storm events that would also resuspend fine sands, advect and deposit with energy decrease. The major difference between these features is their spatial distribution and leading geometry, which might reflect the following dominance

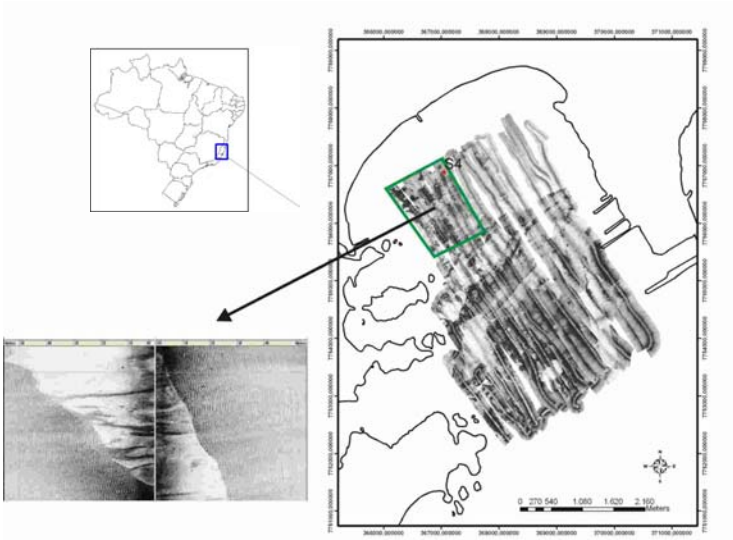

Figure 1. Location of the study area, showing sonographic mosaic for the Espírito Santo Bay. Image on the right show a detail of the storm bedform observed. The red dot in the mosaic is the S4 deployment location.

of cross and/or along-shore sediment transport. Recently, Murray and Thieler (2004) have introduced the term sorted bedforms. They suggest that, in the case of rippled scour depressions, these features are self-organized as a result of a feedback system associated to different-induced bed shear stress due to roughness.

Side-scan sonar survey has revealed the occurrence of sediment-storm bedforms within Espírito Santo Bay, southeast Brazil (Figure1). The occurrence of these features is restricted to the southwest area of the bay. The sedimentological and morphological characteristics of these bedforms match the features described above, i.e., they are characterized by alternating bands of rippled coarse and fine sands with a subtle relief. The term storm bedform is being used here in order not to propose a new type of bedform, but to make clear that it is a storm-induced feature. Hence, the objective of this research is to understand the occurrence and formation of these bedforms within a coastal bay in southeast Brazil (Vitória-ES).

Methods

In order to carry out an investigation of the morphology, sedimentology and formation of these bedforms, an integrated research approach was undertaken, including: seabed mapping, short sedimentary cores, in situ hydrodynamic measurements, estimations of sediment transport and wave refraction modeling. Seabed mapping was undertaken using an Edgetech 4100 side-scan sonar system, operating at 100 kHz. Sidescan data were processed by SonarWiz.Map software (Chesapeak Inc.) in order to produce a sonographic mosaic of the area. A second and higher resolution side-scan survey (operating at 500 kHz) was conducted over the storm bedforms area only. Four short push-cores and eight surficial samples were collected by divers, just after the second geophysical survey, conducted in August 2007. The cores were split, described and analyzed for sediment grain size and composition. Near-bed hydrodynamic data was recorded by an InterOcean S4-DW current meter, for 28 days during the winter 2007. Current and wave data were recorded at 1 m above the bed, comprising 10 min-average interval once every half-hour. A sediment transport model (SEDTRANS, Li and Amos, 2001) was applied to estimate bedload and suspended transport rates and direction under the combined action of waves and currents. Calculations were undertaken considering 0.850 mm D_{50} for rippled coarse sand bed and 0.100 mm for fine sand bed. Based on a coastline orientated 40° from North, current horizontal components were rotated and transformed into along and cross-shore components. In order to investigate the shallow water wave processes in the bay a wave refraction model MIKE21 SW (developed by DHI Water & Environment) has been applied at the region. In these model runs, a constant wave height and period has been modeled approaching the coast from different directions. Results of wave height and radiation stress distributions enable us to define the relative wave energy distributions in the bay for each incident wave direction.

Results and discussion

Seabed mapping revealed that the occurrence of storm bedforms is concentrated over the northwest part of the bay, between depths of 5 to 8 m. The storm bedform area is characterized by alternating bands of low (features muddy fine sands) and high backscatter (rippled coarse sands) signal. Alongshore, towards the east,

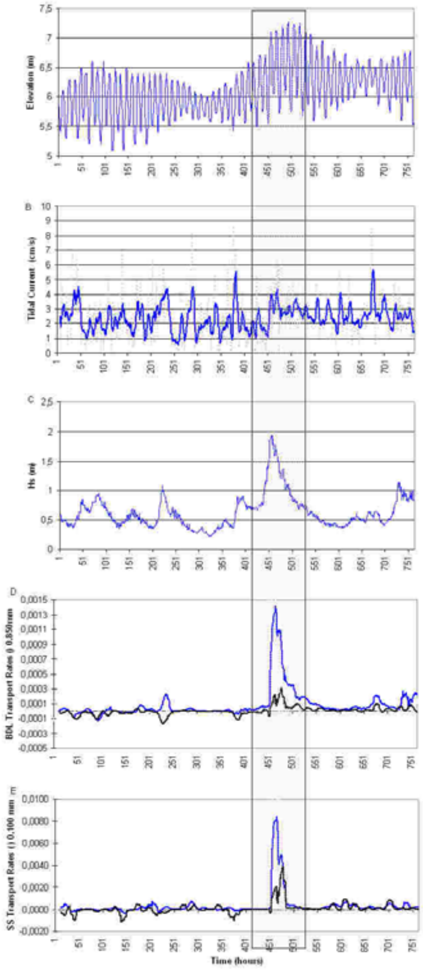

Figure 2. Hydrodymanic measurements and sediment transport estimations using Sedtrans: A) sea-level elevation, B) tidal currents, C) signficant wave height, D) bedload sediment transport, E) suspended sediment transport For D and E, blue line is cross-shore component and black line is along-shore component. Shaded area exhibits the major energetic event during the deployment. Sediment transport is given as kg m^{-1} s^{-1}.

these bedforms are not present, giving place to a featureless muddy sand bottom. Hence, two sedimentary facies can be described: a rippled coarse sand facies and a featureless fine sand facies. A detailed investigation of storm bedforms reveals that the rippled coarse sand bed is characterized by wave-generated ripples with heights ranging from 0.10 to 0.20 m and wavelengths between 0.80 to 1.4 m. Ripple crests are straight to sinuous, but tend to be parallel to the coastline. Short cores exposed a typical storm sedimentary sequence over the fine sand facies, characterized by a 20 to 30 cm thick fine sand deposit overlaying a coarse to very coarse sand layer. It is important to note that these features do not have a clear spatial geometry nor a measurable wavelength. So, differently from what is described by Cacchione et al. (1984), these are not elongated features oblique to the coastline. The beforms observed here are distributed more like patches of rippled coarse sands and fine sands.

Hydrodynamic data and sediment transport estimations showed that tidal currents alone are not capable of transporting sediments and that sediment movement occurs only in the presence of waves. Overall, estimations of bedload and suspended sediment transport showed that coarse sand are mainly transported as bedload, whilst fine sands are, most of the time, transported as suspended load. At least four major sediment transport events can be recognized over the deployment period. The most significant one occurred in the beginning of the second spring tide period and is associated with a storm surge that created a setup of about 40 cm along the coast, and the waves reached 2 m inside the bay. A peak in bedload and suspended sediment transport is clearly observed for this event. Analyzing the along and cross-shore components, it seems that during the major storm event, cross-shore transport was dominant. However, results indicate that after and before this major energetic event, there is no clear evidence of transport direction dominance.

Results from the wave refraction model revealed that wave energy is concentrated mainly over the northwest side of the bay. Due to the morphological configuration of Espírito Santo Bay, incoming waves are refracted at both headlands at the entrance, concentrating energy along the western end of the shoreline. This pattern

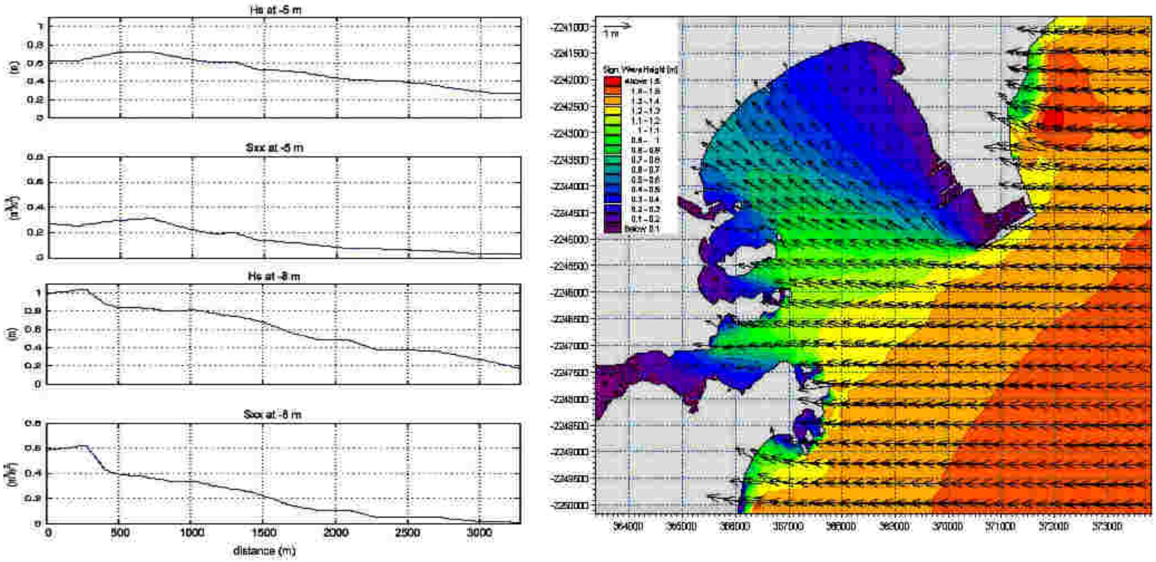

Figure 3. Refraction patterns for waves incident from E. Profiles show the wave significant height (H_s) and radiation stress (S_{xx}) distribution at −5 m and −8 m inside the bay (distance from NW to NE).

creates a low wave energy area over the eastern side of the bay, where the bedforms are not observed and a muddy fine sand bottom occurs. Modeled wave information extracted at −8 and −5 m inside the bay show that for waves approaching from all directions except S and SSE the wave refraction patterns show energy concentration in the northwestern portion of the bay (Figure 3). Considering that the wave climate in the region is dominated by waves approaching the coast from ENE and E (about 50% of occurrence), it is possible to assume that the yearly averaged energy distribution in the bay reflects this energy concentration at the region where the bedforms are found.

Conclusions

The formation and maintenance of these sediment-storm bedforms are probably related to storm-generated near bed currents and fine sand resuspension that are advected by currents and deposited during lower energy conditions. It is possible that the self-organizing mechanism suggested by Murray and Thieler (2004) takes place in this area, but the morphology of the observed storm bedforms are not comparable with rippled scour depressions. So far, it is possible to affirm that the features described here are storm-generated sand patches.

References

Amos, C.L., Li, M.Z., Choung, K.S. (1996), Storm-generated, hummocky stratification on the outer-Scotian Shelf, *Geo-Marine Letters*, 16, 85–94.

Cacchione, D.A., Grante, W.D., Tate, G.B. (1984), Rippled scour depressions on the inner continental shelf off central California, *Journal of Sedimentary Petrology*, 54, 1280–1291.

Green, M.O., Vincent, C.E., Trembanis, A.C. (2004), Suspension of coarse and fine sand on a wave-dominated shoreface, with implications for the development of rippled scour depressions, *Continental Shelf Research*, 24, 317–335.

Kenyon, N.H. (1970), The origin of some transverse sand patches in the Celtic Sea, *Geological Magazine*, 102, 389–394.

Li, M.Z., Amos, C.L. (2001), SEDTRANS96: the Upgraded and Better Calibrated Sediment – Transport Model for Continental Shelves, *Computers and Geosciences*, 27, 619–645.

Murray, A.B., Thieler, E.R. (2004), A new hypothesis for the formation of large-scale inner-shelf sediment sorting and 'rippled scour depressions', *Continental Shelf Research*. 24, 295–315.

Swift, D.J.P., Figueiredo, A.G., Freeland, G.L., Oertel, G.F. (1983), Hummocky cross-stratification and megaripples: A geological double-standard? *Journal of Sedimentary Petrology*, 53, 1295–1317.

Thieler, E.R., Pilkey, O.H., Cleary, W.J., Schwab, W.C. (2001), Modern sedimentation on the shoreface and inner continental shelf at Wrightsville Beach, North Carolina, USA, *Journal of Sedimentary Research*, 71, 958–970.

Mapping of bathymetry and tidal currents in the Dee estuary using marine radar data

PAUL S. BELL

Proudman Oceanographic Laboratory, 6 Brownlow Street, Liverpool L3 5DA UK
email: psb@pol.ac.uk

Keywords: bathymetry, currents, remote mapping, X-band radar

ABSTRACT

Bathymetric maps and tidal currents have been mapped in an estuarine environment through the analysis of marine radar image sequences to a range of 4 km and with 100 m grid spacing. The Dee estuary is located on the southern side of Liverpool Bay in the United Kingdom and contains a complex system of intertidal sand banks and channels with a peak spring tidal range exceeding 10 m. In order to understand how the estuary is evolving it would be helpful to regularly observe the positions of the sand banks and channels and the wave and current forcing driving the evolution of these features. To this end a marine radar has been deployed on an island in the estuary from which ten minute sequences of images of the sea surface are recorded once per hour. By fitting a wave dispersion equation to the observed wave behavior it is possible to map the underlying water depth and mean current provided waves are visible on the radar images. Radar derived water depth and current maps recorded around a single high water were compared with survey data and show that in regions where the waves are feeling the sea bottom, the radar derived depths are generally within ±1 m of the survey data.

Introduction

The monitoring of bathymetry and currents in estuaries can be a difficult problem to overcome due to difficulty of instrument deployment and access over shallow waters and muddy areas. The use of marine radar has been demonstrated several times as a tool for remote mapping of bathymetry (Bell, 1999, 2001; Bell et al., 2006) in a variety of locations on open coastlines. In 2005, a marine radar was deployed on the remote Hilbre Island in the Dee estuary overlooking a complex area comprising intertidal sandbanks and deep subtidal channels. The Dee estuary (Figures 1 and 2) is located about 10 km west of Liverpool in the United Kingdom on the south side of Liverpool Bay. Waves are fetch limited and generally do not exceed 8 s period, while the tidal range at peak springs exceeds 10 m. These factors combine to provide a difficult test for extracting bathymetry and currents from marine radar data.

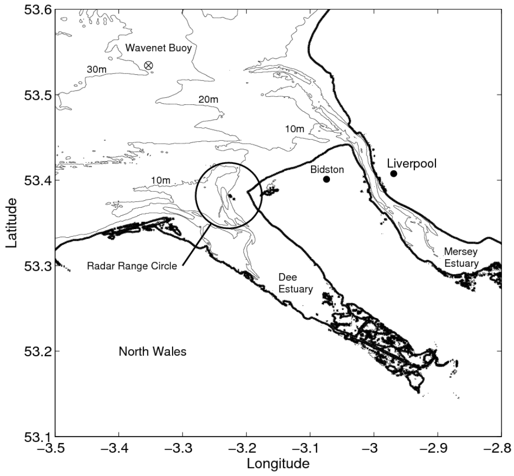

Figure 1. Map showing the location of the Dee and Mersey estuaries in Liverpool Bay. The 4 km recording radius of the radar system is centered on Hilbre Island.

Figure 2. Photograph taken from a light aircraft looking south east into the Dee estuary and showing the extensive intertidal sand banks and deep tidal channels.

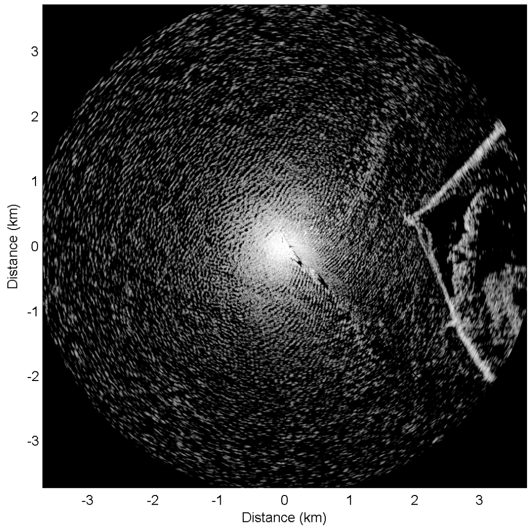

Figure 3. The X-band radar mounted on a tower on Hilbre Island in the Dee estuary.

Figure 4. A raw digitized image from the X-band radar showing the eastern side of the mouth of the Dee estuary during a wave event.

Data collection

A sequence of 256 radar images are recorded at 2.4 second intervals spanning about 10 minutes on an hourly basis using a WaMos (Hessner et al., 2008) radar digitization system with a radial sampling interval of 7.5 m or smaller. The radar is a Kelvin Hughes 10 kW X-band radar operating at 9.8 GHz with a 2.4 m rotating antenna and is mounted on a 15 m high tower (Figure 3), the base of which is approximately 15 m above mean water level. Until the middle of 2007 the data were recorded to a range of just under 4 km, and subsequent to that they were recorded to a range of 7.5 km. An example of a raw radar image recorded in the Dee estuary is shown in Figure 4, clearly showing the wave patterns within the sea clutter signal. A tide gauge operated by the Mersey Docks & Harbour Company is located on the northern tip of Hilbre Island and a wave buoy is located about 15 km offshore, operated by CEFAS as part of the WaveNet system.

Analysis

An analysis window is of a size chosen to include at least two wavelengths (L) of the dominant waves is translated in 2-D across the area viewed by the radar. At each point the window of data is processed using Fourier methods to produce a three dimensional wavenumber (k) spectrum (Young et al., 1985). A wave dispersion equation is then fitted to the observed wavenumber spectrum to determine the water depth (d) and 2-D current (U) that caused that wave behavior. The dispersion equation is based on linear theory with a correction for amplitude dispersion, i.e., the non-linear behavior of large wave in shallow water which travel faster than linear theory alone can predict (Hedges, 1976). There is also a correction for currents to account for the Doppler shift the waves traveling on a mean current:

Water depth $$d = \frac{1}{k}\tanh^{-1}\left[\frac{(\omega - k.U)^2}{gk}\right] - Z \qquad (1)$$

where wavenumber $k = 2\pi/L$, angular frequency $\omega = 2\pi f$ and for monochromatic waves (Booij, 1981), or $Z = 0.35\,H_s$ for spectral waves.

Results

Three records around a single spring high water during a wave event have been analyzed using these algorithms. The bathymetric map derived from these data has been corrected to chart datum and is shown in Figure 5. A radar derived instantaneous water depth and current vector map is shown in Figure 6 with the maximum current magnitude being approximately 1 m s^{-1}. This instant in time was about an hour after high water and hence the current vectors show the water flowing off the sand flats and out of the estuary to the northwest as expected.

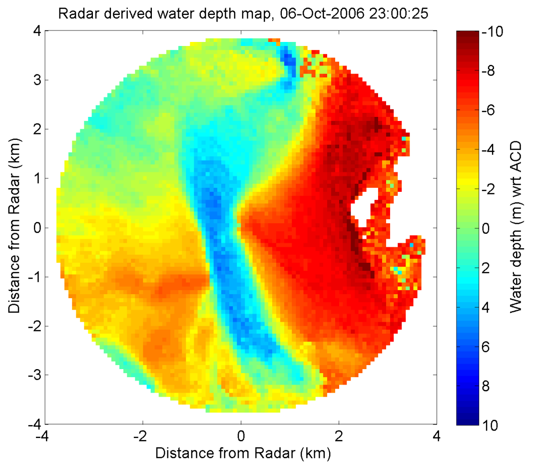

Figure 5. The radar derived bathymetry derived from three records over one spring high water in 2006.

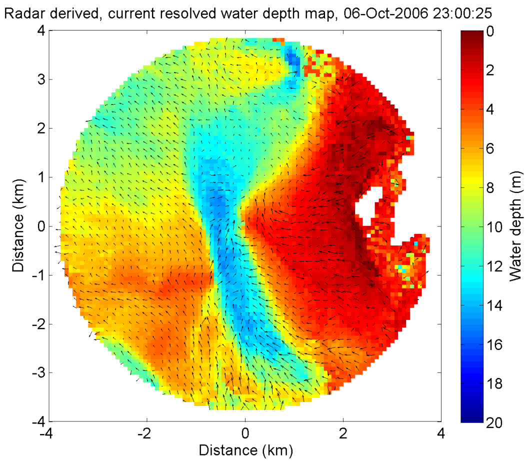

Figure 6. A radar derived instantaneous water depth and current vector map with the maximum current magnitude being approximately 1 m s^{-1}.

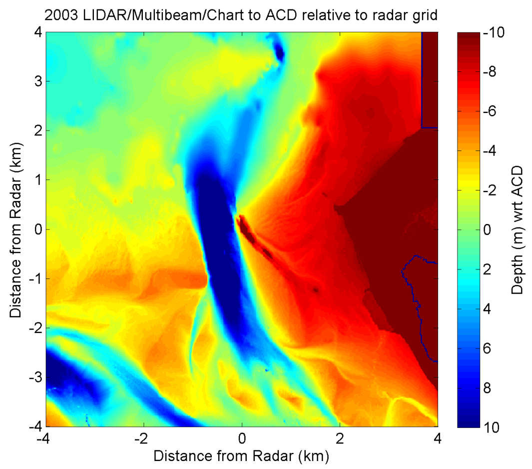

Figure 7. The combined LIDAR, Multibeam echosounder and Admiralty Chart survey of the Hilbre Island area from 2003.

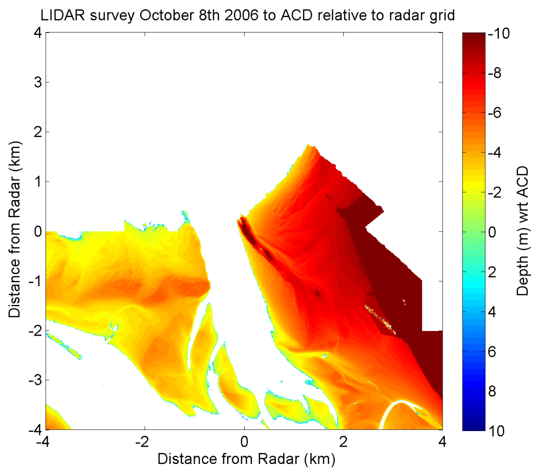

Figure 8. The 2006 LIDAR survey of the Hilbre Island area. Surveys of the deeper areas were not available.

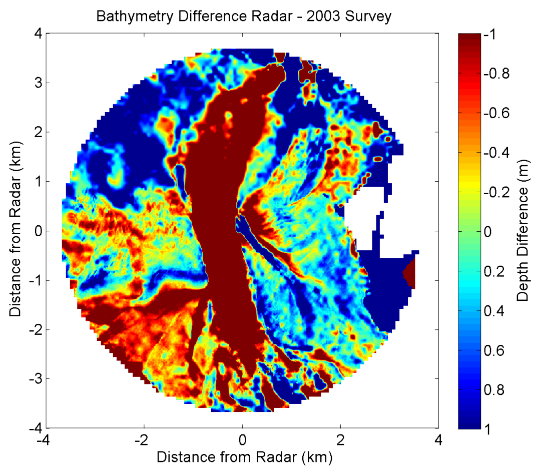

Figure 9. The Difference between the radar derived bathymetry and the 2003 survey data. Red colors indicate that the radar is reading shallower depths than the survey.

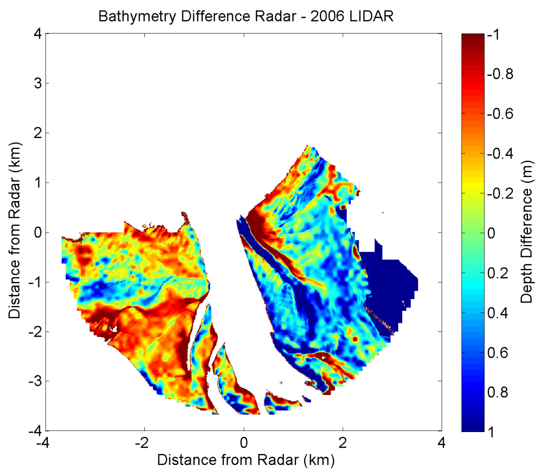

Figure 10. The Difference between the radar derived bathymetry and the 2006 LIDAR survey Red colors indicate that the radar is reading shallower depths than the survey.

The combined 2003 LIDAR-multibeam-chart bathymetric map of the area is shown in Figure 7 and the 2006 LIDAR survey is shown in Figure 8. By subtracting the survey data from the radar derived bathymetry it is straightforward to illustrate the distribution of errors in the radar derived bathymetry. Figures 9 and 10 illustrate the errors relative to the 2003 and 2006 surveys. In Figure 9 a marked deterioration in agreement with the survey data in the northern half of the area in Figure 7 can be explained by the sparsity and age of soundings used in the Admiralty Charts, hence this area of the data is not considered particularly useful for comparisons other than in general form. The consistent over-estimate in depth of around 0.5m over the sand flats to east of the image could potentially be explained by wave setup increasing the local water level over that feature of the bathymetry. The underestimate in depth by around 0.5 m in the south west corner of the study area is thought to be an artifact of the use of a single Hs value for the entire region. One could expect that the wave height behind the sandbanks located 1 km south of the radar and to the west would be substantially lower than to the north of these sand banks, which would lead to an over correction for the effect of wave height in the depth inversion equation.

It is pleasing to note that the radar derived bathymetry show better overall agreement with the 2006 survey than the 2003 survey. In particular the complex of sandbanks located to the west of the study area and 1 km south of the radar have been resolved with no obvious offset in position in Figure 10, while the comparison with the 2003 survey in Figure 9 shows that the sandbanks have migrated approximately 200m to the south in the intervening three years.

The area with the most significant errors in radar derived depth is the deep channel running through the centre of the study area. This is not unexpected since wave periods at this site rarely exceed 8 seconds and hence the waves being used to image the sea bed are barely interacting with the bottom in the deep (25–30 m at high water) channel.

Summary

Marine radar image sequences of waves have been processed to determine water depth and current vectors at ~100 m intervals. The water depth derived from these data have been adjusted to chart datum using tide gauge data and compared with two sets of survey data from 2003 and 2006. The results demonstrate that the radar derived water depths are generally within ±1 m of the survey data in areas where the waves are feeling the bottom. Further work is needed to establish the quality of the derived current data, although they appear qualitatively reasonable for the area and tidal conditions.

References

Bell, P.S. (1999), Shallow water bathymetry derived from an analysis of X-band marine radar images of waves, *Coastal Engineering*, 37(3–4), 513–527.

Bell, P.S. (2001), *Determination of bathymetry using marine radar images of waves*. In: Waves 2001: 4th International Symposium on Ocean Wave Measurement & Analysis, San Francisco, USA, pp251–257.

Bell, P.S., Williams, J.J., Clark, S., Morris, B.D., Vila-Concejo, A. (2006), Nested radar systems for remote coastal observations, *Journal of Coastal Research*, SI39 (Proceedings of the 8th International Coastal Symposium, Itajaí, SC, Brazil, 14-19 March 2004). pp483–487.

Booij, N. (1981), *Gravity waves on water with non-uniform depth and current*. Rep. No.81-1, Department of Civil Engineering, Delft University of Technology.

Hedges, T.S. (1976), Empirical modification to linear wave theory, *Proceedings of the Institution of Civil Engineers*, Part 2–Research and Theory, 61(SEP): 575–579.

Hessner, K.G., Nieto-Borge, J.C., Bell, P.S. (2008), *Nautical radar measurements in Europe – Applications of WaMoS II as sea state, current and bathymetry sensor*. In: Remote Sensing of the European Seas, Barale, V., Gade, M. (Eds.), Springer, Geosciences, Dordrecht, Netherlands, pp435–446.

Young, I.R., Rosenthal, W., Ziemer, F. (1985), A 3-dimensional analysis of marine radar images for the determination of ocean wave directionality and surface currents, *Journal of Geophysical Research – Oceans*, 90(NC1), 1049–1059.

Links between the movements of sandbanks and local beach variability

CLARE COUGHLAN, CHRIS E. VINCENT, TONY DOLPHIN

School of Environmental Sciences, University of East Anglia, Norwich NR4 7TJ UK
email: c.coughlan@uea.ac.uk, c.vincent@uea.ac.uk, tony.dolphin@uea.ac.uk

Keywords: sandbank, beach-bank interaction, sediment transport

ABSTRACT

Links between state of beach and position, height and extent of nearby sandbanks are believed to exist both directly, via exchange of sand, and indirectly through perturbations to the wave and current field. However, few systematic studies of these links exist, and evidence from combined sandbank variations and beach state indicators are rarely available. An understanding of these bank/beach interactions is important for the strategic management of the coastline. The study areas are the beaches at Lowestoft, Suffolk, UK, and the nearby Newcombe Sands, a headland associated sandbank situated off Lowestoft Ness (Figure 1). Newcombe Sand is the southernmost sandbank in a system of sandbanks off the East Anglian Coast.

Sandbanks are, by nature, mobile features, showing significant changes between surveys (Robinson, 1966). Changes in shape, size and location occur on a range of timescales. The smaller scale features superimposed on banks respond rapidly, with sand waves migrating at a rate of the order of a few meters per year (Tonnon et al., 2007), while the morphological timescale of sandbank development is of the order of decades to centuries (Reeve et al., 2001). Dolphin et al. (2007) have discovered both gradual and episodic migration of Newcombe Sand and note that, although tied to the headland, the bank is rarely stationary and that it cycles between a simple elongate form, and a radically different 'deltaic' form (Figure 2). Historically there have been significant changes to both the Lowestoft beaches and Newcombe Sand (Dolphin et al., 2007), and recent changes to the beaches at Lowestoft are thought to be caused by changes in the position of Newcombe Sand (HR Wallingford, 2002), but there is no direct evidence of cause and effect.

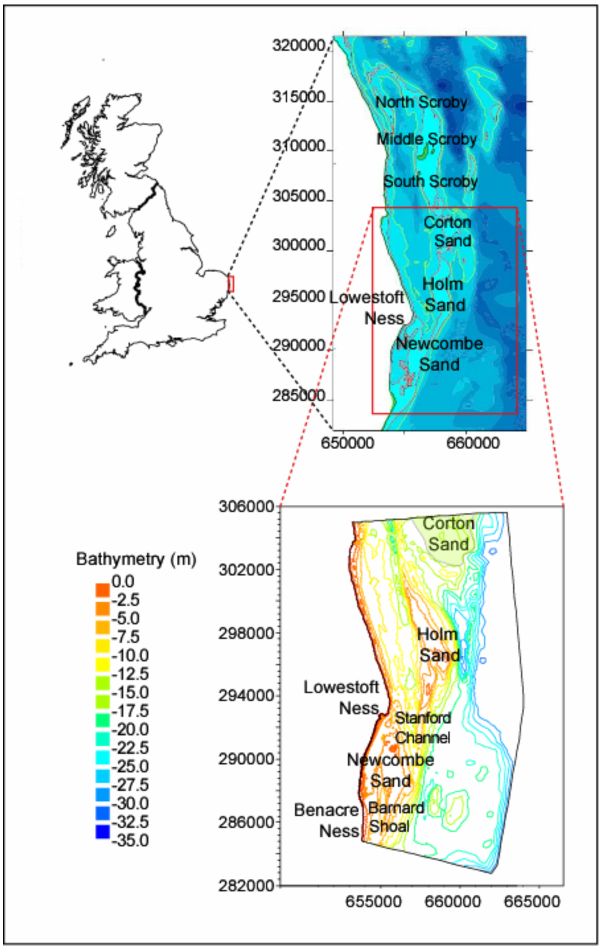

Figure 1. Location of the study site within the Inner Great Yarmouth Banks off the East Anglian Coast, UK (top). Model domain with 2005 bathymetry (bottom)

Methods

Numerical modeling was undertaken using the TELEMAC suite of finite element system (Hervouet, 2000). TELEMAC-2D, the tidal model, was run for a full spring-neap cycle over both the elongate and deltaic bank configurations to investigate the tidal currents around Newcombe Sand and between the bank and the shore. The TELEMAC-2D results (currents and water levels) were input to TOMAWAC, the wave model, to take into account the tidal stage as waves propagate shorewards. This is a superposition of the effects of the wave

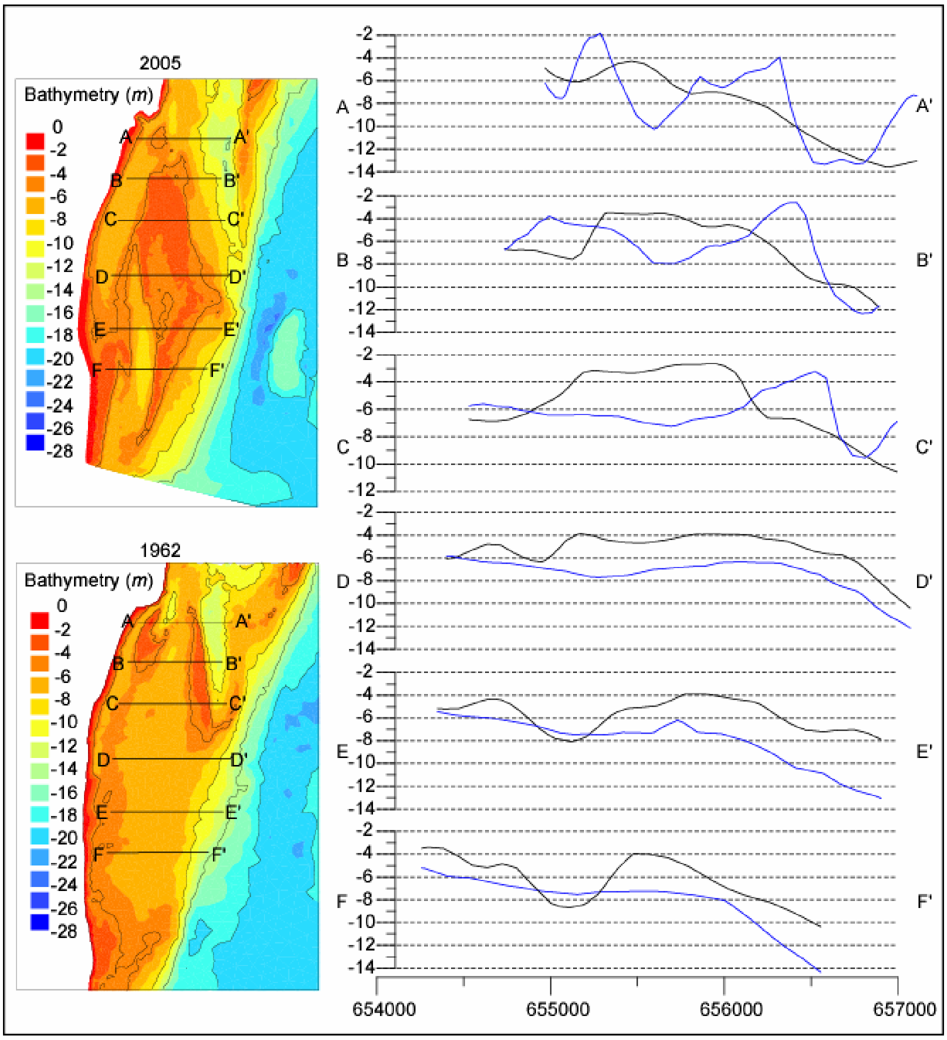

Figure 2. Elongate (top left) and deltaic (bottom left) forms of Newcombe Sand. Right: bathymetric profiles across the elongate (black) and deltaic (blue) bank.

spectrum with the currents; it includes the effects of the current velocity on the wave height and period, but not the effects of waves on the currents. TOMAWAC was run for a representative set of wave conditions to examine the influence and impacts of the movements of Newcombe Sand on the wave climate of the Lowestoft beaches. Sediment transport modeling with SISYPHE was directed towards identifying the likelihood of sediment exchange between the bank and the shore.

In an extension of work carried out by Coughlan et al., 2007, longshore sediment transport rates were calculated from modeled output inshore of each bank configuration to examine the effect of each bank shape on the inshore wave climate. Longshore sediment transport rates were predicted using the CERC equation (CERC, 1984), where the potential longshore sediment transport rate, dependent on an available quantity of littoral material, is related to the longshore component of wave energy flux to give a volume transport rate, Q_l (Equation 1).

$$Q_l = \frac{K}{(\rho_s - \rho) g (1-\varepsilon)} (EC_g)_b \sin\alpha_b \cos\alpha_b \tag{1}$$

$$E_b = \frac{\rho g H_b^2}{8} \tag{2}$$

$$C_{gb} = \sqrt{g d_b} = \left(g \frac{H_b}{\kappa} \right)^{\frac{1}{2}} \tag{3}$$

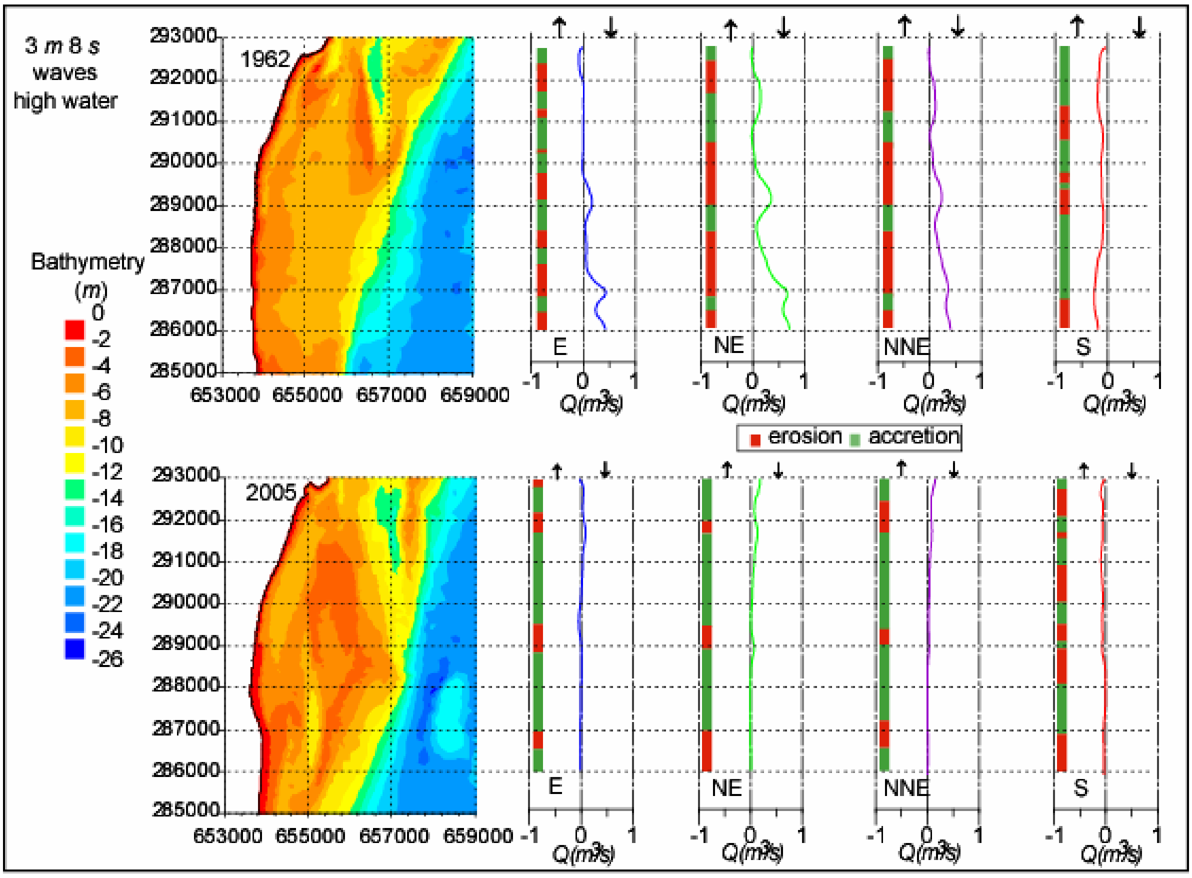

Figure 3. Longshore sediment transport at high water for 3 m, 8 s waves approaching from E, NE, NNE and S over deltaic (top) and elongate (bottom) bathymetries. The arrows show the direction of longshore sediment transport.

The term $(E\,C_g)_b$ is the wave energy flux evaluated at the breaker zone, α_b is the wave breaker angle relative to the shoreline. E_b is the wave energy evaluated at the breaker line (Equation 2) and C_{gb} is the wave group speed at the breaker line (Equation 3). $\kappa = 0.42$ is the breaker index H_b/d_b, ρ is the mass density of sea water (1027 kg $^{-3}$), g is the acceleration due to gravity, ρ_s is the sediment density (2650 kg m^{-3}) and ε is the sediment porosity (0.4). K is a dimensionless proportionality coefficient, taken here as 0.77 (Komar and Inman, 1970).

Wave information was collected at model nodes about 100 m apart, approximately 100 m from the shoreline. The model grid is irregular and so distances between nodes vary. A breaking criteria $\kappa = 0.42$ was used to determine whether or not the waves were breaking, and if not they were transformed using linear wave theory to calculate the breaking wave statistics. At each node the rate of longshore sediment transport was calculated using Equation 1.

Results

Beach state (monthly RTK-GPS^{+} beach surveys) and the position of the bank (6-monthly bathymetric surveys) have been observed to change rapidly and are consistent with historical data on the movement of Newcombe Sands. Modeling has shown that tidal currents alone are not a major factor in sand movement, and that wave action plays a significant role in mobilizing sediment for transport by currents.

The hydrodynamic system inshore of a sandbank is a complex interaction between waves, tidal currents and bathymetry. The influence of a bank on the state of local beaches can either be through direct sediment exchange between the bank and the shore, or indirectly through modification of the inshore hydrodynamic regime. The elongate bank is long, wide and fairly flat, and appears to be moving onshore and rotating slightly anticlockwise. The deltaic bank is composed of two lobes, with the main lobe extending less than half the length of the elongate bank. It is narrower and more sharp-featured (Figure 2) than the elongate bank, and the main lobe appears to be moving offshore. These disparate configurations have very different influences at the shore.

The magnitude of longshore sediment transport and the distribution of areas of erosion/accretion vary significantly for the two bank configurations (Figure 3). In general, the greatest volume of sediment transport occurs at high water when waves are at their highest, but overall the longshore sediment transport is much greater inshore of the deltaic form, particularly in the southern part of the study area where there is little protection from the bank. Gradients in longshore sediment transport are important, as for different transport directions, the effect at the shoreline can be the same.

A large percentage of wave energy is removed by the 2005 bank, and so the beaches are likely to changes less rapidly (more stable). For the 1962 bank configuration, the region is much more exposed to waves, resulting in larger values of potential longshore transport. This suggests that inshore of the deltaic bank the beaches are less stable and more susceptible to change.

Conclusions

There is little evidence of direct sediment transfer between the bank and the shore, but soft ness features such as Benacre Ness are likely to be key regions for transfer between banks and the shoreline. Benacre Ness is migrating northwards at a rate of about 20 m per year (Babtie and Birbeck College, 2000) and is therefore likely to have increasing interaction with Newcombe Sand. Bathymetrically-induced modification of the wave field is a major identifiable impact at the shoreline.

The long, wide and flat elongate bank is effective at dissipating a large amount of wave energy and potential longshore transport calculations suggest that the beaches inshore of Newcombe Sand are likely to be relatively stable. Modeled patterns of sediment transport and erosion/accumulation around the elongate bank show onshore bank migration, in reasonable agreement with observed morphological feature and patterns. Composed of two main lobes, the deltaic bank is narrower, steeper and has a much shorter length span than the elongate bank, and is situated further north. As might be expected, much more wave energy reaches the shoreline, and in terms of potential longshore sediment transport, the beaches within the study area are less stable and more susceptible to change. Residual transport around the deltaic bank is an order of magnitude greater than around the elongate bank.

References

Babtie and Birbeck College (2000), *Spits and Nesses: basic processes and effects on long-term coastal morphodynamics*. Technical report.

CERC (1984), *Shore Protection Manual*. Coastal Engineering Research Centre, Waterway Experiment Station, Corps of Engineers, Vicksburg.

Coughlan, C., Vincent, C.E., Dolphin, T. (2007), Effects of tidal stage on the wave climate inshore of a sandbank, *Journal of Coastal Research*, SI 50, 751–756.

Dolphin, T., Vincent, C.E., Coughlan, C., Rees, J. (2007), Variability in sandbank behaviour at decadal and annual time-scales and implications for adjacent beaches, *Journal of Coastal Research*, SI 50, 731–737.

Hervouet, J. (2000), TELEMAC modeling system: an overview, *Hydrological Processes*, 14, 2209–2210.

HR Wallingford (2002), *Southern North Sea sediment transport study, Phase 2 – Final Report*. Technical Report EX4526.

Komar, P.D., Inman, D.L. (1970), Longshore sand transport on beaches. *Journal of Geophysical Research*, 75(30), 5514–5527.

Reeve, D., Li, B., Thurston, N. (2001), Eigenfunction analysis of decadal fluctuations in sandbank morphology at Great Yarmouth, *Journal of Coastal Research*, 17, 371–382.

Robinson, A. (1966), Residual currents in relation to shoreline evolution of the East Anglian Coast, *Marine Geology*, 4, 133–146.

Tonnon, P. van Rijn, L., Walstra, D. (2007), The morphodynamic modeling of tidal sand waves on the shoreface, *Coastal Engineering*, 54, 279–296.

Study of tidal effect on beach changes with presence of coastal defense structures

SHUNQI PAN, YANLIANG DU, YONGPING CHEN

School of Engineering, University of Plymouth,
Drake Circus, Plymouth PL4 8AA UK
email: shunqi.pan@plymouth.ac.uk, yanliang.du@plymouth.ac.uk,
yongping.chen@plymouth.ac.uk

Keywords: tidal effect, coastal structures, beach changes, numerical modeling

ABSTRACT

Tidal effect on coastline changes is particularly important for the UK shoreline management, as the most UK coasts are subject to macrotides ranging up to more than 10 m. The interaction between tides and coastal defense structures are yet to be fully understood, since many existing coastal defense structures in the UK were designed with the microtide experience. This paper presents the results obtained from a process-based model, which has been extensively developed to include the major important coastal processes in the nearshore areas on the morphological changes under combined wave and tidal conditions. As part of the EPSRC-funded LEACOAST2 research project, the model was applied to the study area at Sea Palling (Norfolk, UK), where a shore-parallel breakwater scheme is present, including four surface-piercing reefs and five submerged reefs. A 200-hour storm event was modeled, which include a significant storm surge, to examine the response of the beach to these storm wave and tidal conditions. Detailed volumetric changes of the sediment derived from the computed bed level changes in the nearshore zones are compared, and sediment transport patterns are studied.

Introduction

Coastal structures, such as segmented shore parallel breakwaters (SSPB), have been used worldwide. In the UK, applications include the breakwaters at Kings Parade, Wirral; Elmer, Sussex; and Sea Palling, Norfolk, with possibly some planned for the future. However, most current UK structures were designed a decade or more ago with the object of providing appropriate levels of flood protection as well as resisting the worst storm conditions likely to be experienced over the lifetime of the structures and also minimizing the long term (25–50 years) impact of the structures on adjacent coastlines. However, existing design guidelines rely heavily on microtidal experience, and even this experience is imperfect as demonstrated by the use of modern computer methods, showing the inability of some engineering criteria to correctly predict the formation of salients and tombolos in the lee of such structures, O'Connor et al. (1995). Recently, the significance of impact of increased future flood risk, which threats some four million people and properties in England and Wales alone and a potential increase in flooding costs by a factor of 20 has been highlighted in the Government's 'Foresight Project'. While much is being done, there is an urgent need for further action as regards the use of such structures and particularly their long-term impact. Immediate action to improve understanding of the impacts and methodology to mitigate the emerging problems and design guidelines for UK conditions is clearly needed.

The recent EPSRC-funded research project – LEACOAST2 uses combined direct measurements of hydrodynamics and morphodynamics, both process-based and probabilistic numerical models and long-term remote-sensing monitoring techniques from video cameras and x-band radar systems to study both the short-term and longer term impacts of the nearshore structures on adjacent beach changes, see www.research.plym.ac.uk/cerg/leacoast2 for details. One of the main objectives of the project is to investigate the effect of tides on the overall sediment transport pathway and morphological changes with the presence of the nearshore structures. This paper presents the preliminary results of the model applications to the Sea Palling site for a storm event in November 2006, which includes different wave, tide and storm surge conditions. The paper also illustrates from the detailed analysis of the volumetric changes in the area for each tidal cycle, the sediment transport patterns under these conditions.

Model description

The process-based model used in the study consists of a number of fully interactive modules, but mainly a wave module to determine wave-period averaged wave energy or wave height and wave direction for the wave transformation from offshore to nearshore; and a current module to compute the depth-integrated current velocity and water surface elevation under both tide and wave actions; and a morphological module to compute the sediment transport rate using equilibrium formulae, as well as the resulting bed level changes, details of which can be found in Pan et al. (2001), O'Connor et al. (2002) and Pan et al. (2007a). The model includes modules for bedform predictions (Pan et al., 2007b) to allow for the bed shear-stresses dynamically computed; the full wave-current interaction; and full hydrodynamic-morphological interaction. The model also allows for the combined variations of tides, wave height and wave direction throughout the computations; see Pan et al. (2005) for details.

The model was setup for the Sea Palling site, as shown in Figure 1. The computational domain covers an area of 5.0 km in the longshore direction by 2.0 km in the cross-shore direction with a grid size of 25.0 m by 12.5 m in the longshore and cross-shore directions respectively.

The model was applied to the study area with a storm event in early November 2006, where comprehensive hydrodynamic and morphological measurements carried out by two of the project partners: Proudman Oceanographic Laboratory (POL) and University of East Anglia (UEA). The field measurements enabled the comparisons between the model results and field measurements to be carried out.

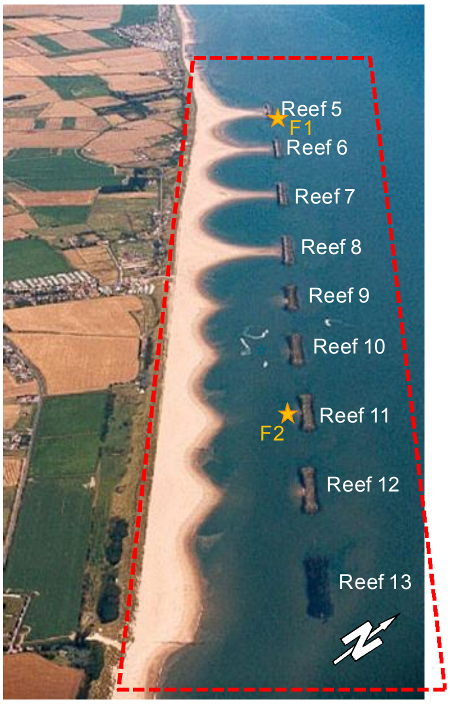

Figure 1. Breakwaters at Sea Palling, with the computational domain and the two measurement locations

Storm event

The model takes the measured wave and tidal conditions from POL Frame F1, as marked in Figure 1, as its offshore boundary conditions with minor adjustments. In order to check the accuracy of the boundary conditions, the computed wave height and water depth at the F1 measurement location were compared with the measurements. As shown in Figure 2 for wave height and Figure 3 for water depth, the overall agreement between the computed and measured quantities can be considered to be satisfactory.

The computed and measured velocity components were also compared at F1 location, as shown in Figures 4 and 5, where three ADVs were mounted on the F1 Frame at the different levels in the water column. The results show that the computed velocities in the easting direction agreed well with the measurements, but the northing velocities were slightly under-predicted by the model. Comparisons of the computed and measured

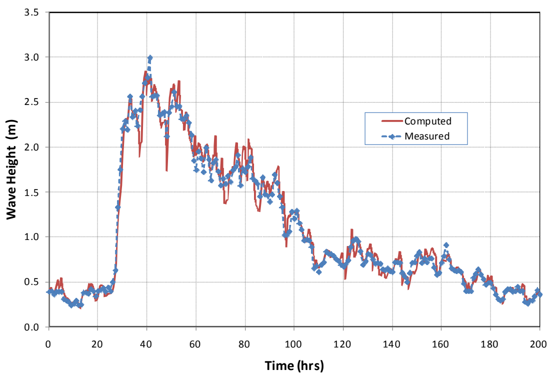

Figure 2. Computed and measured wave height at F1.

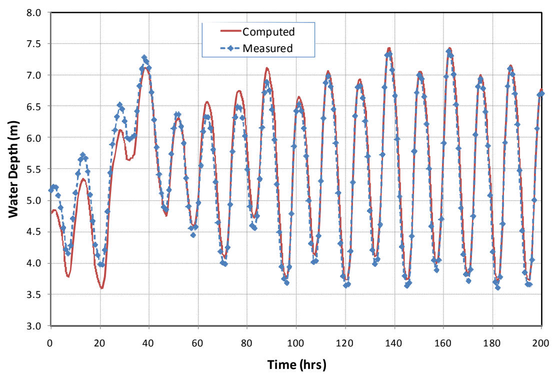

Figure 3. Computed and measured water depth at F1.

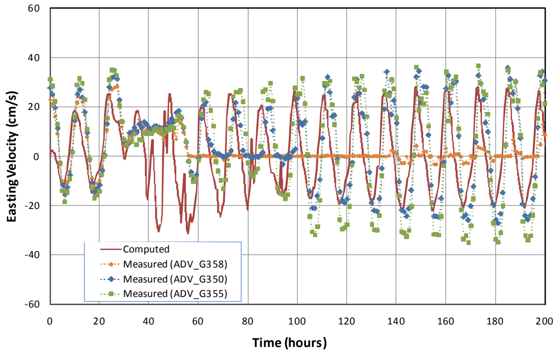

Figure 4. Computed and measured easting velocity at F1.

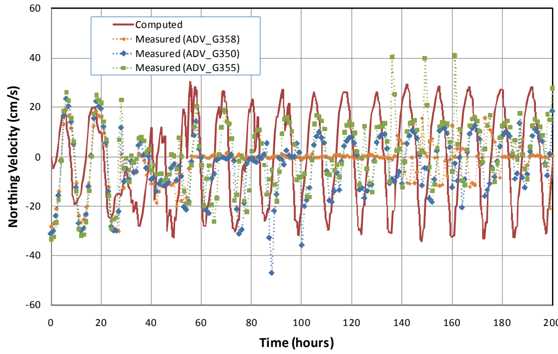

Figure 5. Computed and measured northing velocity at F1.

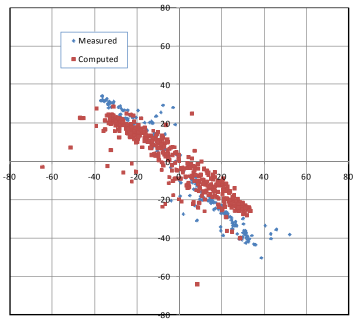

Figure 6. Computed and measured velocity ellipses at F2.

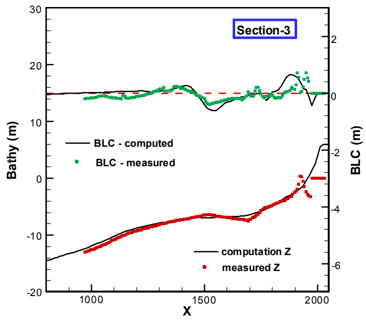

Figure 7. Computed and measured bed level changes along Section-3.

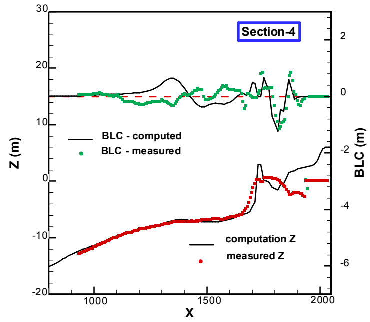

Figure 8. Computed and measured bed level changes along Section-4.

easting and northing velocities from POL F2 Frame, as marked in Figure 1, mounted with a single ADV, were also made, although not shown here, both agreeing well. The tidal ellipses of the computed and measured velocities at F2 location are shown in Figure 6, again indicating a good agreement. The results indicate that the model performed well in reproducing the hydrodynamics in the region for storm conditions.

The model results of morphological changes are also compared with the measurements taken by the UEA team from regular bathymetric and topographic surveys. Shown in Figures 7 and 8 are the total bed level changes (BLC) along two cross-shore transects: Section-3 located at the centre of the embayment between Reefs 7 and 8, see Figure 1, and Section-4 located across the middle of Reef 8. The results clearly indicate that a good level of agreement has been achieved by the model.

Both hydrodynamic and morphological comparisons shown above have provided high confidence on model performance and capability, although fine tunings may still be needed to further improve the accuracy. The computed bed level changes were further analyzed to study the net and accumulative volumetric changes over the whole computational domain. As shown in Figure 9, the net volumetric changes are clearly modulated by tides, but also influenced by wave conditions. Storm surge can significantly affect the sediment transport, and in turn the volumetric changes in the area. During the peak of the storm surge, there is a large quantity of sediment loss over a period of two tidal cycles, but the system gains the sediment during a few tidal cycles right after the peak of the surge. The figure also shows a clear influence of wave height on the volumetric changes. With higher wave energy, i.e., larger wave height, the volumetric changes are more pronouncedly modulated by the tides. The accumulative volumetric changes shown in Figure 9 clearly indicate that the scheme traps sediments over the entire storm duration, despite the loss of sediment over a number of tides while significant surge occurs. However, the rate of gaining sediments is on a decreasing trend when the wave height reduces. Further study with calm conditions, although not shown here, also indicated further reduction of sediments gaining or even loss of sediments in the study area during the neap tides with smaller waves. Detailed study of the sediment volumetric changes in each embayment has also been carried out, showing the complexity of the sediment transport with different types (higher crested and submerged reefs) under different wave and tidal conditions.

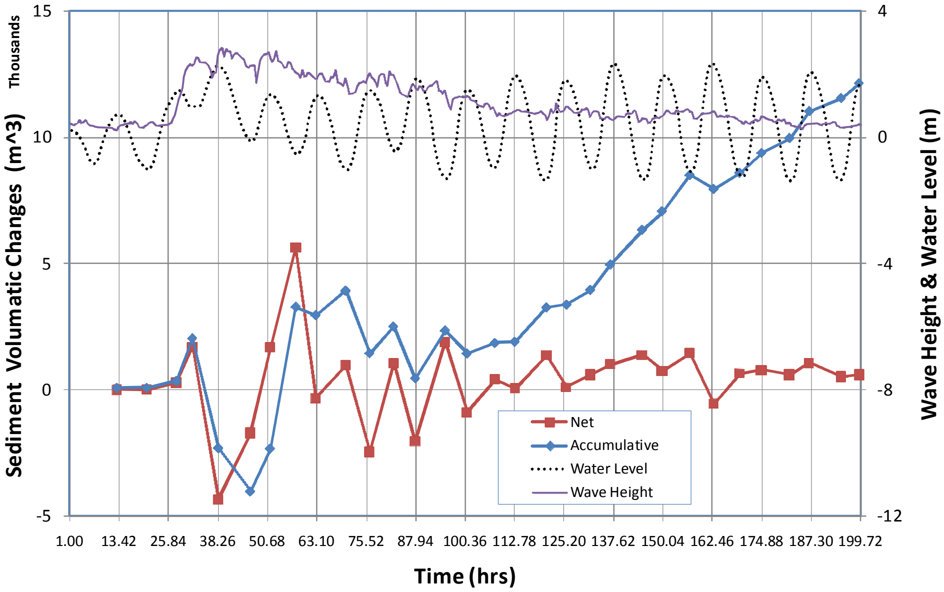

Figure 9. Sediment volumetric changes over a 200-hour storm event.

Conclusions

A 2D process-based model has been developed and applied to the breakwater scheme at Sea Palling for a storm event. The computed hydrodynamics and morphodynamics from the model agreed well with the field measurements. The results clearly show a significant influence of tides on the sediment transport and the resulting bed level changes. Particularly for storm events, the sediment volumetric changes are clearly modulated by the tides. It was also found that storm surge, which is usually associated with high energy sea states, can have a profound effect on the total volumetric changes.

Acknowledgements

This work is partly supported by the Engineering and Physical Sciences Research Council (EPSRC) under the grant number: EP/C010965/2. Thanks also go to all project partners for their support, particularly the POL and UEA teams, who kindly provided the field measurement data.

References

O'Connor, B.A., Nicholson, J., MacDonald, N.J. (1995), *Modelling morphological changes associated with an offshore breakwater*. In: Computer Modelling of Seas and Coastal Regions II, Brebbia, C.A., Traversoni, L., Nrobel, L.C. (Eds.), Computational Mechanics Publications, Southampton, pp215–272.

O'Connor, B.A., Pan, S., Heron, M., Williams, J., Voulgaris, G., Silva, A. (2000), *Hydrodynamic modeling of a dynamic inlet*. In: Proceedings of the International Conference on Coastal Engineering, Sydney, Australia, pp3472–3481.

Pan, S., Fernando, P., Li, M., Zhu, Y., O'Connor, B., Vincent, C., Taylor, J., Dolphin, T. Bacon, J. (2005), *Effect of shore parallel breakwaters on coastal morphology under storm conditions*. In: Allsop, N.W.H. (Ed.), Coastlines, Structures and Breakwaters. Thomas Telford, London, pp64–73.

Pan, S., MacDonald, N., Williams, J. J., O'Connor, B.A., Nicholson, J., Davies, A.M. (2007b), Modelling the hydrodynamics of an offshore sandbank, *Continental Shelf Research*, 27, 1264–1286, doi:10.1016/j.csr.2007.01.007.

Pan, S., O'Connor, B.A., Bell, P., Williams, J. (2001), *Interactive numerical modelling of the hydrodynamics of combined waves and tides in the coastal zone*. In: Coastal Dynamics '01, Hanson, H., Larson, M. (Eds.), ASCE, pp162–171.

Pan, S., Wolf, J., Chen, Y., Bell, P., Du, Y., Fernando, P., Li, M. (2007a), *Modelling nearshore waves with presence of shore-parallel breakwaters*. In: Coastal Structures 2007 (conference proceedings), Venice, Italy, 2nd–4th July 2007.

Modeling surface wave effects on evolved offshore sand waves

FENNEKE VAN DER MEER[1], SUZANNE J.M.H. HULSCHER[1], NICHOLAS DODD[2]

1. Water Engineering and Management, University of Twente,
P.O. Box 217, 7500 AE Enschede, Netherlands
email: f.m.vandermeer@utwente.nl, s.j.m.h.hulscher@utwente.nl

2. School of Civil Engineering, University of Nottingham, University Park,
Nottingham NG7 2RD UK
email: nick.dodd@nottingham.ac.uk

Keywords: offshore sand waves, wind waves, non linear modeling

ABSTRACT

Offshore sand waves are bed forms that occur in water depths of tens of meters. Under normal conditions wind waves rarely interact with the sea bed, however during storm conditions this might no longer be the case. Sand waves show both spatial and temporal variation in their characteristics such as their height (1–10 m), length (100–800 m), asymmetry and migration rate (1–10 m yr^{-1}). The reason for this variation is still not fully understood. A possible explanation for this variation is the occurrence of wind and weather influences.

In this paper we present the results of our non linear sand wave model, including the wind wave effects on sand wave height and show that wind waves can significantly lower the sand wave height and with that might explain some of the occurring variation.

Sand waves

Offshore sand waves are bed patterns that occur in shallow seas (Figure 1). The wavelengths of these bed forms vary between 100 and 800 m, and heights can reach up to one third of the water depth (i.e., a maximum of around 10 m in 30 m of water). These characteristics, together with the fact that sand waves can migrate several meters per year and that they cover the majority of, e.g., the Southern North Sea (van der Veen et al., 2006), mean that they affect human activities in shallow seas. Therefore, we aim to model and so better understand the dynamics of these sand waves.

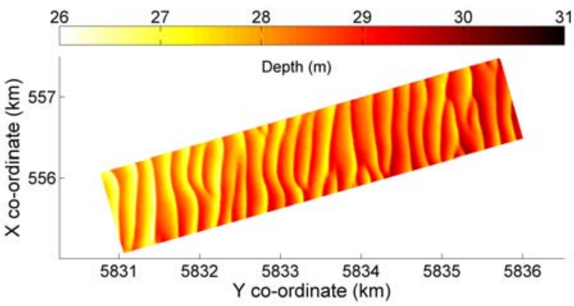

Figure 1. Example of a sand wave patch in the Southern North Sea.

As the water depth is in the order of tens of meters, under normal conditions sediment is transported as bed load and wind waves have a negligible influence on the sea bed. However, during storms, wind waves are considered to initiate the stirring of sediment, such that the sediment transport by the tidal currents increases. This occurs especially in the relatively shallow water e.g. closer to the coast, or on the crests of sand banks. In this case the wind waves might affect sand wave shapes or migration speed. Field observations confirm this hypothesis. For example Passchier and Kleinhans (2005) concluded that the sand wave morphology close to the coast of the Netherlands is a function of the general wind wave climate. Measurement of Harris (1989) already show that sand waves close to Australia change their asymmetry, most likely as a response to the wind driven currents during the trade and monsoon season.

Though the effect of wind waves is incorporated in a few linear studies of sea bed morphodynamics (e.g., Blondeaux and Vittori, 2005), a non-linear investigation into its effect on sand waves, in particular sand wave heights, has not yet been accomplished. In this paper we present a first investigation on the effect of wind waves on the final sand wave height. Our main question is "do wind waves effect the sand wave height, and if so, to what extent?". Here, we implement wind wave effects in an idealized non-linear sand wave model.

Model approach

The Sand Wave Code (SWC) used in this project is based on an idealized model by Németh et al. (2006) and further developed by van den Berg and van Damme (2006). It is a two dimensional vertical model, which is developed specifically to describe sand wave evolution from its generation, to its fully grown state.

Sand wave formation is explained as self organization due to interaction between a sandy seabed and a tidal flow. Sand waves occur as free instabilities in this system, i.e. there is no direct relation between the scales related to the forcing (tide) and those related to the morphological feature (sand wave) (Dodd et al., 2003). Hulscher (1996) described the mechanism of self organization for sand waves, where residual vertical vortices play a crucial role. In short, the process is as follows. Starting from a flat bed with an oscillating current, small perturbations of the sea floor cause small perturbations in the flow field and vice versa. The bed can be either stable, which means that all bed perturbations will be damped, or unstable, which means that certain bed perturbations will grow and the sea bed is changed.

The SWC detects the fastest growing mode (FGM) and simulates the growth for this wave length from the initial disturbance to the final sand wave shape that is in equilibrium with the flow. The SWC consists of the hydrostatic flow equations for 2DV flow. The tidal flow is modeled as a sinusoidal current prescribed by means of a forcing. Boundary conditions at the bed disallow flow perpendicular to the bottom. Further, a partial slip condition compensates for the constant eddy viscosity, which is known to overestimate the eddy viscosity near the bed. At the water surface there is no friction and no flow through the surface. Since the flow changes over a timescale of hours and the morphology over a timescale of years, the bathymetry is assumed to be invariant within a single tidal cycle. The flow and the sea bed are coupled through the continuity of sediment. Only bed load transport is taken into account, for equations we refer to van den Berg and van Damme (2006) and van der Meer et al., (2007).

As sand waves occur in relatively deep water with respect to wind waves, the wind waves are expected not to break. To implement the effect of surface waves we use linear wave theory, i.e., monochromatic waves for which the linear approximation holds (ak<<1, a/h<<1 and a/k^2h^3<<1, where a is wind wave amplitude, k wavenumber and h local water depth). We assume that waves and current are collinear. The absolute frequency of the waves, ω, is assumed to be constant and the wave action, E/σ, is a conserved quantity. We further assume that the currents will influence wave characteristics, while waves don't influence currents (Mei, 1999). With a given incoming wave period the wave number k and wave energy per location over the sand wave is calculated.

$$\omega = Uk + \sqrt{gk\tanh(kh)}\,, \qquad \frac{d}{dx}\big((U + C_g)\,E/\sigma\big) = 0\,, \qquad C_g = \frac{\omega}{k}\left(1 + \frac{2kh}{\sinh(2kh)}\right), \qquad \omega = 2\pi/T\,. \tag{1}$$

U is the depth averaged current velocity, g the gravitational force, E the wave energy, σ is the intrinsic wave frequency, C_g and T represent the group velocity and the wave period of the surface waves respectively. Via surface wave height H_w and wave orbital velocity u_w, we determine the bed shear stress due to wind waves, τ_w.

$$E = \frac{\rho g H_w^2}{8}\,, \qquad u_w = \frac{\omega H_w}{2\sinh(kh)}\,, \qquad \tau_w = \frac{f_w u_w^2}{2}\,, \qquad f_w = 0.237\left(\frac{a}{2.5D}\right)^{-0.52}\,. \tag{2}$$

Here f_w is the bed friction factor according to Soulsby (1997), and D is the grain size. Note that we use the volumetric bed shear stress. To combine both the current and the wave shear stress, we extend the sediment transport equation with an extra term, for the wind wave bed shear stress. This causes an extra transport by the tidal flow and affects the slope adjustment, both due to the stirring effect of the wind waves:

$$q_b = \alpha \left|\tau_{bf}\right|^{1/2}\left(\left|\tau_{bf}\right| + \gamma\left|\tau_{bw}\right|\right)\left(\frac{\tau_{bf}}{\left|\tau_{bf}\right|} - \lambda\frac{dh}{dx}\right)\,. \tag{3}$$

We follow Roos et al. (2004) and Calvete et al. (2001), here rewritten for a z-coordinate dependent situation, i.e., for bed shear stress τ instead of depth averaged velocity u. The bed load sediment transport and the bed shear stress due to the current are represented by q_b and τ_{bf} respectively and γ is a dimensionless with value 1.

Results

We present below, an overview of the effect of wind waves on the modeled sand wave height. Parameters (Table 1) are typical for the North Sea. We modeled four different cases with a water depth of 15 or 30 m and a flow velocity of 0.5 and 1 m s^{-1}. With these cases different wind waves were included as listed in Table 2.

Table 1. Parameter values used in the simulations typical for the North Sea.

Physical quantity	Parameter	Value	Dimension
Water depth	h	15–30	m
Tidal velocity	U	0.5–1.0	m s^{-1}
Eddy viscosity	A_v	0.03	m^2 s^{-1}
Slip parameter	S	0.01	m s^{-1}
Slope parameter	λ	1.7	–

Table 2. Wind wave characteristics, corresponding to the IJmuiden munition dump in the North Sea (21 m water depth), after De Leeuw (2005).

Probability of exceedance (%)	Wind wave height (m)	Wind wave period (s)
100	0.0	0.0
50	1.0	5.3
10	2.4	7.0
1	4.2	8.9
0.1	5.5	10.7

In Figure 2 the effect of variation in wind waves on the sand wave height is shown. We see that if we include the wind waves continuously, the sand waves are lowered for increasing wind waves. For deeper water the decrease rate increases with larger waves, in shallower water the decrease rate slows down if wind waves increase. Also, we see that the larger tidal currents tend to decrease the effect of wind waves. Though not shown, we note that in the case of deep water sometimes both the trough and the crest position move down when wind waves increase. This leads to a more constant sand wave height, which however not means that the wind waves have no influence on the sand wave.

If we take into account that the different wind wave types have different probabilities of occurrence (Table 2), the effect of wind waves shows a different picture (Figure 2, right panel). The smallest wind waves, which occur longer periods do decrease the sand wave height more than the larger wind waves that occur rarely. We also included a combined wind wave climate, with all the different wind waves and their probabilities of occurrence. The sand wave height was in this case lowered by approximately 35% of the original height (Figure 3).

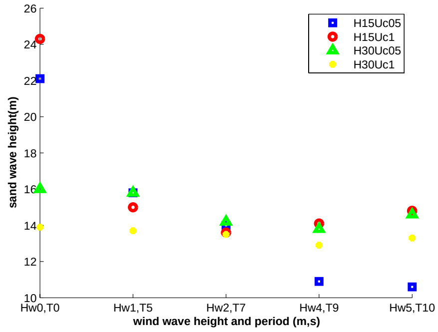

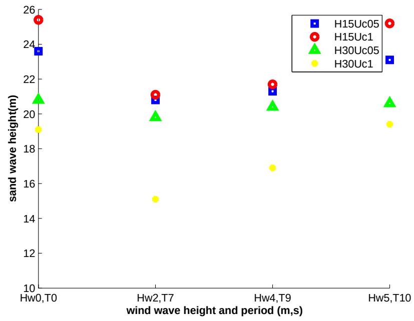

Figure 2. Final sand wave heights under different wind wave conditions. Wind waves have height, H_w and period, T, both increasing towards the left (on x-axis). Symbols indicate different water depths and flow velocities. Left: results for wind waves continuously on. Right: probability of exceedance is taken into account.

Discussion

The results clearly show that wind waves are able to affect the sand wave height. Overall, wind wave periods can lower the sand waves with a few meters up to 35% of the sand wave height for a combined wind wave climate.

Though larger wind waves have a stronger effect on the sand wave height, due to their low frequency in time their effect is relatively small. If the wave exceedance is taken into account, we see that sand waves are most affected by the small, frequently occurring, wind waves. Even though an individual large storm can decrease the sand wave height by a few decimeters, this effect diminishes within a few years to a decade. For smaller waves the effect of an individual storm is smaller but due to their frequency the sand wave has no time to recover fully and will lower further in the next event. This causes a new equilibrium, with smaller sand waves than when these wind waves are excluded. High occurrence of wind waves seems more important than their size.

Physical surroundings influence the effects that wind waves can have. Decreasing water depth increases the wind wave effect significantly (Figure 2). In deep water, smaller waves are less likely to reach the bed than in shallower water, leading to smaller changes in the sand wave shape. The fact that in some deep water cases only the crest lowers, while the trough remains unchanged, agrees with this idea. In that case, wind waves only reach the crests and not the troughs of the sand waves. For increasing wind waves, wind waves reach a bigger part of the bed, leading to an increased lowering of sand waves. For shallower water the opposite occurs, small waves already reach the total bed, lowering the sand waves. When wind waves increased, the bed changed less quickly. It shows that sand waves tend to a new equilibrium that already establishes including a relatively small disturbance, after which the height remains more robust.

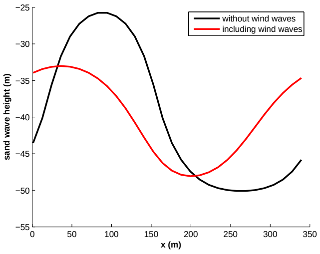

Figure 3. Final sand wave shapes with and without wind wave climate. Left: water depth 20 m and flow velocity 0.41 m s^{-1}; right: water depth 40 m, flow velocity 0.43 m s^{-1}, additional 0.02 m s^{-1} residual current. Note the location of the crest and trough is different due to migration of the sand wave.

Changing the current velocity gives a less clear view. It slightly increases sand wave lowering. Two processes act here in different directions. On the one hand, increasing the current decreases the relative effect of wind waves; on the other, sediment that is stirred by wind waves is transported further, thereby increasing the wind wave effect. When including the wind wave probability of exceedance, the current effect is clearer, increasing the sand waves lowering by wind waves (steeper lines in Figure 2).

Conclusion

We presented a first investigation on the influence of wind waves on sand wave height. Results of the idealized process based SWC show that wind waves can significantly lower the sand waves. A general wind wave climate lowers the sand waves by approximately 35%. Though larger wind waves lower the sand waves more, due to their low frequency of occurrence the effect on sand waves is smaller than that of smaller, but more frequent wind waves. The relative importance of smaller wind waves coincides with observations indicating that the general wind wave climate is more important than individual large storms (Passchier and Kleinhans, 2005). Including wind waves improves model predictions, and might explain part of the observed variation in sand wave height. Further investigations will focus on effects of wind waves on other sand wave characteristics.

Acknowledgement

This research is supported by EncoraNL and the Technology Foundation STW, applied science division of NWO and the technology program of the Ministry of Economic Affairs. Their support is gratefully acknowledged.

References

van den Berg, J., van Damme, D. (2006), *Sand wave simulations on large domains*. In: Parker, G., Garcia, A., (Eds.), River, Coastal and Estuarine Morphodynamics: RCEM 2005.

Blondeaux, P., Vittori, G., (2005), Flow and sediment transport induces by tide propagation: 2. the wavy bottom case, *Journal of Geophysical Research*, 110, C08003, doi:10.1029/2004JC002545.

Calvete, D., Falqués, A., de Swart, H.E., Walgreen, M., (2001), Modelling the formation of shoreface-connected ridges on storm-dominated inner shelves, *Journal of Fluid Mechanics*, 441, 169–193.

Dodd, N., Blondeaux, P., Calvete, D., de Swart, H., Falqués, A., Hulscher, S.J.M.H., Rózynski, G., Vittori, G. (2003), Understanding coastal morphodynamics using stability methods, *Journal of Coastal Research*, 19(4), 849–866.

Harris, P.T., 1989. Sand wave movement under tidal and wind-driven currents in a shallow marine environment: Adolphus Channel, northeastern Australia, *Continental Shelf Research*, 9(11), 981–1002.

Hulscher, S.J.M.H. (1996), Tidal-induced large-scale regular bed form patterns in a three-dimensional shallow water model, *Journal of Geophysical Research*, 101, 727–744.

de Leeuw, C.J., (2005), *Model predictions of wave-induced sediment transport on the shoreface*. M.Sc. thesis. University of Twente, Netherlands. April 2005.

van der Meer, F.M., Hulscher, S.J.M.H., Hanes, D.M., Elias, E. (2007), *San Francisco Bay sand waves: modelling and observation*. In: Dohmen-Janssen, C.M., Hulscher, S.J.M.H. (Eds.), River, Coastal and Estuarine Morphodynamics: RCEM 2007. Taylor & Francis Group, London.

Mei, C.C., (1999), *The applied dynamics of ocean surface waves*. In: Advanced Series on Ocean Engineering. World Scientific Publishing Co Pte Ltd. Vol. 1.

Németh, A.A., Hulscher, S.J.M.H., van Damme, R.M.J. (2006), Simulating offshore sand waves, *Coastal Engineering*, 53, 265–275.

Passchier, S., Kleinhans, M.G. (2005), Observations of sand waves, megaripples, and hummocks in the Dutch coastal area and their relation to currents and combined flow conditions, *Journal of Geophysical Research*, 110, F04S15, doi:10.1029/2004JF000215.

Roos, P.C., Hulscher, S.J.M.H., Knaapen, M.A.F. (2004), The cross-sectional shape of tidal sandbanks: Modeling and observations, *Journal of Geophysical Research*, 109, F02003, doi:10.1029/2003JF000070.

van der Veen, H.H., Hulscher, S.J.M.H., Knaapen, M.A F. (2006), Grain size dependency in the occurrence of sand waves, *Ocean Dynamics*, 56(3–4), 228–234.

Morphodynamic modeling and data assimilation

POLLY J. SMITH[1], SARAH L. DANCE[1], MICHAEL J. BAINES[1],
NANCY K. NICHOLS[1], TANIA R. SCOTT[2]

1. Department of Mathematics, University of Reading, Reading RG6 6AX UK
   email: p.j.smith@reading.ac.uk, s.l.dance@reading.ac.uk, m.j.baines@reading.ac.uk, n.k.nichols@reading.ac.uk

2. Environmental Systems Science Centre, University of Reading,
   Reading RG6 6AL UK
   email: trs@mail.nerc-essc.ac.uk

Keywords: data assimilation, morphodynamic modeling, parameter estimation, state augmentation

ABSTRACT

Data assimilation is a means for combining observational data with model predictions to produce state and parameter estimates that most accurately approximate the current and future states of the true system. The technique is commonly used in atmospheric and oceanic modeling, combining empirical observations with model predictions to produce more accurate and well-calibrated forecasts. Here we consider its application within a coastal environment and describe how the method can also be used to deliver improved estimates of uncertain morphodynamic model parameters. This is achieved using a technique known as state augmentation. A simple 1-D model of bed-form propagation is used to demonstrate the method within a three-dimensional variational assimilation framework. Preliminary results are positive and suggest the potential for application to more complex morphodynamic models.

Introduction

Coastal morphodynamics presents a challenge to modelers. Modeling is difficult because longer term morphological changes are driven by shorter term processes such as waves and tides. State of the art models are growing more sophisticated in an attempt to accurately model coastal morphology. In practice, models suffer from uncertainty in their initial conditions and parameters which can lead to significant errors between the predicted and actual states of the system, so that coastal area morphodynamic models often perform poorly in detail. A complementary approach to improving model performance is to combine model integrations with observations of morphology using data assimilation techniques.

Data assimilation is a means for combining observational data with model predictions to 1) produce a model state that most accurately estimates the current and future states of the true system 2) provide estimates of the model parameters. It is routinely used in atmospheric and oceanic prediction, but the possibility of transferring the technique into the coastal environment has only recently been investigated (e.g., Scott and Mason, 2007). The overall aim of this work is to apply data assimilation within a morphodynamic model, exploiting the information content of empirical observations to provide more accurate and well-calibrated forecasts. Here, we focus on the second of these applications and present a method for using data assimilation to deliver improved parameter estimates.

The dynamical system we wish to model depends on parameters whose exact values are not known, for example those that arise from parameterization of the sediment transport flux. Inaccurate representation of model parameters can lead to the growth of model error and therefore affect the ability of our model to accurately predict the true system state. A key question in model development is how to estimate these values a priori. Generally, parameters are determined theoretically or by calibration of the model against observations. Here we present an alternative approach, using the technique of state augmentation to develop a scheme that enables model parameters to be estimated alongside the model bathymetry as part of the assimilation process. Ideas are currently being developed and tested using simplified 1-D models of bed-form propagation with the long term aim of implementing the scheme in a full assimilation-forecast system.

Data assimilation

In reality, a model cannot represent the behavior of a morphodynamic system exactly. Over time the model bathymetry will diverge from the true bathymetry and errors will arise due to imperfect initial conditions and inaccuracies in physical parameters and numerical implementation. Data assimilation can be used to compensate for the inadequacies of a model and help keep the model bathymetry on track. By periodically incorporating measured observations into the model, data assimilation nudges the model bathymetry back towards the true bathymetry, thus improving the ability of the model to predict future bathymetry.

We suppose that the true state of the system is represented by a vector $\mathbf{z}^\mathbf{t}$, and we have a background estimate $\mathbf{z}^\mathbf{b}$, based on some prior knowledge of what we expect the present state to be. These are both 1-D vectors of dimension m, where m is the number of model grid points. We also have another vector $\mathbf{y}$ of dimension r containing the observations to be assimilated, where r is the number observations to be assimilated. The aim is to combine the measured observations $\mathbf{y}$ with the model predictions $\mathbf{z}^\mathbf{b}$ to derive a model state $\mathbf{z}^\mathbf{a}$ that most accurately describes the true state of the system $\mathbf{z}^\mathbf{t}$. This optimal estimate is called the *analysis*.

A wide variety of data assimilation schemes exist, many of which have been derived using statistical techniques (e.g., Kalnay, 2003). In this work we apply a standard method based on statistical estimation theory known as three dimensional variational data assimilation (3D Var). 3D Var is based on a maximum a posteriori estimate approach and derives the analysis by looking for a state that minimizes a cost function measuring the misfit between the model state $\mathbf{z}$ and the background $\mathbf{z}^\mathbf{b}$ and observations $\mathbf{y}$,

$$J(\mathbf{z}) = (\mathbf{z} - \mathbf{z}^\mathbf{b})^\mathrm{T}\, \mathbf{B}^{-1}(\mathbf{z} - \mathbf{z}^\mathbf{b}) + [\mathbf{y} - \mathbf{h}(\mathbf{z})]^\mathrm{T}\, \mathbf{R}^{-1}[\mathbf{y} - \mathbf{h}(\mathbf{z})]\,. \tag{1}$$

$\mathbf{h}$ is known as the observation operator. It is used to generate model equivalents of the observations by mapping $\mathbf{z}$ from model- to observation-space, e.g., interpolation from the model to the location of an observation; a forward model that takes values of bathymetry to values of lidar reflectance. The $m \times m$ matrix $\mathbf{B}$ and $r \times r$ matrix $\mathbf{R}$ are covariance matrices of the background and observation errors, $\boldsymbol{\varepsilon}_\mathbf{b} = \mathbf{z}^\mathbf{b} - \mathbf{z}^\mathbf{t}$ and $\boldsymbol{\varepsilon}_o = \mathbf{y} - \mathbf{h}(\mathbf{z}^\mathbf{t})$. These matrices represent errors associated with the background and observations, determining the relative weighting of $\mathbf{z}^\mathbf{b}$ and $\mathbf{y}$ in the analysis. (Discussed further in the 'Error Covariances' section.)

State augmentation

The equations used to describe the dynamical system we wish to model depend on parameters whose values are imprecisely known. Data assimilation provides us with a method for estimating these parameters using observational information. This can be achieved through 'state augmentation'. State augmentation is a conceptually straightforward technique that allows us to estimate uncertain model parameters alongside the original model state (Jazwinski, 1970). In theory, state augmentation can be applied to any of the standard data assimilation methods. A vector containing the parameters we wish to estimate is simply appended to the state vector and the chosen assimilation algorithm is applied to the augmented system in the usual way. However, practical implementation of the approach relies strongly on the relationships between the parameters and state components being well defined and assumes that we have sufficient knowledge to reliably describe them. Since it is not usually possible to observe the parameters themselves, the parameter updates are only influenced by the observations through the cross covariances that describe the correlations between the error of the model state estimate and the error of the model parameter estimate. Successful parameter estimation will therefore only be possible if these cross correlations are adequately specified.

Error covariances

Error covariances play an important role in variational data assimilation. Before we can implement our 3D Var algorithm we need to define the error covariance matrices $\mathbf{B}$ and $\mathbf{R}$. We are assuming that our model is perfect, i.e., the model equations provide an exact representation of the dynamical system. Obviously, this assumption is unrealistic. In practice it is impossible to describe the true system behavior completely and the model will also contain errors as a result of uncertain parameters and inaccurate initial and boundary conditions. In addition, the observations we wish to assimilate are likely to incorporate some kind of error, however small. Our assimilation scheme needs to take account of the errors that arise as a result of these imperfections as the precision of the analysis is determined by the precision of the background and observations. The error covariance matrices $\mathbf{B}$ and $\mathbf{R}$ represent our uncertainty in the background $\mathbf{z}^\mathbf{b}$ and observations $\mathbf{y}$. For the augmented system we also need to consider the errors in the parameter estimates and the relationship between these errors and the errors in the background state. These are combined with the standard $\mathbf{B}$ matrix to form an augmented background error covariance matrix $\mathbf{B}^*$. Correct specification of

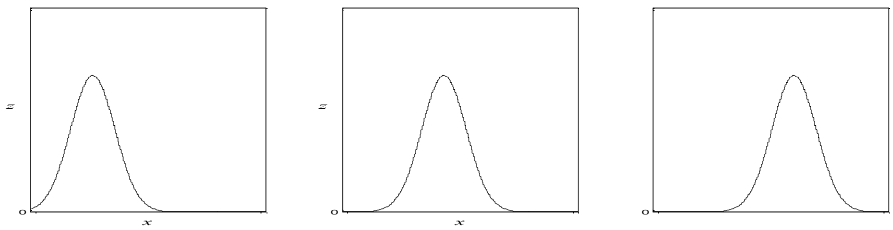

Figure 1. Solution to the linear advection equation.

these matrices is crucial to the quality of the analysis. If we can ensure that these matrices provide appropriate representation of the true error statistics, our data assimilation algorithm will produce optimal results.

The observation error covariance matrix **R** gives a statistical description of the errors in **y**. These errors originate from instrumental error, errors in the forward model **h** and representativeness errors (observing scales that cannot be represented in the model). For ease of computation we assume that the observation errors are spatially and temporally uncorrelated and take **R** to be a constant diagonal matrix with error variance σ_o^2.

Specification of the matrix **B** is one of the key parts of the assimilation problem. Background errors arise from errors in both the initial conditions and model errors. Since, by the nature of the problem, these errors are not known exactly they have to be approximated in some manner. There are various ways of doing this; Fisher (2003) provides a useful review of current operational techniques.

Formulation of the matrix **B** can be made considerably easier by specifying the error correlations as analytic functions. A number of correlation models have been proposed (Daley, 1991). One of the simplest ways of representing **B** is to assume that background error covariances are homogenous and isotropic. **B** is then equal to the estimated error variance σ_b^2 multiplied by a correlation matrix defined using a pre-specified correlation function. Although this method is somewhat crude it makes the data assimilation problem far more tractable.

For the augmented system we have the added difficulty of specifying the background error covariance matrices for the parameter vector and for the cross correlations between the state and parameter errors. For simplicity we take these matrices to be of a functional form similar to that used for the state background error covariance matrix. Since successful parameter estimation relies upon these correlations being suitably specified it is important to ensure that the choice of function is appropriate to the particular model application. In this work **B*** was identified using a combination of theory and practical experiments.

The model

We choose to start with the simple case of a model with a single unknown parameter. For this we use the 1-D linear advection model described in Smith et al. (2007)

$$\frac{\partial z}{\partial t} + a\frac{\partial z}{\partial x} = 0\,, \tag{2}$$

where $z(x, t)$ is the bathymetry or bed height, a is the advection velocity and t is time. The idea is to explore the application of the state augmentation technique within the framework of this simplistic model before moving on to more complex morphodynamic models. The advantage of the linear advection Equation (2) is that it can be solved analytically. This provides a reference solution against which we can assess the performance of our scheme.

We assume that Equation (2) gives an accurate representation of the true system evolution but that the model inputs are incorrect. We wish to investigate whether, given an uncertain initial bathymetry and unknown advection velocity, we are able to use our augmented data assimilation scheme to produce a more accurate estimate of the true velocity, thereby improving the ability of our model to predict the true system state. For the purpose of these experiments we set the true advection velocity $a = 0.5$ and use a Gaussian exponential function to give a smooth bell-shaped bed-form. The evolution of the solution is illustrated in Figure 1. As time increases, the bed moves undistorted across the model domain with constant speed a.

Results

Experiments were carried out with the initial advection velocity both over and underestimated. Figures 2a and 2b show the updating of the parameter a, for initial estimates of $\tilde{a} = 0.25$ and $\tilde{a} = 0.75$. Results are given

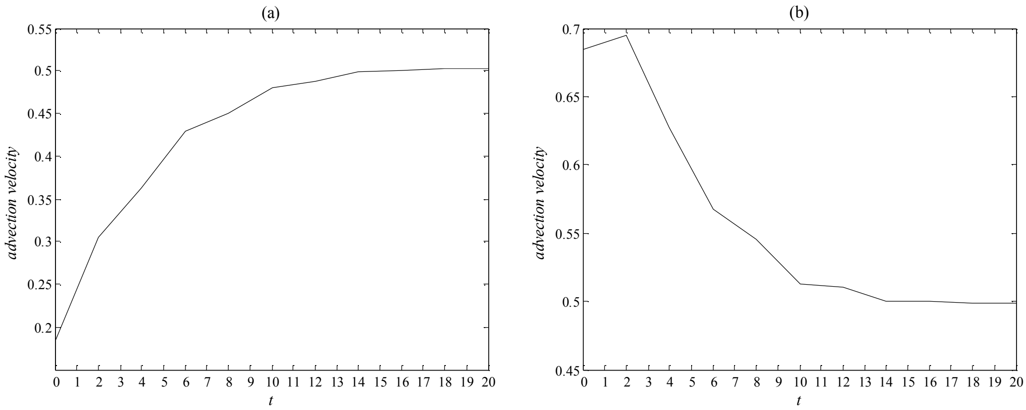

Figure 2. Convergence of parameter estimate estimates towards true value $a = 0.5$ (a) initial estimate $\tilde{a} = 0.25$ (b) initial estimate $\tilde{a} = 0.75$.

for times $t = 0$ to 20 with time step $\Delta t = 0.1$. The assimilation process was carried out sequentially with a new set of observations being assimilated every 20 time steps. At the end of each cycle the analysis was integrated forward using the model to obtain the background state for the next analysis time. A grid spacing of $\Delta x = 0.1$ was used and observations were generated from the true solution at fixed intervals of $20\Delta x$. The cost function was minimized iteratively using a Quasi-Newton descent algorithm (Gill et al., 1981).

In the examples illustrated above, the scheme managed to successfully recover the true value of a after approximately 15–20 time units. In both cases the final value of a was 0.50 to 2 d.p. Other starting values and observation combinations have also been tested. Not unsurprisingly, the speed of convergence varies depending on the initial background guess, the location and frequency of the observations and the time between successive assimilations.

Conclusions

We have presented a novel approach to model parameter estimation using data assimilation. So far the technique has only been developed and tested in a simplified 1-D single parameter model. The results are promising. The method has been shown to be capable of recovering near-perfect parameter values and therefore improving our ability to predict future model states. This suggests the potential for successful application of the technique in more complex morphodynamic models.

Acknowledgements

This work is funded under the UK Natural Environment Research Council (NERC) Flood Risk From Extreme Events (FREE) program, with additional funding provided by the Environment Agency as part of the CASE (Co-operative Awards in Science and Engineering) scheme.

References

Daley, R. (1991), *Atmospheric data analysis*. Cambridge University Press.

Fisher, M. (2003), *Background error covariance modeling*. In: Recent developments in data assimilation for the atmosphere and ocean. ECMWF Seminar Proceedings, ECMWF Reading UK, pp45–64.

Gill, P.E., Murray, W., Wright, M.H., (1981), *Practical optimization*. Academic Press.

Jazwinski, A.H. (1970), *Stochastic processes and filtering theory*. Academic Press.

Kalnay, E. (2003), *Atmospheric modeling, data assimilation and predictability*. Cambridge University Press.

Scott, T.R., Mason, D.C. (2007), Data assimilation for a coastal area morphodynamic model: Morecambe Bay, *Coastal Engineering*, 54, 91–109.

Smith, P.J., Baines, M.J., Dance, S.L., Nichols, N.K., Scott, T.R. (2007), *Simple models of changing bathymetry with data assimilation*. Numerical Analysis Report 10/2007, Department of Mathematics, University of Reading, available from www.reading.ac.uk/maths/research/maths-numanalrpts.asp.

Wave-orbital speed and sediment entrainment on an estuarine intertidal flat

TONY DOLPHIN[1], MALCOLM O. GREEN[2]

1. School of Environmental Science, University of East Anglia, Norwich NR4 7TJ UK
   email: tony.dolphin@uea.ac.uk

2. National Institute of Water and Atmospheric Research,
   P.O. Box 11-115, Hamilton 3251, New Zealand
   email: m.green@niwa.co.nz

Keywords: estuary, tides, waves, sediment transport, sand, silt

ABSTRACT

Sediment transport on estuarine intertidal flats is complex, due to variability in sediment size (i.e., silts and sands), water levels and exposure to spatially and temporally varying skin friction resulting from both tidal currents and the locally generated wave field. The historical emphasis of estuarine intertidal flat research has been on tidal currents and not waves (Malvarez et al., 2001), presumably because tides are periodic and more easily measured/predicted. Although there are few detailed studies into the influence of waves in estuaries, there is a general recognition of their importance on intertidal flats where tidal flows are typically weak (e.g., Allen, 1971; Dyer, 1989). An accurate understanding of the processes that mobilize and transport sediments on estuarine intertidal flats (and in channels) is imperative to understanding wider estuarine evolution, the burial and dispersal of contaminants, habitat change, and numerical modeling efforts. In this paper we present the results of field experiments into the parameters that control sediment entrainment on an intertidal flat (called Wiroa) in a large New Zealand estuary (fetch lengths up to 25 km).

Setting

Manukau Harbour is a large, meso-tidal, barrier-enclosed estuary adjacent to the city of Auckland, New Zealand (Figure 1). The estuary is shallow and infilled, with over 40% of its surface area exposed at low tide. Large intertidal and subtidal flats/banks are dissected by deep tidal-channels. The tide is semi-diurnal with a spring range of 4.4 m. Strong tidal flows are experienced in deep tidal channels (up to 200 cm s^{-1} in the inlet gorge), but weaken significantly across intertidal flats (0–40 cm s^{-1}).

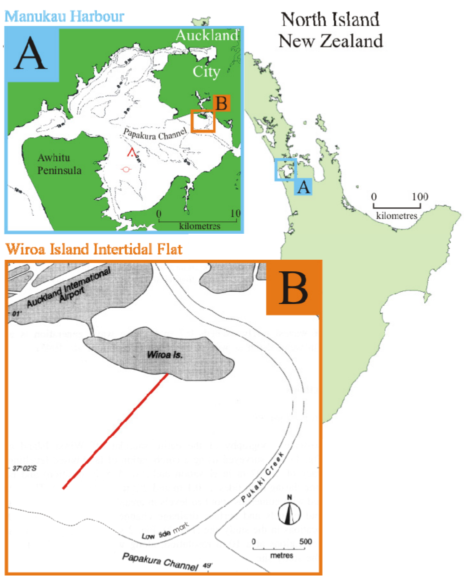

Figure 1. Location map of Wiroa Island Intertidal Flat and Manukau Harbour. Red line in map B marks instrumented transect.

The estuary is sheltered from oceanic swells by a large Pleistocene barrier (10 × 25 km) and a very large and shallow ebb-tidal delta (1250 × 10^6 m^3; Hicks and Hume, 1996). Maximum fetch is at high tide (25 km), but on the falling tide intertidal banks emerge cutting fetch in sudden steps until, for some locations, fetch equates to channel width (1–2 km). Optimum conditions for wave generation require coincidence of very strong winds with high spring tides, when fetch is at its maximum. Under such conditions waves can grow to over 1 m.

Experiments were conducted on the Wiroa intertidal flat (Figure 1B). The site is exposed to prevailing south-westerly winds. The intertidal flat is approximately 2 km wide and has five distinct regions distinguished by variation in slope and sediment size distribution; the channel margin (1:40), lower flat (1:450), middle flat (1:400), upper flat (1:1000) and the estuarine beachface (1:10). On the channel margins and lower flat, silts make up 3–4% of bed sediments; landward the low gradient sand flat (<2% mud) often features wave ripples; on the upper flat low amplitude multiple bars are present (Dolphin et al., 1995), sandy sediments give way to mud deposits around discrete patches of mangrove forest; and the upper flat breaks into a steep, shelly coarse-sand beach face.

Methods

A transect parallel to the prevailing south westerly wind (red line, Figure 1) was instrumented at 16 stations. The data used here are from Dobie-O wave-turbidity gauges (Druck pressure sensor and Downing optical backscatter sensors (OBS)) and the tripod Alice. Alice measures total pressure using a Paroscientific pressure sensor; water currents using four vertically offset Marsh-McBirney 3.8-cm electromagnetic current meters; suspended silt concentration using four vertically offset OBSs; suspended sand concentration using a three-frequency (1.08, 1.97, 4.38 MHz) acoustic backscatter system (ABS); and suspended sediment concentration and particle size distribution using a purpose built water sampler, Zelda. Zelda samples were analyzed in the lab with a Galai time-of-transition particle sizer and using standard filtration techniques for suspended sediment concentration.

The particle-size distribution during storm events is distinctly bi-modal, consisting of silts (10–30 µm) and sands (125–225 µm). Following Green et al. (1999, 2000), we used the OBSs to estimate the suspended silt concentration as they are comparatively insensitive to sand in suspension (assuming only silt is present in a 1:1 silt:sand mixture gives a 10% error), and we used the ABS to estimate the suspended sand concentration as it is comparatively insensitive to silt in suspension (assuming only sand is present in a 1:1 silt:sand mixture gives a 0.5% error).

Results

Wave modulation

During onshore winds, wave growth is controlled by wind speed, fetch, duration and water depth ($\overline{h}$). In mature (infilled) estuaries such as Manukau, fetch (and duration at a given fetch) is systematically controlled by tidal stage and the periodic emergence and submergence of intertidal banks. As a result, and notwithstanding changes in wind speed, wave height (H) is controlled by fetch length (Figure 2), which varies on a ~12.4-h cycle in phase with the tidally varying water level. Wave heights rise and fall dramatically around the time of the fetch transition associated with the submergence and emergence of the Hangore Bank. The fetch more than doubles on the rising tide (7→16 km) and halves on the falling tide (16→7 km). Coinciding with fetch transitions is the anticipated change in bottom friction that occurs as relative water depth over sandbanks increases/decreases (e.g., Figure 2 and Black et al., 1999). The reduction in wave height that occurs prior to the emergence of the Hangore Bank (Figure 2), when local h is low, is probably due to energy dissipation on central harbor banks.

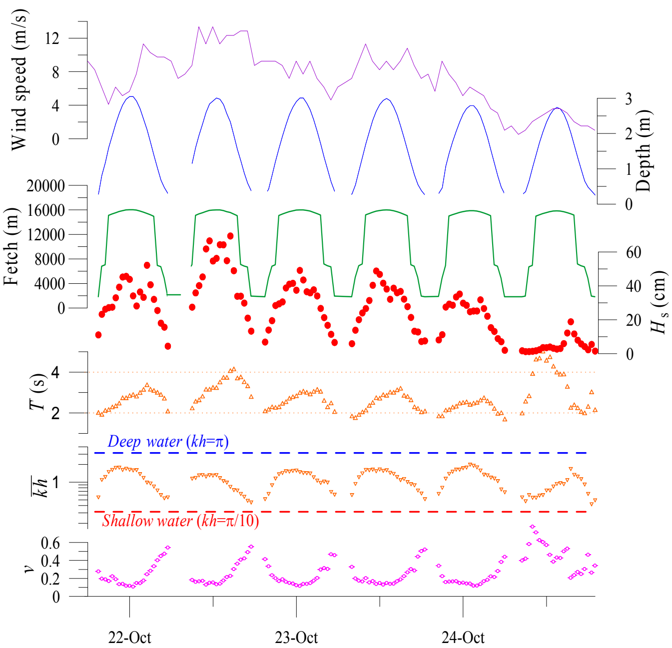

Figure 2. Temporal variation in wave characteristics during a period of strong onshore winds. ν is the spectral width parameter. See text for other symbols.

Wave period (T) also changes with fetch, rising steadily and peaking after high tide. This implies that penetration to the bed of wave orbital motions continues to rise after high tide when depth is falling. Changes in wave period across the range 1–4 s (typical for this site), exerts strong control over penetration [$\chi = 1/\sinh(kh)$] and near-bed wave orbital speed, $U_{\mathrm{w,bed}}$. Over a tidal cycle, temporal patterns in $U_{\mathrm{w,bed}}$ are determined by a subtle balance between $\overline{h}$, H and T, all of which increase and decrease more-or-less simultaneously (Figure 2). On the rising tide, the increasing depth acts to reduce χ, but this is countered by the effect of increasing period on χ, and by increasing H. The result is that $U_{\mathrm{w,bed}}$ can be in-phase with H, peaking at or around high tide (maximum fetch) when waves are largest, or $U_{\mathrm{w,bed}}$ can be 180° out of phase with H because increasing local depth leads to sufficiently small χ such that, despite increasing H, $U_{\mathrm{w,bed}}$ falls as H increases. On the Wiroa flat the latter is most likely to occur on spring tides, due to a greater tidal range and rate of water level rise/fall.

Entrainment

In Figure 3, sand suspension is categorized into 'suspension' and 'no-suspension' bursts and plotted in terms of the Shield's parameters for waves alone θ_w and currents alone θ_c. The predicted sand entrainment threshold of $\theta_{cr,sand} = 0.056$ was determined for local sands using Soulsby and Whitehouse (1997), and is a good predictor of entrainment at Wiroa. The effect of wave-current interaction on entrainment is negligible, as shown by Figure 3 and also by the Larsen et al. (1981) wave-current interaction model, which gave no improvement over treating waves and currents in isolation (Dolphin, 2004).

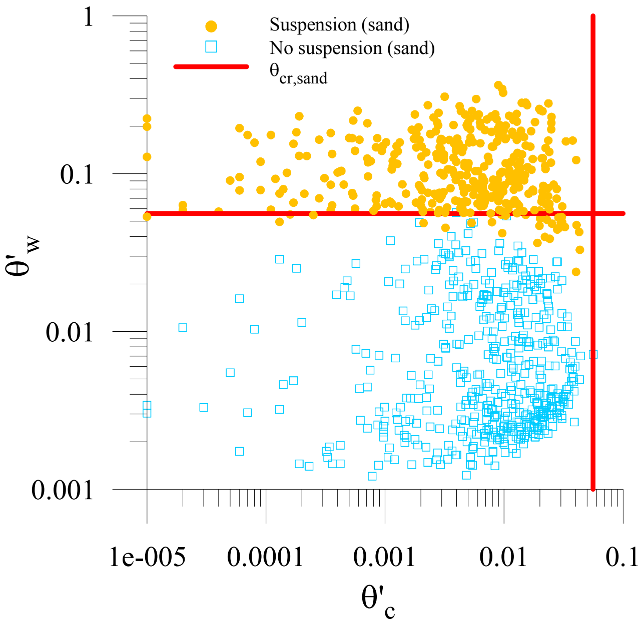

Figure 3. Plot of skin friction due to waves (θ'_w) and currents (θ'_c). Filled symbols indicate 'suspension' and hollow symbols indicate 'no suspension'.

Entrainment on the Wiroa intertidal flat is clearly dominated by waves. As expected, tidal currents are weaker on the intertidal flat compared with channels and channel margins. Tidal currents were never capable of mobilizing bed sands, except on channel margins. However, for similar settings with higher tidal energy, the lower intertidal flat is likely to experience regular tidal reworking. In comparison, reducing tidal currents with increasing elevation and distance across flats leads implies subcritical tidal currents and entrainment by waves alone on upper flats (as is the case here). A wave dominated upper flat (given sufficient fetch) is anticipated, especially for estuaries where fetch is tidally modulated and greatest at high tide. The result is a spatial gradient from tidally dominated skin friction on the lower flats to wave dominated skin friction on the upper flats. Differences in intertidal flat profile, tidal energy, wind speed and fetch length will control the extent of such zones.

Silt entrainment is considered in Figure 4. As the silt suspension signal (OBS) can be related to sediment load in catchment runoff, bursts recorded during rainfall events were distinguished (marked with an X). The remaining data are bursts of bed resuspension (both local and 'far-field', due to slow settling speed for silts). Unlike sands, the entrainment of silt is not related to the predicted Shields threshold. Instead, silt entrainment occurs at more-or-less the predicted value for sands. That is, $\theta_{cr,silt} \approx \theta_{cr,sand}$, implying that silt particles reside within the interstitial spaces between sand grains, are shielded from bed shear stress, and are therefore released into suspension during sand entrainment. The silt suspension bursts with $\theta_w < \theta_{cr}$,sand are likely to be due to long settling times for silts and/or suspension events occurring elsewhere in the estuary that are advected passed the measurement station during subcritical periods (e.g., Green et al., 2000).

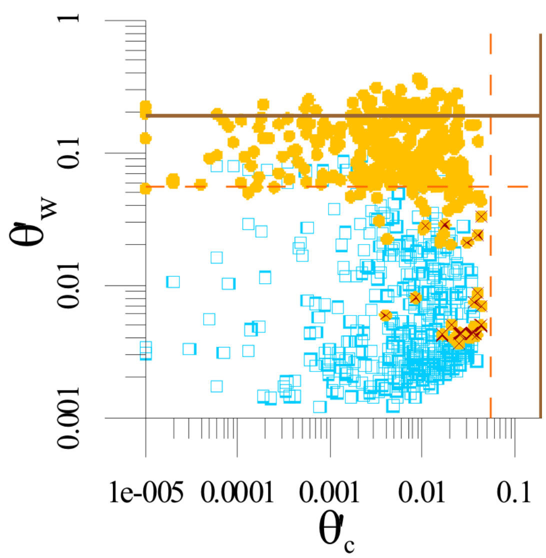

Figure 4. Plot of skin friction due to waves and currents. Filled symbols indicate 'suspension' and hollow symbols indicate 'no suspension'. Dashed red lines = $\theta_{cr,sand}$; solid lines = $\theta_{cr,silt}$.

Conclusions

Tidal flows are typically subcritical on the upper reaches of intertidal flats, if not across the entire flat (as is the case here). In such cases, only waves can mobilize bed sediments (both sands and silts in this case), and thus waves are the primary control on where and when sediment mobilization occurs.

Tidal modulation of fetch leads to H and T evolving in phase with $\overline{h}$. However, conditions near the bed are also controlled by penetration. When the tidal range is larger (i.e., spring tides), increasing depth can dominate over increasing H and T, giving rise to out-of-phase $U_{w,bed} - \overline{h}$ (i.e., $U_{w,bed}$ low at high tide). The opposite (in phase $U_{w,bed} - \overline{h}$) can occur when waves are sufficiently large or for shallower depths (i.e., neap tides). Rather different patterns for estuaries exposed to constant fetch are observed (e.g., Green and MacDonald, 2001).

The critical Shields parameter is a very good predictor of entrainment for sands, but not for silts. Because of shielding, silts are released at the same time as sands. Cohesion does not appear to be significant.

Despite the short wave-periods and intense white-capping associated with the developing sea of a large estuary, the motion under waves at Wiroa is relatively symmetrical (Dolphin, 2004) and relative water depth (*kh*; Figure 2) is almost always intermediate. Under such conditions the component of the burst averaged sediment flux advected by wave motion will be small. Instead the sediment flux at Wiroa is dominated by advection of the wave-induced suspension by tidal currents. So sediment transport on mesotidal flats like Wiroa, and on the upper reaches of macro-tidal flats, is likely to be controlled by local $U_{w,bed}$ (suspended sediment concentration) and tidal speed/direction (transport pathway and excursion).

These results suggest that studies of estuarine intertidal flat sediment transport ought to include waves as, for all or part of the intertidal flat, they are the only entraining mechanism. The sediment transport equation complex and local; entrainment on upper flats is dominated by waves, but tidal currents can become significant on the lower flats; temporal patterns in $U_{w,bed}$ can peak near inundation/exposure or at high water; and spatial variability in $U_{w,bed}$, tidal current, and sediment-size modes make for a complex but fascinating transport regime.

References

Allen, G.P. (1971), Relationship between grain size parameter and currernt patterns in the Gironde estuary, *Journal of Sedimentary Petrology*, 42 (3), 74–88.

Black, K.P., Green, M.O., Healy, T., Bell, R.G., Oldman, J., Hume, T.M. (1999), *Lagrangian modeling techniques simulating wave and sediment dynamics determining sand-body equilibria*, In: J. Harff, W. Lemke, K. Stattegger (Eds), Computerized Modelling of Sedimentary Systems, Springer, Berlin, pp3–21.

Dolphin, T.J., Hume, T.M., Parnell, K.E. (1995), Oceanographic processes and sediment mixing on a sand flat in an enclosed sea, Manukau Harbour, New Zealand, *Marine Geology*, 128, 169–181.

Dolphin, T.J. (2004), *Wave-induced sediment transport on an estuarine intertidal flat*, PhD Thesis, University of Waikato, Hamilton, New Zealand, 154pp.

Dyer, K.R. (1989), Sediment processes in estuaries: Future research requirements, *Journal of Geophysical Research*, 94(C10), 14327–14339.

Green, M.O., Dolphin, T.J., Swales, A., Vincent, C.E. (1999), Transport of mixed-sediments in a tidal channel, *Coastal Sediments '99*, Vol. 1, 644–658.

Green, M.O., Bell, R.G., Dolphin, T.J., Swales, A. (2000), Silt and sand transport in a deep tidal channel of a large estuary (Manukau Harbour, New Zealand), *Marine Geology*, 163, 217–240.

Green, M.O., MacDonald, I.T. (2001), Processes driving estuary infilling by marine sands on an embayed coast, *Marine Geology*, 178, 11–37.

Hicks, D.M., Hume, T.M. (1996), Morphology and size of ebb tidal deltas at natural inlets on open-sea and pocket-bay coasts, North Island, New Zealand, *Journal of Coastal Research*, 12(1), 47–63.

Larsen, L.H., Sternberg, R.W., Shi, N.C., Marsden, M.A.H., Thomas, L. (1981), Field investigations of the threshold of grain motion by ocean waves and currents, *Marine Geology*, 42, 105–132.

Malvarez, G.C., Cooper, J.A.G., Jackson, D.W.T., Navas, F. (2001), The role of wave action on sedimentation of tidal flats: Application of high spatial resolution numerical modelling in Strangford Lough, Northern Ireland, *Journal of Coastal Research*, Special Issue 34, 172–182.

Soulsby, R.L., Whitehouse, R.J.S. (1997), *Threshold of sediment motion in coastal environments*, In: Proceedings of: Pacific Coasts and Ports: The 13th Australasian Coastal and Ocean Engineering Conference, Vol. 1, 149–154, Centre for Advanced Engineering, Christchurch, New Zealand.

Modeling the sand-mud morphodynamics of tidal flats

MAARTEN VAN DER VEGT[1, 2]

1. Department of Physical Geography, University of Utrecht,
   P.O. Box 80115, 3508 TC Utrecht, Netherlands
   email: m.vandervegt@geo.uu.nl

2. Hydraulic and Offshore Engineering Section,
   Faculty of Civil Engineering and Geosciences, Delft University of Technology,
   P.O. Box 5048, 2600 GA Delft, Netherlands

Keywords: sand-mud, tidal flat, morphodynamics, biological activity

ABSTRACT

Tidal flats are found along many sheltered estuaries and tidal inlet systems. They often form the connection between low-lying saltmarshes and the marine waters and are important as both sink and source of sediments in the estuary or tidal basin. Tidal flats are of ecological importance since they serve as feeding grounds for fish, birds and biota. The sediments that are found on tidal flats consist of sand, mud and organic matter or a mixture of these. In general the landward part of the flat is often muddier and the seaward part sandier and strong spatial gradients in sediment composition can be present. Sediment composition is also a function of time caused by sequences of erosion and deposition. Biota are thought to play an important role in this erosion and sedimentation cycle because they strongly alter the critical threshold for erosion and the erosion rate and have a strong seasonal cycle. During winter the biological activity is small and sediment can easily be eroded. In summer sediment is stabilized by for instance the presence of algae mats. In addition, biota living in the upper layer of the bed often mix the sand and mud in the upper layer, and thereby influence the mud content. This layer can extend till a depth of several tens of centimeters.

In general it is believed that the shape of tidal flats depends on the availability of sediment and the strength of the eroding forces. Observations suggest that eroding tidal flats have a concave upward profile and accreting profiles a convex upward profile (Kirby, 2000). Biota can act as ecosystem engineers and are able to locally increase the bed level by adapting their environment such that sediment is deposited and less stresses by the currents and waves are experienced.

Our knowledge of the dynamics of tidal flats is still very limited, and predicting the evolution of tidal flats on longer timescales is almost impossible. Only in recent years models have been developed that can capture the processes that are important for the dynamics of tidal flats. In a study by Roberts et al. (2000) it has been shown that the bed profile of a mud flat can be considered as a morphodynamic equilibrium. However, in most modeling studies it has been assumed that the sediment consists of mud only and the influence of biota on the dynamics of the tidal flat have not been explicitly included. In a study by Paarlberg et al. (2005) an interesting attempt has been made to include as well sediment mixtures as to explicitly account for the effects of biota. They used a numerical model to study the seasonal change of bed level and mud content of a tidal flat in the Western Scheldt estuary. Longer timescales were not considered.

The main aim of this study is to model and understand the sand-mud morphodynamics of tidal flats on the time scale of years. It will be studied whether a morphodynamic equilibrium exists, as is the case for mudflats, and how biological processes influence the evolution of tidal flats. In addition it will be studied how the sand and mud is distributed over the tidal flat. To this end an idealized model is developed and analyzed and the model description and results are presented in this paper.

Model description

The geometry of the idealized model consists of a tidal flat flanked by a channel with x- and y-axis pointing in the cross- and along-channel direction, respectively (Figure 1, left panel). The model is uniform in the along-channel direction and only cross-channel variations are studied. The seaward boundary of the flat is positioned in the channel and only one half of the channel-shoal system is modeled.

Figure 1. Left panel: Geometry of the model. Only cross-shore variations are considered and model is alongshore uniform. Right panel: Sediment in model consists of sand and mud and is transported as suspended load. Conservation of mud in the bed is explicitly modeled.

The hydrodynamics are described by the shallow water equations. The along-channel currents are not considered on first instance because we focus on the shallow parts of the tidal basin. For the momentum equation in the cross-channel direction it is assumed that inertia, friction and advection can be considered small with respect to the pressure gradient. The cross-shore tidal currents are calculated by solving the continuity equation under the assumption that sea surface elevation is spatially uniform. This solution is similar to the pumping mode solution as obtained for tidal basins. Main difference is that the tidal velocity is not zero at the landward boundary but equals the propagation speed of the tidal front.

Sediment is only transported as suspended load. The sediment mass concentrations are calculated by solving the depth-integrated advection-diffusion equation. Both sand and mud are considered (see Figure 1, right panel). The erosion rate of the mud (sand) fraction is a function of the mud (sand) content of the bed and is linear in the bed shear stress. No critical shear stress for erosion or deposition is taken into account. The deposition flux near the bed is the product of the fall velocity times the near bed concentration of the fraction considered. This near bed concentration is calculated by assuming a balance between settling of sediment and vertical diffusion due to turbulent eddies. For simplicity a vertically uniform and time independent vertical eddy coefficient is assumed. The boundary conditions for the mud fraction at the seaward boundary is that during inflow the concentration is prescribed while during the ebb-phase it is assumed that there is no gradient in the mud concentration. At the landward boundary the diffusive flux is zero and sediment can only be transported by the currents. For the sand fraction at the landward boundary it is assumed that the change in sand concentration is balanced by erosion and deposition while at the landward side the diffusive flux is zero.

The bed level can change as a result of net exchange of sediment between the water column and the sediment bed. This net exchange flux of sediment is the sum of erosion of sand and mud minus the deposition of sand and mud.

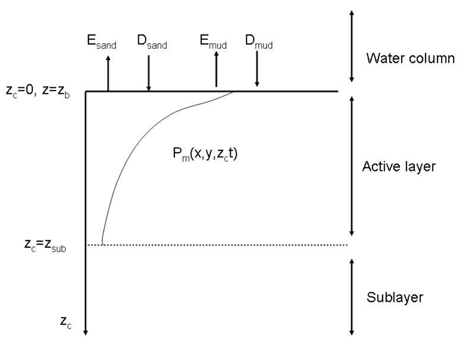

Figure 2. Geometry of the bed module. The Lagrangian coordinate z_c is used. It has its origin at the water-bed interface and is positive downward. In the model the mud content in the bed is calculated. The mud content can change as a result of erosion and deposition of sand and mud and due to mixing by biota in the active layer.

Due to exchange of sand and mud with the water column the mud fraction, $p_m(x, y, z_c, t)$ of the sediment bed can change (Figure 2). The sand and mud fraction can also change due to physical and biological mixing processes. This mixing only occurs in the upper layer, which is called the active layer. In the sublayer no active mixing of sediment takes place. A Lagrangian approach is used to solve the diffusion equation for the mud fraction in the sediment bed. The vertical coordinate z_c is used and it is positive downward. The level $z_c = 0$ always coincides with the actual bed level and thus the origin shifts when bed level changes. The evolution of mud content in the sediment bed is described by:

$$\frac{\partial p_m}{\partial t} + \frac{\partial z_b}{\partial t}\frac{\partial p_m}{\partial z_c} - \frac{\partial}{\partial z_c} D_{mix} \frac{\partial p_m}{\partial z_c} = 0 . \qquad (1)$$

The mixing coefficient is throughout this paper $D_{mix} = 10^{-7} e^{-Z_c/0.2}$ m^2 s^{-1}. Boundary conditions have to be prescribed at $z_c = 0$ and $z_c = z_{sub}$. At the water-sediment bed interface the net flux of sediment is prescribed and equals the deposition flux minus the erosion flux of mud, $E_{\text{mud}} - D_{\text{mud}}$. At $z_c = z_{\text{sub}}$ the mud content equals the mud content of the sublayer in case of erosion while for accretion a weak condition is used and the change with depth of the mud content is zero.

Results

The results of the default experiment are shown in Figure 3. An M_2 tide with amplitude of 2 m has been prescribed at the seaward boundary. The concentration of mud during inflow is 20 mg l^{-1}. The erosion coefficient for sand and mud was linear in the sand and mud fraction of the top layer of the sediment bed: $E_s = E_0(1 - P_m(x, 0, t))$, $E_m = E_0 P_m(x, 0, t)$. A period of 140 years has been simulated starting from an initial linear bed level. The results show that the bed level is gradually decreasing in time. Although the evolution is slowing down no equilibrium is obtained. Also for longer simulation times no equilibrium was obtained. After 140 years the seaward side of the intertidal flat has a linear profile, the middle part is concave while for bed levels larger than 0 the profile is convex. In the right panel of Figure 2 the mud content in the upper layer after 70 and 140 years is shown. Initially there is no mud in the bed. Although there is net erosion of the intertidal flat the upper layer of the bed is becoming muddier, especially at the landward side. There are sharp changes in the mud content in the intertidal part of the flat. Analysis of the results has shown that sand is being exported in the seaward direction while mud is being imported and stored in the sediment bed. Because the export of sand is larger than the import of mud there is overall erosion. However, because mud is imported the upper layer can become muddy even in the case of net erosion.

Sensitivity experiments have been performed to better understand the several factors that influence the evolution of the intertidal flat. In a first experiment the value of E_0 is a factor two smaller and still spatially uniform. This more or less represents the presence of biota that stabilizes the bed. In a second experiment it has been assumed that only in the intertidal area the value of E_0 is a factor two smaller. For depths larger than 2 m it keeps its default value. In a third experiment a spatially uniform E_0 is prescribed that is varying periodically between a value 50% larger during winter and 50% smaller in summer than the default value. This models the change in biological activity during the year. In summer biota stabilize the bed while in winter they destabilize it. In a fourth experiment E_0 is a linear function of the mud content. It is zero when the bed consists of 100% mud and equals the default value when the mud content of the upper layer of sediment is 0%. This represents that cohesive sediment is more difficult to erode than a sediment bed that is formed by sand grains. In a fifth experiment E_0 has its default value but now the prescribed concentration of mud at the seaward boundary is 100 mg l^{-1} instead of 20 mg l^{-1} in the default experiment.

The bed levels after 140 years of simulation for the different experiments are shown in the left panel of Figure 4. In neither of the runs equilibrium was achieved and the profiles were still evolving. The profiles have all in common that at the seaward side the profile is linearly sloping; in the middle the profile is concave while in the upper part of the intertidal part the profile is convex. However there are differences between the several experiments. The convexity of the upper part of the intertidal flat depends on the model setting. When the prescribed mud concentration is large (100 mg l^{-1}) the overall profile has accreted (black dotted line in Figure 4). The deposition of the mud fraction is larger than the erosion of the sand fraction in this case. This is also the case for E_0 that is a factor two smaller than default (blue line). By decreasing the erodibility of the

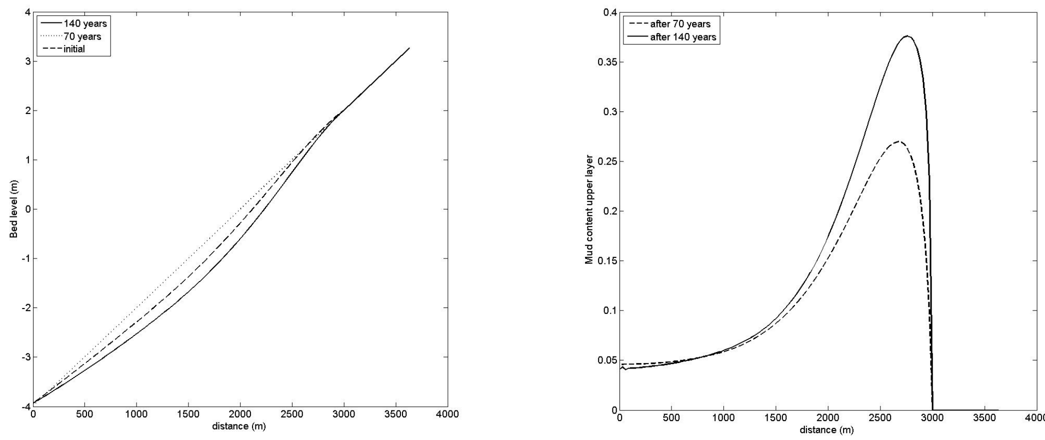

Figure 3. Results of default experiment. Left panel: initial bed profile and bed profile after 70 and 140 years of simulation. Right panel: mud content of upper layer of the bed after 70 and 140 years of simulation. Initially the mud content was zero.

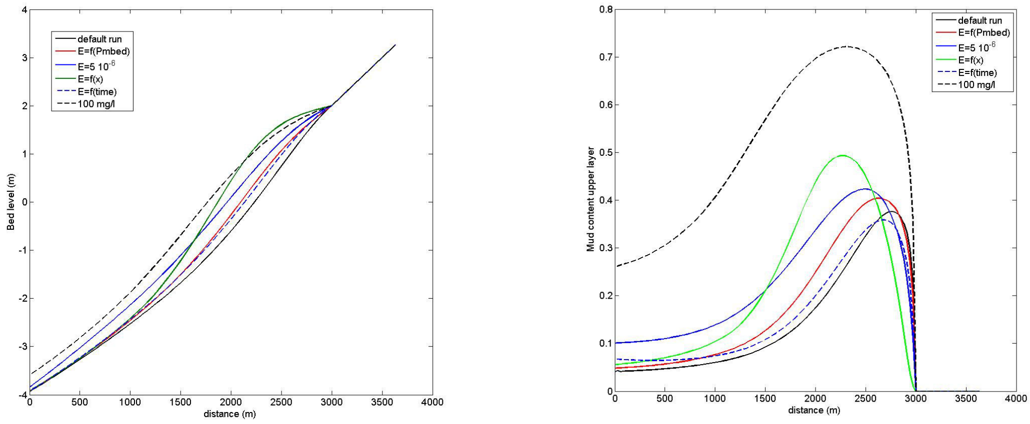

Figure 4. Left panel: Bed level after 140 years for different sensitivity experiments. For more information see text. Right panel: Same as left panel, but now mud content in the upper layer.

sediment less sand is exported from the system. A spatially varying E_0 (green line) results in erosion at the seaward side similar to the default experiment, while there is much larger accretion in the intertidal part. This profile has the most convex shape in the intertidal area. Using a time-dependent erosion coefficient results in less erosion than in the default case and bed levels are therefore higher. Although the yearly averaged value of E_0 is equal to the default case, feedbacks cause a bed profile which is larger. When E_0 is a linearly decreasing function of the mud content a bed profile is obtained which more or less is similar to the case of a time-varying value of E_0.

In the right-hand panel of Figure 4 the mud content of the top layer of the bed is shown for all the sensitivity experiments performed. The results have all in common that the seaward side is sandier while the landward end is muddier. When the prescribed mud concentration at the seaward boundary is larger the top layer is much muddier after 140 years. This is mainly caused by the large influx of mud in the system. In all the other runs the influx of mud is much smaller and differences between the results are mainly caused by differences in the amount of eroded sand. This difference in eroded sand mainly influences the modeled bathymetry but not the modeled mud content of the upper layer.

Conclusions

From the model several conclusions can be drawn. First, no morphodynamic equilibria could be obtained when sand, mud and the presence of biota in the bed are included in the model. It will be further studied whether this can also proofed from a theoretical framework. Second, all modeled flats have in common that they develop towards a profile which is linearly sloping at the seaward side; in the middle of the flat there is a part which has a concave shape and at the seaward end the profile is convex. The amount of concavity in the middle part and convexity at the landward end of the profile depend on model parameters. A profile which is accreting has much more pronounced convex shape than a profile that is accreting. This is in agreement with observations by Kirby et al (2000).

The model results show that there are strong gradients in the mud content of the upper layer. The landward part is in all cases much muddier than the seaward part of the tidal flat. There are many processes that have been neglected. The most important ones are the effects of the alongshore tidal currents and the effects of waves. These will be included in a further study.

References

Kirby, R. (2000), Practical implications of tidal flat shape, *Continental Shelf Research*, 20, 1061–1077.

Paarlberg, A.J., Knaapen, M.A.F., de Vries, M.B., Hulscher, S.J.M.H., Wang, Z.B. (2005), Biological influences on morphology and bed composition of an intertidal flat, *Estuarine, Coastal and Shelf Science*, 64, 577–590.

Roberts, W., le Hir, P., Whitehouse, R.J.S. (2000), Investigation using simple mathematical models of the effect of tidal currents and waves on the profile shape of intertidal mudflats, *Continental Shelf Research*, 20, 1079–1097.

On the equilibrium bed profiles of tidal embayments and their linear stability

MIRIAM C. TER BRAKE, HENK M. SCHUTTELAARS

Delft Institute of Applied Mathematics, Delft University of Technology, Mekelweg 4, 2624 CD Delft, Netherlands
email: m.c.terbrake@tudelft.nl, h.m.schuttelaars@tudelft.nl

Keywords: tidal embayments, equilibrium bed profiles, linear stability

ABSTRACT

To gain understanding of the mechanisms resulting in bottom patterns as observed in many tidal embayments, an idealized model is developed and analyzed. Contrary to many other models, the suspended sediment fluxes induced by topographic variations are included. Unlike the model results without this flux, the profiles obtained with this sediment flux included show good agreement with the width-averaged observed bottom profiles. Due to this additional flux, the growth rates of the two-dimensional perturbations on the equilibrium profiles are reduced, and the resulting channel and shoal patterns can change completely.

Introduction

Chains of barrier islands are found in many coastal areas all over the world, for example along the Dutch, German and Danish Wadden coast. Tidal embayments, that are a dynamic part of these barrier systems, are important for economic and ecological activities. When the sea bed of tidal embayments consists of sand and/or mud, channels and shoals develop due to the interaction of the prevailing currents generated by tides, wind and density differences with the erodible bed. Morphological changes have a significant effect on the flow dynamics and hence on the general tendency of the tidal embayment to import or export sediment. External conditions, such as mean sea level rise and human interferences can also strongly influence the morphologic behavior. Taking into account these complex morphodynamic interactions and the importance of these areas, it is crucial to accurately model, simulate and predict the morphodynamic development.

Several researchers developed width-averaged idealized models to study the water motion in tidal embayments. These one-dimensional models have been extended to include the feedback between water motion, sediment transport and bed evolution (see Schuttelaars and de Swart, 1996; van Leeuwen et al., 2000). To compare the model results with observations, the external tidal forcing has to include both the M_2 and the M_4 tidal constituents. However, when using realistic parameter values in the above-mentioned models, the obtained equilibrium profiles are strongly convex and the maximum length is only about 25% of the observed length. In these models, the sediment transport was described by an advection-diffusion equation, where sediment fluxes induced by spatial variations in the water depth – and directed towards deeper water – were assumed to be compensated by fluxes induced by waves and secondary circulations in the vertical plane. In this paper we demonstrate that inclusion of these spatial fluxes is necessary to obtain realistic embayment lengths for realistic parameter values and external forcing of the water motion by the M2 and M_4 tidal constituents. Results obtained with inclusion of these fluxes are compared with observations. Furthermore, we investigate the stability of the two-dimensional bed perturbations on these one-dimensional equilibrium profiles and compare these results with those of Schuttelaars and de Swart (2000) and van Leeuwen et al. (2004).

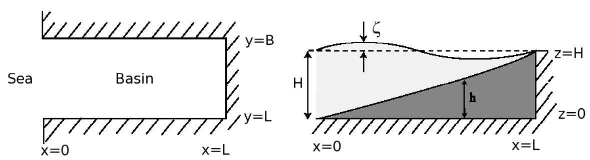

Figure 1. Left: top view, right: cross-sectional view of the embayment.

Model description

The embayment considered is of rectangular shape with width B and length L. The basin is bounded at the landward side and its prescribed length L is assumed to be small compared to the frictionless tidal wavelength $L_g = T\sqrt{gH}$ with T the tidal period of the M_2-tidal constituent, the gravitational constant g and H the undisturbed water depth. Tidal resonance is not considered. The coastlines of the embayment are fixed and the bed (described by $z = h$) is erodible. The sediment of the bed consists of fine grain particles (d ~120 μm), hence bedload transport is negligible compared to suspended load transport. The basin has an open connection to the adjacent sea. The water depth H at the entrance of the embayment is prescribed and the local water depth is given by $H - h + \zeta$, with ζ the sea surface elevation.

The water motion is described by the cross-sectionally averaged shallow water equations for a homogeneous fluid. The continuity equation reads

$$\zeta_t + [(\zeta + H - h)\, u]_x = 0, \tag{1}$$

where u is the depth-averaged velocity. Using that $L \ll L_g$ and assuming that the frictional time-scale is at least of the same order as the tidal period T, the momentum equation reduces to

$$\zeta_x = 0. \tag{2}$$

with boundary conditions

$$\zeta = \mathrm{A}_{\mathrm{M}_2} \cos(\sigma t - \phi_{\mathrm{A}_{\mathrm{M}_2}}) + \mathrm{A}_{\mathrm{M}_4} \cos(2\sigma t - \phi_{\mathrm{A}_{\mathrm{M}_4}}) \quad \text{at } x = 0, \tag{3}$$

$$(H - h + \zeta)\, u = 0 \quad \text{at } x = L, \tag{4}$$

where $\mathrm{A}_{\mathrm{M}_2}$ ($\phi_{\mathrm{A}_{\mathrm{M}_2}}$) and $\mathrm{A}_{\mathrm{M}_4}$($\phi_{\mathrm{A}_{\mathrm{M}_4}}$) are the tidal amplitudes (phases) of respectively the M_2 and M_4 tidal constituents. The frequency of the first harmonic (M_2) is denoted by σ. Hence, at the open boundary the system is forced with a basic tide and its first overtide. At the landward boundary, no net water flux is allowed.

The sediment transport is described by the cross-sectionally averaged concentration equation. Using that $\zeta_x = 0$, the resulting depth-integrated concentration equation reads

$$\frac{\partial}{\partial t}C + (uC)_x - \tilde{\kappa} C_{xx} - \tilde{\kappa}\frac{w_\mathrm{s}}{\kappa_\mathrm{v}}[\beta_\mathrm{b} h_x C]_x = \alpha u^2 - \frac{w_\mathrm{s}^2}{\kappa_\mathrm{v}}\beta_\mathrm{b} C, \tag{5}$$

where the parameter β_b is defined by $\left(1 - e^{-\frac{w_\mathrm{s}}{\kappa_\mathrm{v}}(\zeta + H - h)}\right)^{-1}$. Here C is the depth integrated concentration, $\tilde{\kappa}$ is a constant diffusion coefficient and α is a coefficient related to sediment properties. Equation (5) is derived by integrating the width-averaged 3D concentration equation over the depth. In this derivation it is assumed that the downward settling flux of particles is balanced by the upward diffusive flux of sediments. This yields $C_{3\mathrm{D}} = c_\mathrm{b} e^{-w_\mathrm{s}(z-h)/\kappa_\mathrm{v}}$, where c_b is the suspended sediment concentration at the bed, w_s the settling velocity and κ_v the vertical diffusion parameter. This expression is used to relate the concentration at the free surface and the bed to the depth-integrated concentration C.

The bed evolution equation is derived from continuity of mass in the sediment layer. Assuming suspended load transport to be dominant (neglecting the bedload transport mechanism), the bed evolution equation reads

$$\rho_\mathrm{s}(1 - p)\, h_t = -\left\langle \alpha u^2 - \frac{w_\mathrm{s}^2}{\kappa_\mathrm{v}}\beta_\mathrm{b} C \right\rangle, \tag{6}$$

where $\langle\cdot\rangle$ stands for the averaging over the tidal period, p the bed porosity and ρ_s denotes the density of the sand. The corresponding boundary conditions are

$$\left\langle \alpha u^2 - \frac{w_\mathrm{s}^2}{\kappa_\mathrm{v}}\beta C \right\rangle = 0 \quad \text{at } x = 0 \tag{7}$$

$$\left\langle uC - \tilde{\kappa} C_x - \left[\tilde{\kappa}\frac{w_\mathrm{s}}{\kappa_\mathrm{v}}\beta h_x C\right] \right\rangle = 0 \quad \text{at } x = L. \tag{8}$$

The first condition assumes that the bed level stays constant at the entrance ($h = 0$), the second states that no net sediment flux is allowed through this boundary. The time dependent boundary condition for the concentration at the entrance and the coast are $C'(x, t, \kappa) = C'(x, t, \kappa = 0)$, with $C' = C - \langle C\rangle$ the time fluctuating part of the concentration. This condition implies that no diffusive boundary layer develops in the fluctuating part of the concentration (C') at these boundaries.

Equation (6) indicates that tidal averaging is allowed, the bottom evolves on a much longer timescale (τ) than the tidal period. Hence the bed evolution equation can be written as

$$h_\tau = -\langle F \rangle_x \tag{9}$$

where the sediment flux F is given by $F = uC - \tilde{\kappa} C_x - \tilde{\kappa} \frac{w_s}{\kappa_v} \beta_b h_x C$. Hence bed changes are determined by the convergence and divergence of the tidally averaged sediment flux consisting of an advective contribution $F_{adv} = uC$, a diffusive contribution $F_{diff} = -\tilde{\kappa} C_x$ resulting from suspended load processes *and* a diffusive flux induced by the spatial variations in the water depth $F_{vd} = -\tilde{\kappa} \frac{w_s}{\kappa_v} \beta_b h_x C$. The occurrence of the extra sediment transport term (which was neglected in previous studies) can be easily understood if one considers the vertical distribution of sediment in the water column. The concentration is highest near the bed and reduces with decreasing depth. Hence, there is a horizontal concentration gradient between the water columns, resulting in a diffusive sediment flux directed towards deeper water.

Solution method

It is known (see, e.g., Schuttelaars and de Swart, 1996) that the equilibrium solution for a short embayment without $\langle F_{vd} \rangle$ and constant deposition is unique and is characterized by a constant sloping bed, getting shallower towards the end of the embayment. By slowly changing the model formulation (either by introducing additional physical processes or by changing parameter values) and using a previously obtained numerical or analytical solution as an initial guess, equilibrium bed profiles can be calculated using standard continuation techniques. The Newton–Raphson method was used to numerically solve the resulting system of nonlinear equations.

Results

The first important result is that the maximum length of the embayment, obtained when the topographically induced sediment flux is taken into account, can be much bigger than the maximum length obtained without this flux. These differences in length are shown in the sensitivity plot Figure 2(a), where the maximum length of the embayments is plotted as a function of the settling velocity. The other parameters are taken as observed in the Frisian Inlet System.

The sensitivity of the equilibrium bed profile to the grain size is investigated by varying w_s. Finer sediment results in more convex bed profiles. When the grain size is coarser ($d \sim 200$ µm) the profile becomes concave. In Figure 2(b) the sensitivity of the model to the phase difference ϕ is shown. For a tidal asymmetry smaller than default, the bed profile becomes more concave. When the tidal asymmetry is decreased, the bed profile becomes more convex.

First the Frisian Inlet System is considered. Next the model results are compared with the observations in the Dutch Wadden Sea. In Figure 3(a) the dotted (blue) line indicates the depth profile obtained from the observation of the depth in the Frisian Inlet system that is averaged over the width of the basin. When the topographically induced sediment flux is neglected, no equilibrium bed profiles can be found for the observed embayment length of 15 km (a maximum length of 5 km is found, see orange profile). Including the topographically induced sediment flux results in a good comparison with the data. We also compared our model results for parameter values of the Ameland Inlet, resulting in the same observations, see Figure 3(b).

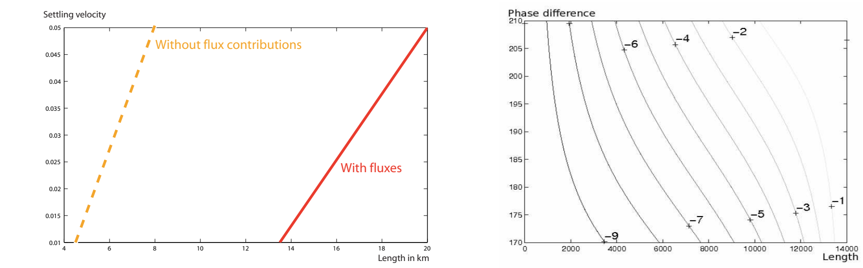

(a) Comparison of the maximum length of the embayment as function of the settling velocity.

(b) Depth contours of the equilibrium bed profile for a varying phase difference.

Figure 2. Sensitivity analyses.

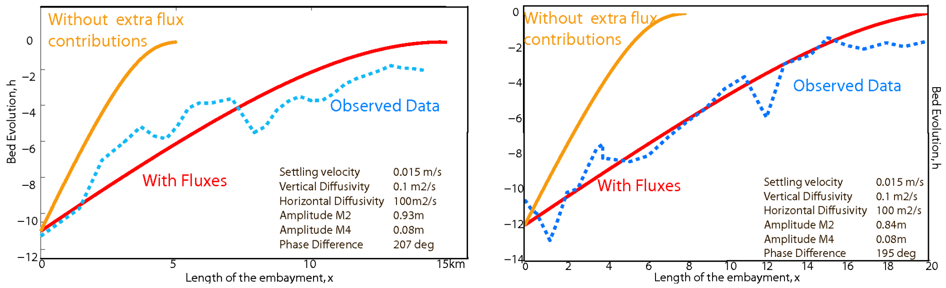

(a) Frisian Inlet. (b) Ameland Inlet.

Figure 3. Compare model results with data observations.

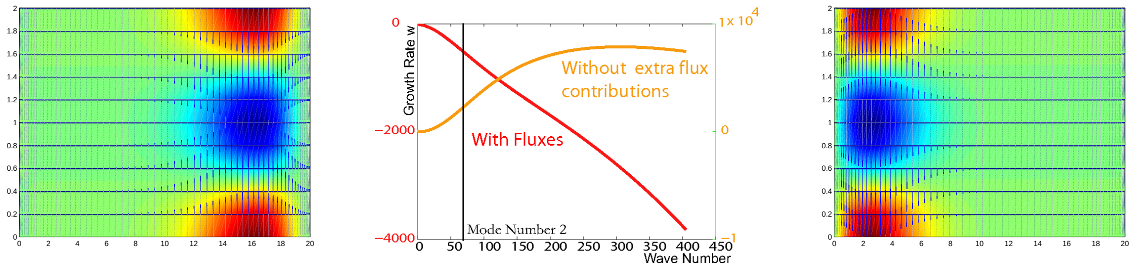

(a) Perturbations: With Fluxes. (b) Growth Rate of perturbations.

Figure 4. Comparison of bed perturbations and their stability of the case with or without fluxes.

Outlook

To study the linear stability of the obtained equilibrium profiles, the temporal evolution of small two-dimensional bottom perturbations is investigated. First results indicate that the channel and shoal patterns can be quite different when comparing results with and without the additional flux. For example the position of the bottom perturbations depends strongly on the grain size: compare Figures 4a and 4c. Furthermore the growth rate of these perturbations is much smaller when the extra flux is taken into account (the red line represents the growth rates from the perturbations obtained with extra flux, and the orange line without).

Conclusions

The contribution of the topographically induced suspended sediment flux is essential for obtaining realistic embayment lengths. When this flux is not included the maximum length of the embayment is 9 to 12 km shorter, for fine sand. When this flux contributes to the sediment transport, the equilibrium bed profile, its stability and the location of the bed perturbations strongly depend on the grain size. Furthermore, due to this flux the growth rates are much smaller than when this flux is neglected.

References

van Leeuwen, S.M., Schuttelaars, H.M., de Swart, H.E. (2000), Tidal and morphologic properties of embayments: effect of sediment deposition processes and length variation, *Physics and Chemistry of the Earth*, *B*, 25(4), 365–368.

van Leeuwen, S.M., de Swart, H.E. (2004), Effect of advective and diffusive sediment transport on the formation of local and global bottom patterns in tidal embayments, *Ocean Dynamics*, 54, 441–451.

Schuttelaars H.M., de Swart, H.E. (1996), An idealized long-term morphodynamic model of tidal embayment, *European Journal of Mechanics – B: Fluids*, 15, 55–80.

Schuttelaars, H.M., de Swart, H.E. (2000), Multiple morphodynamic equilibria in tidal embayments, *Journal of Geophysical Research*, 105(C10), 24105–24118.

Numerical modeling of the formation of tidal channels in Hangzhou Bay, China

DONG-FENG XIE[1], ZHENG-BING WANG[2, 3], SHU GAO[1], HUIB DE VRIEND[2, 3]

1. Ministry of Education Key Laboratory for Coast and Island Development, Nanjing University, Nanjing, China
   email: eastwind111@hotmail.com, shugao@nju.edu.cn

2. Deltares, Rotterdamseweg 185, P.O. Box 177, 2600 MH Delft, Netherlands
   email: zheng.wang@deltares.nl, huib.devriend@deltares.nl

3. Hydraulic and Offshore Engineering Section,
   Faculty of Civil Engineering and Geosciences, Delft University of Technology,
   P.O. Box 5048, 2600 GA Delft, Netherlands

Keywords: tidal channel, cohesive sediment transport, morphology, Delft3D; Hangzhou Bay, China

ABSTRACT

Hangzhou Bay is a macro-tidal bay located south of the Yangtze Estuary in China. Along the northern shore of this bay a large-scale tidal channel system has developed, with a length of more than 50 km and a width of 10 km, and a secondary southern tidal channel. A process-based morphodynamic model based on Delft3D, is used to analyze the physical mechanisms and processes underlying the formation and evolution of this tidal channel system, employing the cohesive sediment transport module. The long-term model results agree with patterns from nature at least qualitatively. The results show that tidal asymmetry, enhanced by the shape of the coastline, is responsible for the formation of the main tidal channel in this system, due to a combination of various factors such as restriction by funnel-shaped geometry, hindering of flood currents by nearby islands and the effects of the southern tidal flat etc. It is proved that long-term modeling of cohesive-floored coastal environments is feasible through suitable parameter settings.

Introduction

Hangzhou Bay, located in East China Sea, is one of the largest strong tidal estuaries in the world. It is a funnel-shaped estuary with a width of 98.5 km at the mouth and 19.4 km at Ganpu of upstream and a length of 85 km, with an average tidal range of 3–5 m, and an average depth of 10 m. A large-scale tidal channel with length of 50 km and width of 10 km developed in the northern Hangzhou Bay, with average water depth larger than 12 m, and a maximum of 50 m. Sediments in Hangzhou Bay are mostly clay or silt and transported as suspension. Several numerical models (Li, 1993; Wang, 1994; Ni, 2003) were set up to simulate hydrodynamics and salinity transport of Hangzhou Bay. However, few of the models simulated sediment transport and morphological evolution of Hangzhou Bay. There is a large gap between the understanding of the morphologic development and hydrodynamic of the tidal channels.

In recent years, morphologic evolution of tidal channels has received the attention of morphologists, coastal engineers, and coastal managers. Wang (2007) reported morphologic evolution processes of the Xinqiao Channel in the Yangtze estuary, based on analyses of historic maps. On the other side, with the development of computer capacity, estuarine morphological models have been increasingly used. Most research has focused on estuaries floored by non-cohesive sediments and are based on conceptual or highly idealized 1-D or 2-D models (Schuttelaars and de Swart, 1999; Hibma et al., 2003, 2004; Lanzoni, 2001; van der Wegen, 2007). Although they give good insight into the mechanism under these morphological processes, it is widely recognized that currently available models have limited capabilities for simulating long-term (decadal or longer) geomorphologic evolution within estuarine regimes (Prandle, 2004).

This present paper aims to provide more insight into the physical processes that determine the formation of the tidal channel system of Hangzhou Bay. A process-based morphodynamic model based on Delft3D is used

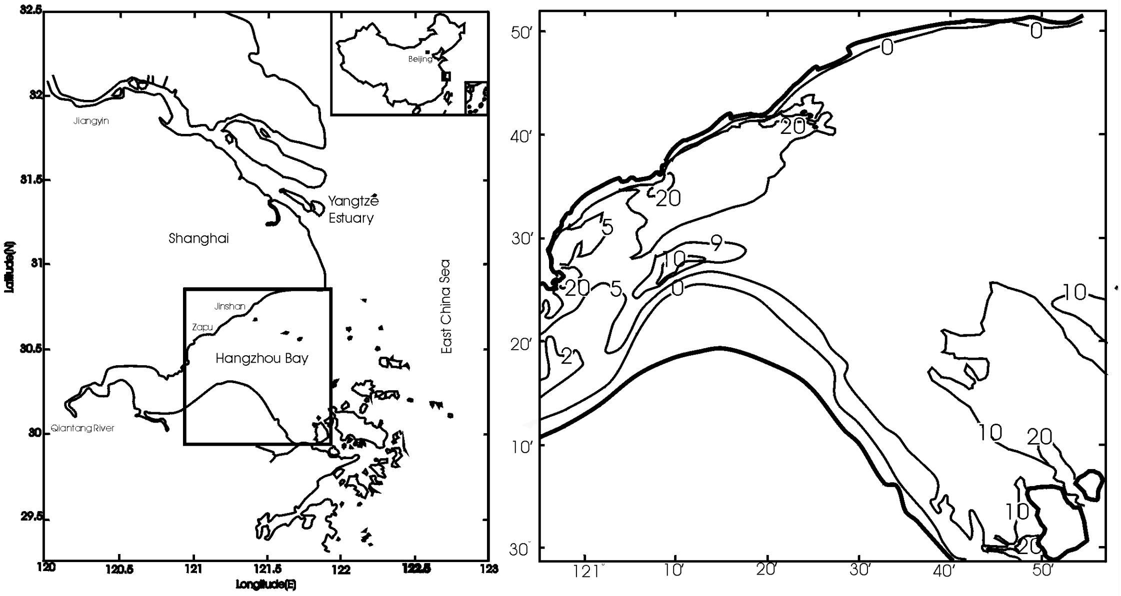

Figure 1. Location of Hangzhou Bay and Yangtze Estuary (left) and Bathymetry of Hangzhou Bay (right).

to analyze the physical mechanisms and processes underlying the formation and evolution of this tidal channel system. Since sediments in Hangzhou Bay are mainly composed of mud or silt, the cohesive sediment transport module is used, instead of the non-cohesive module which was used by the above-mentioned research.

Model description

The depth-averaged two-dimensional numerical model from Wang (1994) is used for the flow modeling of Hangzhou Bay. It includes both Hangzhou Bay and the Yangtze estuary, since the Yangtze estuary has important influences on the hydrodynamics and the sedimentation in Hangzhou Bay. The M_2 constituent is the dominant tidal component in Hangzhou Bay (ECCHE, 1992), for long-term morphodynamic modeling, and hence for simplification only M_2 is taken into account. Waves in Hangzhou Bay are weak and hence ignored. Two major rivers flowing into the model area, i.e., the Yangtze River and Qiantang river, are considered. The flow module has already been well validated (Wang, 1994). Suspended sediment concentrations at seaward boundaries are set to be zero. Since our aim is to understand the formation of the tidal channel system in Hangzhou Bay, a flat initial bathymetry of 11 m was used in the tidal channel system in the model. The model was then run to try to reproduce the observed tidal channel patterns.

Transport of the suspended sediment in the model is based on the advection-diffusion equation, in which the erosion and the deposition terms are calculated with the well-known Partheniades-Krone formulations. In Hangzhou Bay, no field or laboratory data were present for setting model parameters, such as settling velocity, erosion parameter and shear stresses. Sediment parameters are set empirically, consistent with what are generally used in modeling (Whitehouse et al., 2000; Van der Ham and Winterwerp, 2001; Lumborg, 2005). The elevation of the bed is dynamically updated based on the conservation of sediment mass. Morphological updating is initiated after ten tidal cycles when the distribution of suspended sediment concentrations becomes stable. A morphological scale factor of 30 is applied. We carried out a simulation over 11 months, resulting in 25 years of morphological change, until an equilibrium tidal channel system is formed.

Results

Analysis of the initial state

Understanding the hydrodynamic processes is an essential precondition for an evaluation of the sediment transport problem. To analyze the main contributions of these processes, the hydrodynamics generated by the models at the initial stage of the morphodynamical evolution was post-processed.

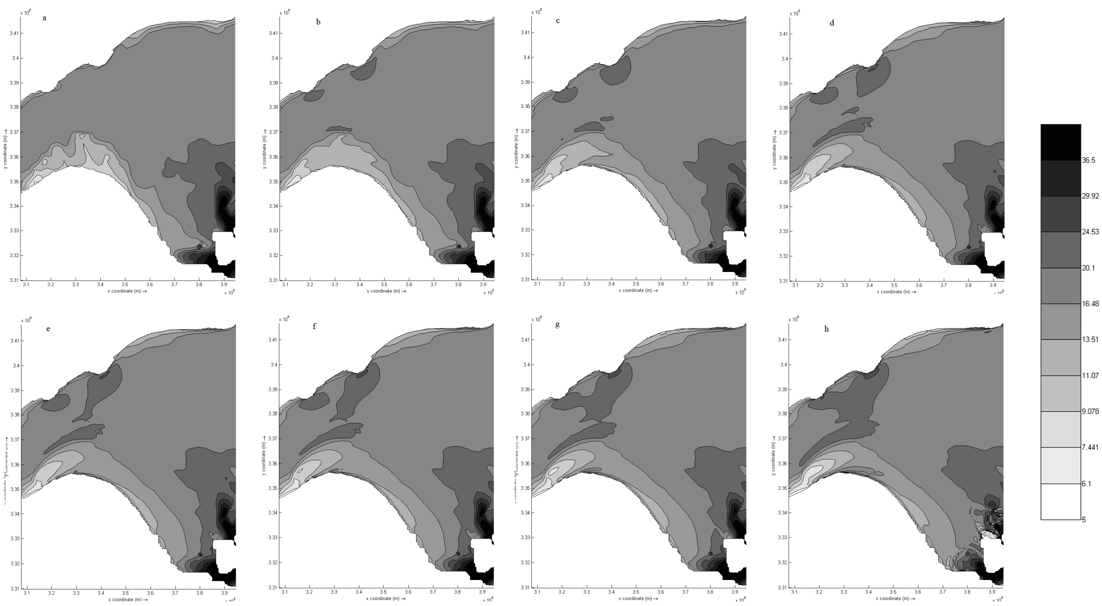

Figure 2. Initial bathymetry and formation of tidal channel system in Hangzhou Bay (three years time span).

Tidal waves propagate in a north-west direction into Hangzhou Bay and the Yangtze estuary. At the mouth of Hangzhou Bay, flood currents mainly enter from the north and much less from the south because the islands hinder the tidal currents and the channels between islands are small. Tidal amplitudes of in the south of the mouth of the bay are smaller than those in the north, 0.7–0.8 m compared to around 1.0 m. When tidal waves propagate northwestwards, they are restricted by the funnel-shaped geometry of Hangzhou Bay so that flood currents from the north and the south converge near Jinshan, where the flood currents are enhanced strongly. Tidal amplitudes increase westwards, from less than 1.0 m at mouth to about 2.0 m at Ganpu. At the same time, amplitude difference between the south and the north decrease gradually. Flood velocities increase westwards from 0.7 m s^{-1} at the mouth to 1.6 m s^{-1} off the coast of Jinshan. In the west of Jinshan, flood velocities are larger than ebb velocities while flood durations are smaller than the ebb durations, revealing that the tidal channel areas are dominated by flood currents. In the east of Jinshan, flood velocities are smaller than those of the ebb, and flood durations are larger in the northeast but smaller in the southeast, revealing that the ebb dominates in the southeast. In the northern tidal channel area, the maximum current velocities (2 m s^{-1} for flood and 1.5 m s^{-1} for ebb) appear off the coast of Jinshan and Zapu.

Modeled suspended sediment concentration of Hangzhou Bay range between 0-0.4 m3/m3, with a large area of high concentration in the middle of Hangzhou Bay. Initial residual sediment transport analysis shows that in the north sediments are transported landward while in the southern part, sediments are transported seaward. This is consistent with the measurements that showed sediments in Hangzhou Bay ‘entering in the northern part while leaving in southern part’ in one tidal cycle (ECCHE, 1992).

Long-term model results

Figure 2 illustrates the morphological development of the tidal channels system of Hangzhou Bay. In the first 15 years, two secondary tidal channels were gradually formed off the coast of Jinshan and Zapu. At the same time, a southern tidal channel started to develop in the northwest of the southern tidal flat. Then the channel off the coast of Jinshan began to extend southwestwards. After 25 years, the northern tidal channel formed with a depth of about 12 m and a width of about 15 km. The results also show a high depositional rate in the inner reach of Hangzhou Bay and a shoal formed to the west of Zapu, revealing that the eroded sediment from the tidal channels deposited to the west of the Zapu. The comparison of model results of the tidal channel system with the real situation (shown in Figure 1) is satisfactory, showing that the model could reproduce the formation of the tidal channel system in Hangzhou Bay qualitatively. Time scale for the formation of the tidal channel system is 25 years, much shorter than that of non-cohesive sediment, which is of the order of 102 years (e.g. Lanzoni, 2001; Hibma, 2003; van der Wegen, 2007).

Conclusions

The tidal channel system in Hangzhou Bay was reproduced by a process-based morpholodynamic model Figure 2 Initial bathymetry and formation of tidal channel system in Hangzhou Bay (time space of three years) based on the cohesive sediment transport module of Delft3D. The results agree with patterns from nature at least qualitatively. The tidal asymmetry, which is caused by the funnel-shaped geometry of Hangzhou Bay, the hindering of tidal currents by the islands and the convex southern tidal flat, is the controlling factor for the formation of the tidal channel system. Both the northern and the southern tidal channels in Hangzhou Bay are flood-dominated.

References

ECCHE (Editorial Committee for Chinese Harbors and Embayments) (1992), *Chinese Harbours and Embayments (Part V)*. China Ocean Press, Beijing (in Chinese).

Hibma, A., de Vriend, H.J., Stive, M.J.F. (2003), Numerical modelling of shoal pattern formation in well-mixed elongated estuaries, Estuarine, *Coastal and Shelf Science*, 57, 981–991.

Lanzoni, S., Seminara, G. (2001), Long-term evolution and morphodynamic equilibrium of tidal channels: 1, *Journal of Geophysical Research*, 107(C1), 3001, doi:10.1029/2000JC000468.

Li, S.D., Gu, S.M. (1993), 3D numerical simulation of tidal waves in Hangzhou Bay, *Oceanologia et Limonologia Sinica*, 24 (1), 7–15 (in Chinese with English Abstract).

Lumborg, U., Pejrup, M. (2005), Modelling of cohesive sediment transport in a tidal lagoon-an annual budget, *Marine Geology*, 218, 1–16.

Ni, Y.Q., Geng, Z.Q., Zhu, J.Z. (2003), Study on characteristic of hydrodynamics in Hangzhou Bay, *Journal of hydrodynamics*, 18(4), 439–445 (in Chinese with English Abstract).

Prandle, D. (2004), How tides and river flows determine estuarine bathymetries, *Progress in Oceanography*, 61, 1–26.

Schuttelaars, H.M., de Swart, H.E. (1999), Initial formation of channels and shoals in a short tidal embayment, *Journal of Fluid Mechanics*, 386, 15–42.

Wang, Y.H., Ridd, P.V., Wu, H.L., Wu, J.X., Shen, H.T. (2007), Long-term morphodynamic evolution and the equilibrium mechanism of a flood channel in the Yangtze Estuary, *Geomorphology*, 91(1–2), 65–79.

Wang, Z.B. (1994), *Hangzhou Bay environmental study: Hydrodynamic modelling*. Rep. Z588, WL|Delft Hydraulics, Delft, Netherlands.

van der Wegen, M., Roelvink, J.A. (2008), Long-term morphodynamic evolution of a tidal embayment using a two-dimensional, process-based mode, *Journal of Geophysical Research*, 113, C03016, doi:10.1029/2006JC003983.

Tidal inlet evolution along the Escoffier curve and empirical prism-cross section relationship using a 2-D process-based approach

MICK VAN DER WEGEN[1], ALI DASTGHEIB[1], DANO ROELVINK[1, 2]

1. UNESCO-IHE, P.O. Box 3015, 2601 DA Delft, Netherlands
   email: m.vanderwegen@unesco-ihe.org, a.dastgheib@unesco-ihe.org, d.roelvink@unesco-ihe.org

2. Deltares, Rotterdamseweg 185, P.O. Box 177, 2600 MH Delft, Netherlands

Keywords: tidal inlet, morphodynamic modeling, Escoffier curve

ABSTRACT

Tidal inlets and embayments in alluvial environments are dynamic systems that react to changing physical conditions (such as sea level rise) as well as to anthropogenic impact (such as dredging and bank protection works). They have been studied extensively in the past. This resulted in various empirical relationships that are available and which assume a certain type of (dynamic) equilibrium. The focus of the current research is on (long-term) modelling of the morphodynamic evolution of a tidal inlet and its basin morphology. Use is made of a 2-D process based, numerical model.

Results are evaluated against well known concepts in inlet stability research, such as the empirical 'PA' relationship between tidal prism (P) and cross sectional area (A) and the Escoffier curve, describing the relationship between cross-sectional area and maximum tidal velocities in the inlet.

Firstly, a simplified configuration is studied that describes the morphodynamics of an isolated tidal inlet that is subject to relatively constant hydrodynamic forcing. A straightforward comparison with the Escoffier curve is made. The second step focuses on a more complex configuration, i.e., a long and shallow tidal embayment, so that a closer analysis is made on the impact of changing conditions like basin geometry and tidal wave characteristics. Model results are evaluated against the empirical PA relationship.

The model results show two-time scales in inlet evolution. One timescale is related to the adjustment of the cross-sectional profile to governing hydrodynamic conditions (made explicit in the Escoffier curve). The second timescale is related to basin evolution and the prevalent tidal wave characteristics in the basin developing over time. It has a timescale depending on the basin geometry and may extend to thousands of years.

Introduction

Understanding of tidal inlet stability and predicting the adjustment of the basin morphology due to fluctuation in the hydrodynamic environment require detail knowledge of the hydrodynamic and sedimentary processes in the vicinity of the tidal inlet. Thus far research focused on empirical relationships of assumed equilibrium conditions [e.g., O'Brien (1931), Jarret (1976), Bruun (1978), Hume and Herdendorf (1992)] and characterization of dominant hydrodynamic processes in fixed tidal inlet/basin configurations [e.g., by Brown (1928), Keulegan (1951) or Dilorenzo (1988), summarized by Walton (2004)]. Semi-empirical and highly parameterized models were developed to study adaptation timescales of the inlet in case of changing forcing conditions like land reclamation and sea level rise (for example, van de Kreeke, 2004).

The aim of the current research is to investigate morphodynamic evolution of a tidal inlet and its embayment. Use is made of a 2-D process based, numerical model that is capable of describing long-term morphodynamic basin evolution and pattern development.

To validate the results comparison is made with well known concepts in inlet stability research, such as the Escoffier curve and the empirical PA relationship between tidal prism and cross sectional area.

Firstly, a simplified configuration (inlet model) is studied that describes the morphodynamics of an isolated tidal inlet that is subject to relatively constant hydrodynamic forcing. The second step focuses on a more complex configuration (basin model), which includes the basin morphodynamics.

Inlet model

In this model, a tidal basin of about 6 × 10 km^2 is connected to the ocean by a 1 km long and 1 km wide inlet. The basin and ocean are 40 m deep and have a fixed bed. The inlet has an initial depth of about 2.5 m and is erodible. The model is forced at the seaward boundary by a sine wave with amplitude 1 m. Sediment transport is predicted by the Engelund Hansen transport formulation. Figure 1 (to the right) shows the computational grid.

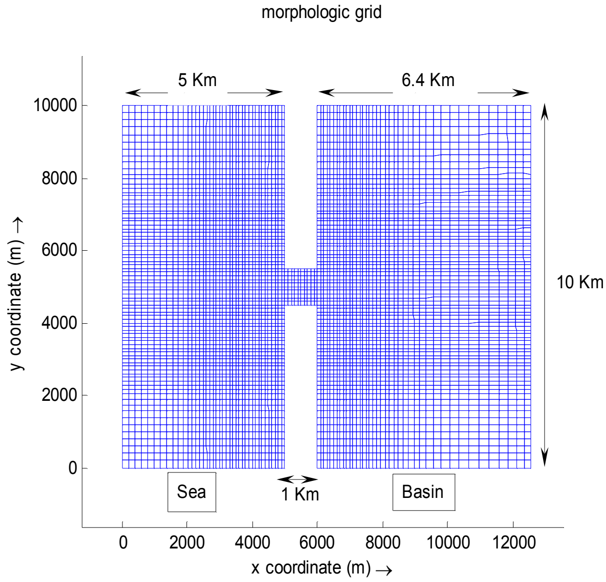

Figure 2 (left) shows analytical harmonic model results comparable to the work of Brown (1928), Keulegan (1951) or Dilorenzo (1988) using similar settings as in the 2-D process-based model for different basin width. The green lines show equilibrium velocities as suggested by van de Kreeke (2004). The model starts with the smallest cross-section on the left and follows the Escoffier curve reproduced by the analytical model. The plotted final cross-sections were reached after 480 days. Model results compare well with the analytical solution although the velocities are over estimated. This is attributed to the evolving shape of the cross-sectional profile. Small deviations on the long term are attributed to the formulation of the wetting and drying procedures in the process-based model. Figure 2 (right) shows that model results evolve towards equilibrium relationships empirically found by Jarret (1967) and Eysink (1991) for different initial inlet depths.

Basin model

The inlet model is highly schematized. The question arises what the impact would be of evolving basin geometry. The following figure (left) shows an impression of process-based modeling results of a shallow 80 km long basin initially varying in depth from −15m MSL at the mouth to MSL at the head. (Details of the model description are given by van der Wegen and Roelvink (2008) and van der Wegen et al. (2008).) The figure (right) shows good comparison (even along the basin!) of the model results with the empirical

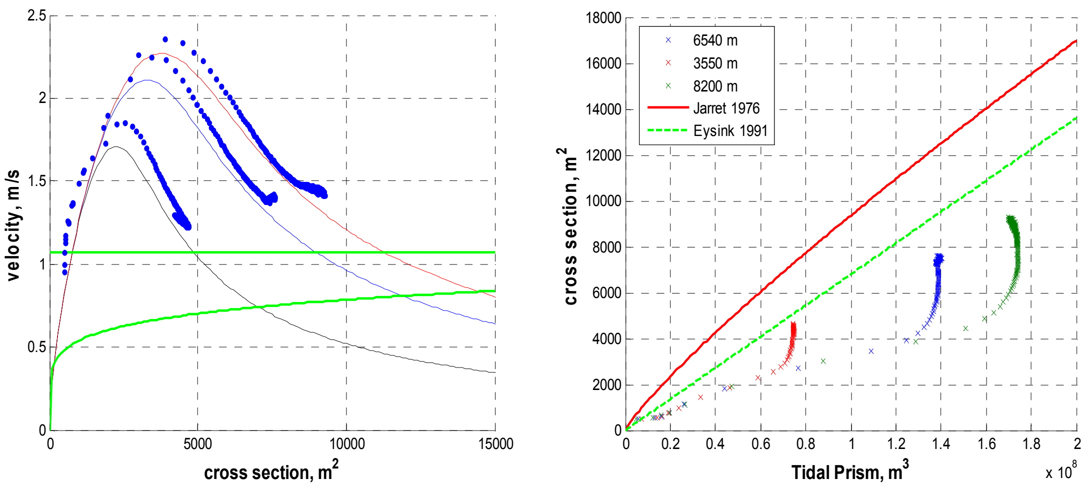

Figure 2. Process-based model results versus analytical model results represented in the Escoffier curve for different basin width (left) and model results versus empirical relationships for different initial inlet depths (right).

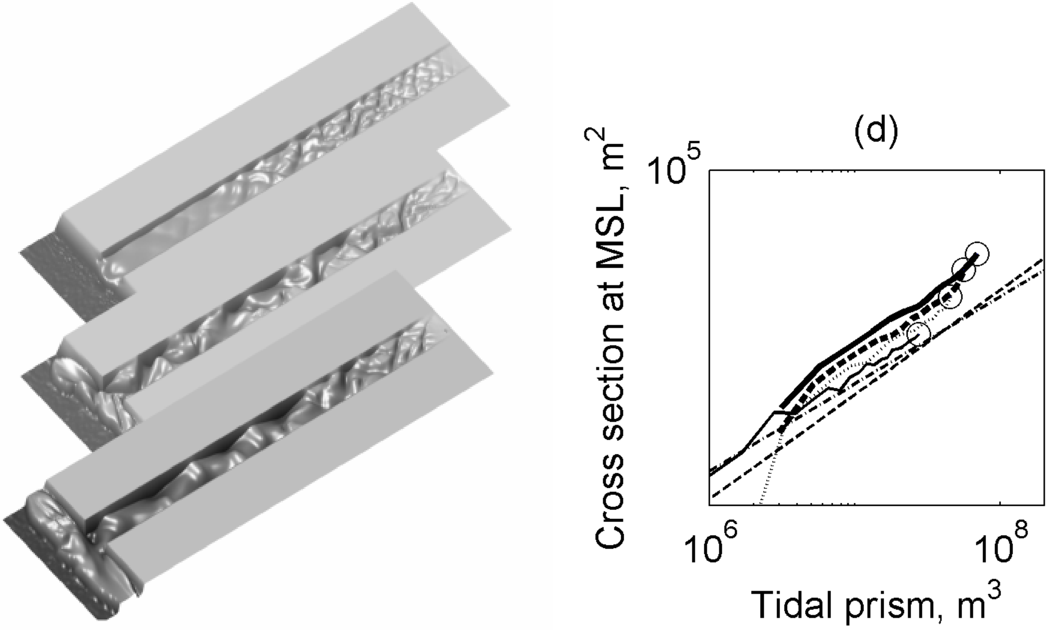

Figure 3. Results of process based model after 25, 400 and 3200 years (left) and tidal prism versus cross sectional area (straight dotted lines represent equilibrium relationships by Jarrett, 1976); along basin model results are given for1, 200, 800 and 3200 years showing increasing prism and cross sections at the mouth and subsequent section along the basin.

relationship between tidal prism and cross-sectional area given by Jarrett (1976), although significant development occurs over (long) time. On the longer term the cross sections are overestimated. This is attributed to the application of uniform sediment sizes without clogging mechanisms in the deeper parts of the channels and the absence of wave induced alongshore transport towards the inlet. Closer analysis shows that the time evolution leads (finally) to smaller tidal asymmetries in the basin. In particular the phase lag between water levels and velocities appears to be a relevant indicator describing the tidal asymmetries. When the time lag is about $\frac{1}{2}\pi$ (i.e., ebb and flood velocities take place at the same water level), the basin is in equilibrium and the relation between tidal prism and cross-sectional areas remains constant in time.

Conclusions

Process-based modeling of tidal inlet morphodynamics shows two-time scales in inlet evolution. One timescale is related to the adjustment of the cross-sectional profile to governing hydrodynamic conditions (made explicit in the Escoffier curve) and has a typical timescale of 50 days. The second timescale is related to basin evolution and the prevalent tidal wave characteristics in the basin developing over time. It has a timescale depending on the basin geometry. Highly schematized modeling suggests that the timescale can be in the order of thousands of years for an 80-km long basin.

The model results presented here do not involve wave induced and along shore sediment transports. This will be subject of future research.

References

Dastgheib A., Wang, Z.B., de Ronde, J., Roelvink, J.A. (2008), *Modelling Of Mega-Scale Equilibrium Condition Of Tidal Basins In The Western Dutch Wadden Sea Using A Process-Based Model*, Proceedings of PIANC-COPEDEC VII Conference 2008, Dubai.

DiLorenzo, J.L. (1988), The overtide and filtering response of small inlet/bay systems. In: *Hydrodynamics and Sediment Dynamics of Tidal Inlets*, Aubrey, D.G., Weishar, L. (Eds.), Springer, New York, USA, pp24–53.

Hume, T.M., Herdendorf, C.E. (1993), On the use of empirical stability relationships for characterising estuaries, *Journal of Coastal Research,* 9(2), 413–422.

Jarrett, J.T. (1976), *Tidal prism-inlet relationships*. GITI. Report 3, US Army Corps of Engineers, Waterway Experiment station, Vicksburg, MS, USA.
Keulegan, G.H. (1967), *Third progress report on tidal flow in entrances: water level fluctuations of basins in communication with seas*, Report No. 1146, National Bureau of standards, Washington DC, USA,
van de Kreeke, J. (2004), Equilibrium and cross-sectional stability of tidal inlets: application to the Frisian inlet before and after basin reduction, *Coastal Engineering*, 51, 337–350.
O'Brien, M.P. (1931), Estuary tidal prism related to entrance areas, *Civil Engineering,* 1(8), 738.
Walton, T.L. (2004), Escoffier curves and inlet stability, *Journal of Waterway, Port, Coastal and Ocean Engineering*, 130, 54–57.
van der Wegen, M., and J. A. Roelvink (2008), Long-term morphodynamic evolution of a tidal embayment using a two-dimensional, process-based model, *Journal of Geophysical Research*, 113, C03016, doi:10.1029/2006JC003983.
van der Wegen, M., Wang, Z.B., Savenije, H.H.G., Roelvink, J.A. (2008), Long-term morphodynamic evolution and energy dissipation in a coastal plain, tidal embayment, *Journal of Geophysical Research*, doi:10.1029/2007JF000898. (In press.)

Numerical modeling of the morphodynamic evolution of the Gironde estuary

CATHERINE VILLARET[1], REGIS WALTHER[2]

1. EDF-LNHE, 6 quai Watier, 78400 Chatou, France
   email: catherine.villaret@edf.fr

2. Sogreah, 6 rue de Lorraine, 38130 Echirolles, France
   email: regis.walther@sogreah.fr

Keywords: sediment transport, mixed sediments, estuary, morphodynamic evolution

ABSTRACT

In the central part of the macro-tidal Gironde estuary (south-west of France), drastic bathymetric evolutions have been observed in the past ten years, leading to a progressive fill-up of a secondary channel. In this paper, we combine numerical modeling, in-situ measurements and analysis of bathymetric records, in order to get a better understanding of this complex multi-channel system.

The finite element tidal code Telemac-2d and the morphodynamic model Sisyphe are applied to predict sediment transport rates and resulting bed evolution. The effects of the variability in the mixed sediment composition on transport processes and resulting bed evolution is discussed. The model is validated against bathymetric records and applied to predict the bed evolution in the next decade.

Introduction

The necessity to build a predictive morphodynamic modeling tool is illustrated here, in the case of the Gironde macro-tidal estuary. In the central part of this multi-channel complex system, an increase of the sediment deposit has been observed in the past ten years, in the vicinity of the Blayais nuclear power plant, located approximately 50 km north of the harbor of Bordeaux (see Figure 1). This deposit induces a global reduction of the dilution of the thermal plume. We present here un-going developments in order to calculate the natural bed evolution due to seasonal variability in the flow regime, at the fortnight semidiurnal tidal cycle and assess the effect of human interference, like dredging activities and built-up of dikes.

The modeling framework is the Telemac finite element system (cf. Hervouet, 2007). The length scale of the sedimentological unit is about 50 km. Recent progresses in the numerical methods and improvements of the coupling methodology between the morphodynamic model (Sisyphe) and the hydrodynamic tidal model (Telemac-2d) are detailed in Hervouet et al., 2008. A significant reduction in CPU computer time has been achieved, such that filtering methods, presented in previous work by Chini and Villaret (2007), now become obsolete for medium term predictions (up to ten years).

After presenting the site of interest, the sediment transport model formulation will be described briefly. We then present a sensitivity analysis, to show the effect of both the cohesive and non-cohesive sediment characteristics on the calculated bed evolutions. Some preliminary results for the non-cohesive sand fraction will be discussed and the model will be validated by comparison with measurements of bathymetric evolutions for the period (1995–2000). The model will then be applied to predict bed evolutions for the next decade.

Presentation of the site

The 150 km long Gironde estuary extends from the Bay of Biscay on the French Atlantic coastline to the confluence of the Dordogne and Garonne rivers. The cumulated mean yearly-averaged river discharge is approximately 1000 $m^3 s^{-1}$. Seasonal variations of the river-discharge determine the hydrodynamics in the lower part of the estuary and variations in the suspended mud discharge at the river mouth. The position of the maximum turbidity fluctuates seasonally along the estuary, from the upper estuary during summer ebb period, and moving downstream during winter floods (cf. Allen et al., 1971).

The central part which extends downstream to the limit of intrusion of marine sands, is characterized by a complex pattern of shoals and channels, separated by elongated islands (see Figure 1).The hydrodynamics is dominated by tidal forcing, with semi-diurnal tidal range varying between 3 and 5 m, from neap to spring tide. The tidal signal amplification and deformation as the tide propagates downstream in the estuary can be reasonably well described by a local two-dimensional tidal model (cf. Chini*,* 2007).

The morphodynamic pattern evolves yearly with periods of sand banks formation, growth and decay, as described by Nagy Breitenstein (1993). However, dredging activities and built-up of dikes are intended to increase the hydraulic power of the navigation channel on the left hand side, leading to a global increase in the fine particles deposit downstream of the release area, with possible consequences on the equilibrium of secondary channels.

The sediment bed composition is highly variable with alternate presence of cohesive and non-cohesive sediments and sand-mud mixtures. Fine to medium sand accumulates on the banks, whereas cohesive sediments are predominant in deeper channels. Tidal flats are made of consolidated mud mixed with a small percent of sand. The structure of the sediment banks was described by Allen et al. (1971): a liquid mud layer varies seasonally, whose thickness depends essentially on the fluctuating position of the turbidity maximum. Underneath, a stable sand layer is accumulated on top of a consolidated mud cover. Sediment samples, taken in March 2006 in the mid-channel, show clearly the presence of both cohesive very fine particles and fine to medium sand. Sediment granulometry displays typically a bi-modal distribution as shown on Figure 2. The non-cohesive fraction is made of fine sand with mean diameter between 200 and 300 μm. The mean diameter of the cohesive fraction is very fine (less than 10 μm).

In this application, we are mainly concerned with the drastic growth of the Patiras sand bank which was formed and progressively re-attached to the downstream end of the Patiras island between 1985 and 1990. In 1995, a submerged dike was built at the downstream end of the mid channel, as shown on Figure 1. This induced a rapid growth of the Patiras sand bank, moving downstream at a rate of 1.5 m yr^{-1} and expending laterally. The bank evolution is associated to a global feel-up of the mid channel (see Figure 3).

Sediment transport model

The morphodynamic model Sisyphe (cf. Villaret, 2005) takes into account both cohesive and non-cohesive sediment transport, either by bed load or suspended load. The effect of rigid beds, sloping bed and bed stability are included. Recent improvements in the internal coupling with hydrodynamics code Telemac-2d and gain in computer time make the use of tidal filtering methods obsolete for medium term predictions (order of decades).

For non-cohesive sediments, the bed load is calculated by a semi-empirical formula (Meyer-Peter), including correction terms for sloping bed effects. The suspended load is calculated by solving a 2-D transport equation for the depth-averaged sediment concentration, with an additional correction term of the convection velocity in order to account for vertical gradients in the concentration. The net exchange rate between the bed-load and suspended load is expressed as a function of an equilibrium concentration, calculated at a given reference elevation, based on the Zyserman and Fredsoe formula. The sediment bed-continuity equation (Exner equation) is solved including the erosion and deposition terms, by using a finite volume conservative scheme. Along the open boundary, transport rates of the non-cohesive fraction are calculated assuming equilibrium conditions.

The cohesive fraction is transported as suspended load without any correction term for the convection velocity. Erosion and deposition rates are calculated based on the classical Krone and Partheniades erosion/deposition laws. A set of additional semi-empirical parameters have to be specified and calibrated (erosion parameter, critical shear strength for erosion and deposition, settling velocities, fresh sediment bed deposit) as well as the mud concentration discharge at the river mouth.

Ongoing developments include a multi-layer consolidation algorithm for sand-mud mixture based on the formulation proposed by B. Waeles (2005).

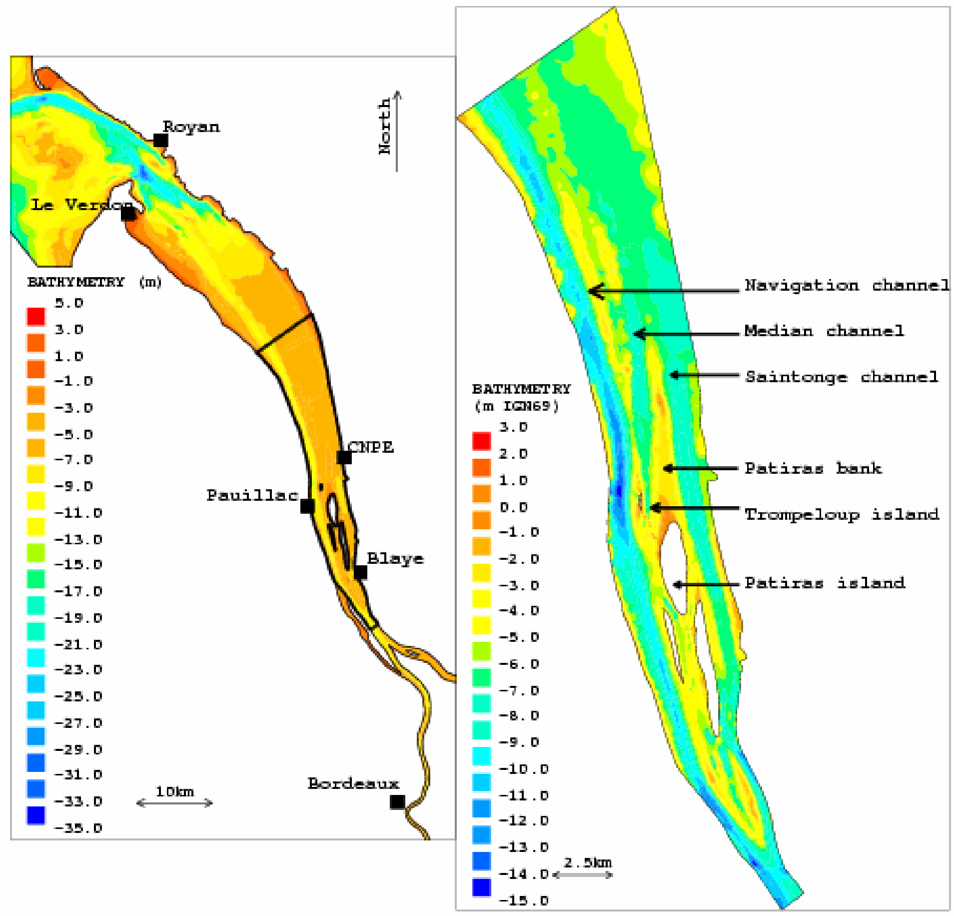

Figure 1: Location map, showing a map of the complete estuary on the left, and a zoom of the central part on the right.

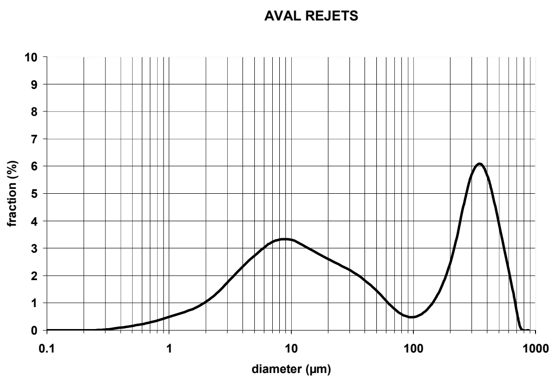

Figure 2: Granulometry distribution (sample taken downstream of point E)

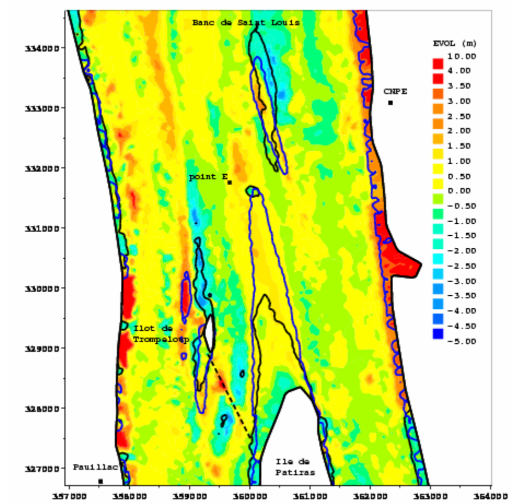

Figure 3: Bed evolution from 2002 to 2006, based on data collected by the Port Authority of Bordeaux.

Model implementation

A numerical model restricted to the central part of the estuary (40 km long) has been developed, with grid mesh varying from 300 m down to 20 m in the area of interest (central mid-channel, sand bank, submerged dike), with a total of 11500 nodes.

The hydrodynamic boundary conditions on the open boundaries (either the flow rate or the free surface) are interpolated from the results of a large scale model of the whole estuary, as explained in Chini (2007). The local model reproduces well the tidal signal amplitude and asymmetry, as well as the residual currents pattern in good agreement with ADCP measurements.

For morphodynamic applications, the hydrodynamic forcing is simplified: the same typical fortnight tidal cycle (August 2006) is reproduced with tidal range varying from neap to spring tide. The river discharge which is imposed at the upstream boundary, is considered constant and equal to its mean (yearly-averaged) value.

Sensitivity analysis and preliminary model results

For the non-cohesive fraction, the sediment diameter is the most sensitive parameter, whereas for cohesive sediments model results are highly dependent on the set of model parameters (erosion parameter, critical erosion and deposition velocity, settling velocity), which are still poorly specified. For non-cohesive sediments, the bed-evolutions are generally underestimated in comparison with observations. For the cohesive fraction only, transport rates are overestimated (deposition rates) downstream of the bank in the absence of consolidation. The effect of consolidation is to stabilize the freshly deposited mud.

Conclusions

The effect of cohesive sand fraction is to increase drastically the rate of deposit downstream of the bank, in comparison with results obtained for the sand fraction. The effect of consolidation and sand mud mixtures will be included and presented at the conference.

References

Allen, G.P., Courtois, G., Jeanneau, B., Klingebiel, A. (1971), *Etude des déplacements de sables sur une bare d'estuaire*, Bulletin de l'Institut de Géologie du Bassin d'Aquitaine, N°11/2.

Chini, N., Villaret, C. (2007), Numerical modeling of the bed evolution downstream of a dike in the Gironde estuary, *Rivers, Coasts and Estuarine Morphodynamics*.

Hervouet, J.-M. (2007), *Hydrodynamics of free surface flows, modelling with the finite element method*. Wiley & sons.

Hervouet, J.-M, Razafindrakoto, E., Villaret, C. (2008), *Telemac release notes*, Report EDF-LNHE H-P74-2008-453.

Nagy Breitenstein, G. (1993), *Analyse quantifiée de l'évolution hydro-morphologique sédulaire de l'estuaire amont de la Gironde*, Thèse, Université de Bordeaux I.

Villaret, C. (2005), *Sisyphe release 5.5, User manuel Sisyphe*, EDF-LNHE report HP-76/05/009/A.

Waeles, B. (2005), *Modélisation morphodynamique de l'embouchure de la Seine*, Thèse, Université de Caen-Basse Normandie.

Morphodynamics of the Dee estuary

ROWENA D. MOORE[1, 2], JUDITH WOLF[1], ALEJANDRO J. SOUZA[1], STEPHEN S. FLINT[2]

1. Proudman Oceanographic Laboratory, 6 Brownlow Street, Liverpool L3 5DA UK
   email: rodmo@pol.ac.uk, jaw@pol.ac.uk, ajso@pol.ac.uk

2. Department of Earth and Ocean Sciences, University of Liverpool,
   4 Brownlow Street, Liverpool L69 3GP UK
   email: flint@liverpool.ac.uk

Keywords: hydrodynamic model, harmonic analysis; Dee estuary, UK

ABSTRACT

The evolution of estuarine morphology is a process of dynamic equilibrium in the short-term (decades to centuries), while estuaries may be regarded as ephemeral in the long-term (millennia). Short-term processes of erosion and deposition are controlled by the estuarine hypsometry, tidal asymmetry, sediment supply and river flow. The Dee estuary, UK, is a macrotidal funnel-shaped estuary, known to have undergone significant infilling over the past two centuries. In macrotidal estuaries (such as the Dee), tidal asymmetry may be the main factor affecting morphological change (Dronkers, 1986; Wang et al., 2002). Tidal asymmetry is a result of higher order harmonic overtides (particularly the M_4 constituent) which are generated by the effects of friction, convergence and continuity (Speer and Aubrey, 1985). While the estuary as a whole may be ebb- or flood-dominated, different processes dominate in the tidal banks and channels. The balance between these processes may determine whether the estuary acts as a net sediment source or sink.

This study has employed three-dimensional hydrodynamic numerical modelling techniques (to a resolution of 180 m – the model used is POLCOMS – *Proudman Oceanographic Laboratory Coastal Ocean Modelling System*) to investigate tidal propagation and asymmetry in the Dee. Harmonic analysis allows separation of the tidal constituents, and the tidal currents ellipses for the principal lunar M_2 constituent can be seen in Figure 1.

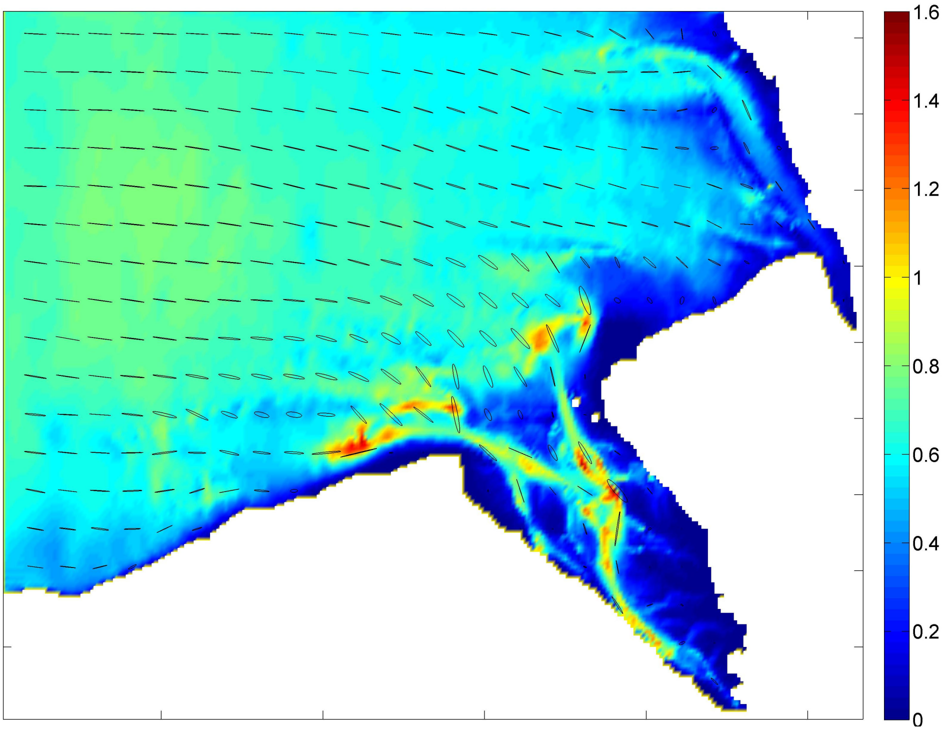

Figure 1. M_2 constituent tidal current ellipses superimposed on major axis velocity (m s^{-1}).

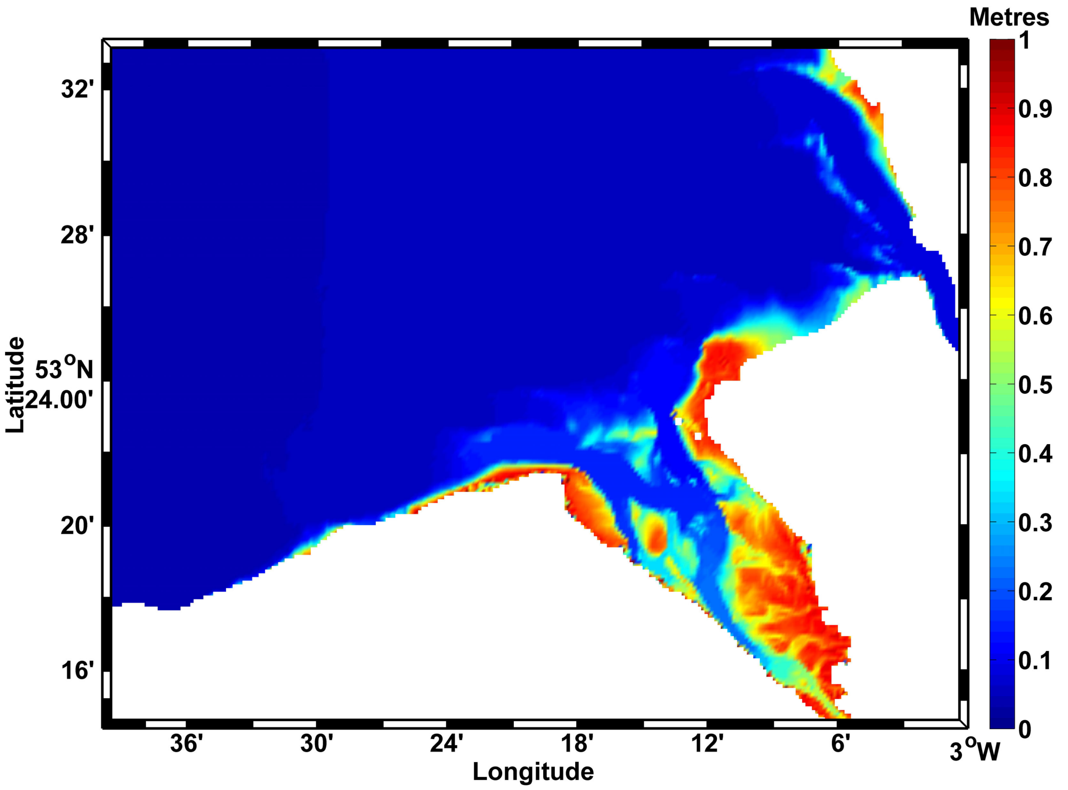

Figure 2. M_4/M_2 amplitude ratio in the Dee estuary and Liverpool Bay as a proxy for tidal distortion (> 0.01 is representative of significant tidal distortion).

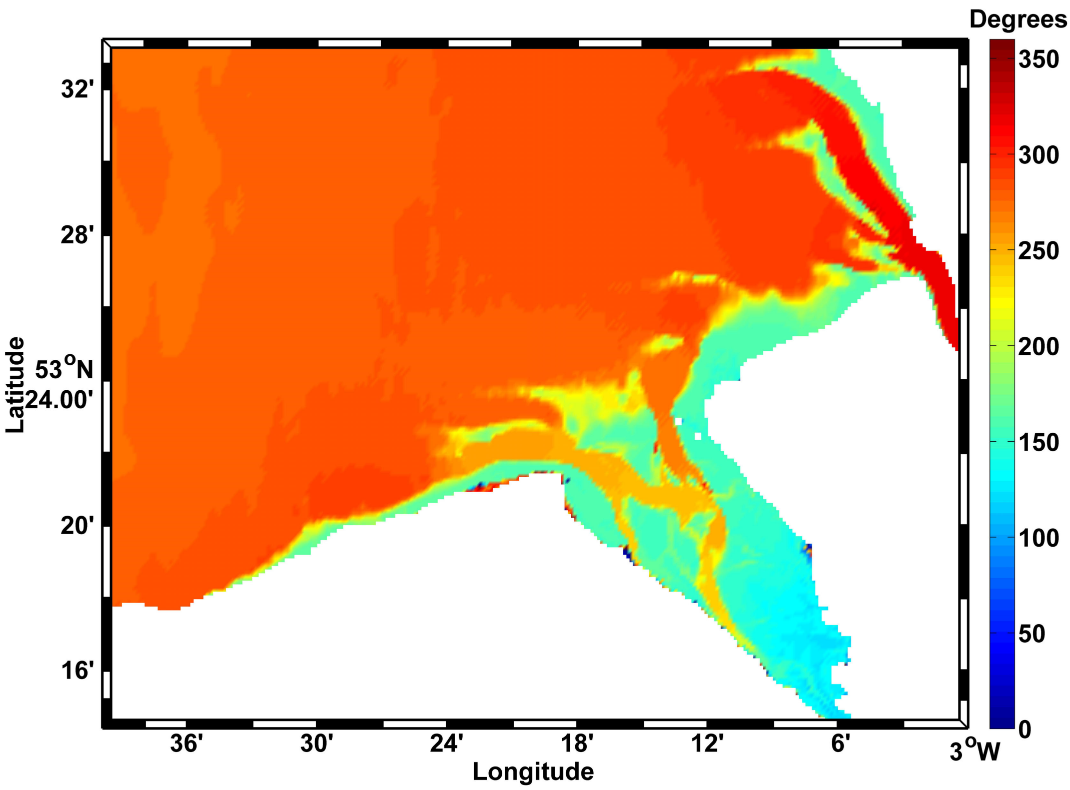

Figure 3. $2M_2 - M_4$ phase difference in the Dee estuary and Liverpool Bay as a proxy for tidal asymmetry (0–180° = flood dominance, 180–360° = ebb dominance).

Comparing the M_2 and M_4 constituents (as used in Friedrichs and Aubrey, 1988) we see that the Dee is highly tidally distorted, with apparent flood dominance of the intertidal areas (Figures 2 and 3. This may explain much of the infilling of the Dee, as a flood dominance results in net sediment import.

Recent high resolution LIDAR surveys also show net accretion between 2003 and 2006 (Figure 4), in agreement with the tidal asymmetry analysis. Results using a coupled suspended sediment transport model with POLCOMS are also presented for this study.

The LIDAR data has also been used for hypsometry analysis (approach of Boon and Byrne, 1981), which has suggested that the Dee is a fairly 'mature' (infilled) estuary and may be approaching equilibrium (when there is no net sediment flux). The increase in extent and elevation of tidal flats during the infilling process is thought to gradually reduce the flood dominant nature of the estuaries until an equilibrium configuration is reached. However, the process of achieving equilibrium may be affected by changing sea levels and climatic alterations such as increased storminess and man-made interventions such as canalisation and dredging.

Concluding remarks

The Dee has undergone huge levels of sedimentation over the past two centuries, resulting in land reclamation and salt marsh colonization. This has been largely due to man-made canalization of the upper estuary and tidal asymmetry. Numerical modeling analysis has shown the Dee to be still tidally distorted, with large areas of flood-dominance, particularly of the intertidal areas. This implies the Dee is still net importing sediment, a fact which is independently verified by LIDAR surveys which show net accretion between 2003 and 2006. Hypsometrical analysis suggests the Dee may be approaching equilibrium and that rates of accretion may, therefore, reduce in the future.

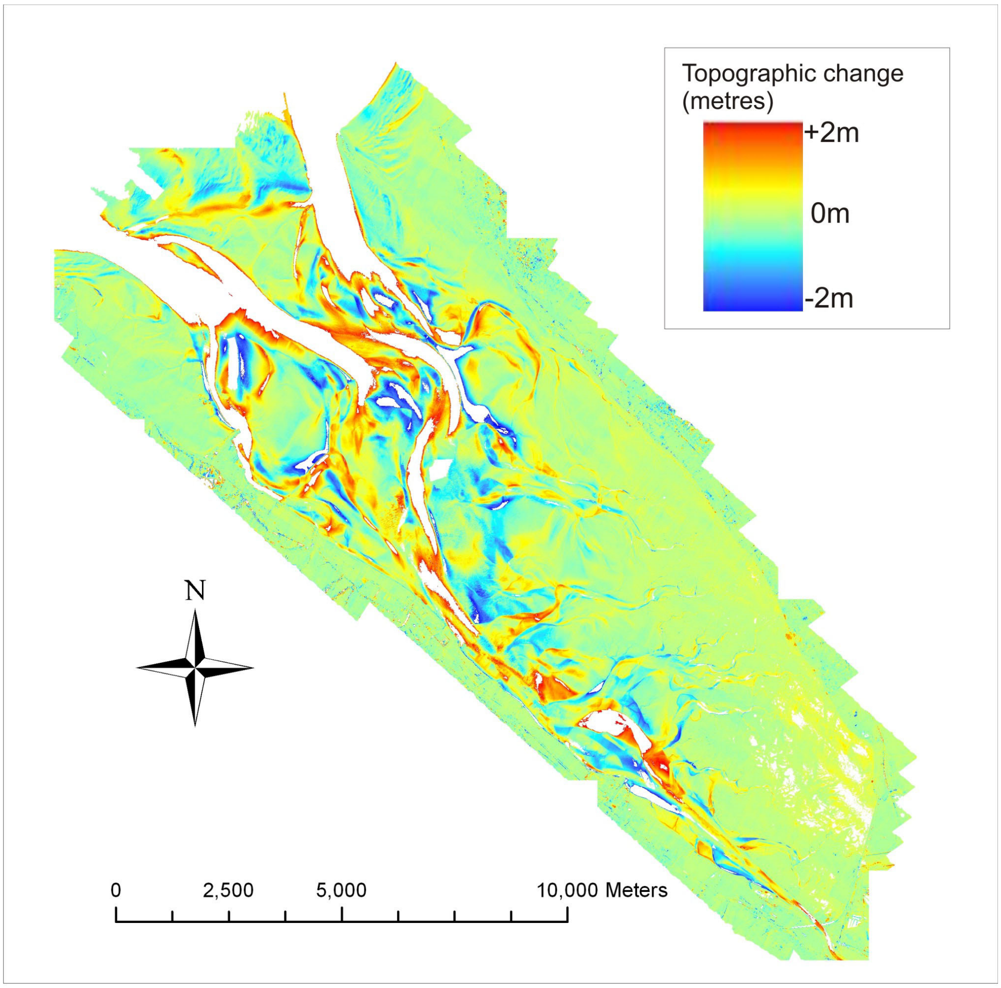

Figure 4. Morphological changes in the Dee estuary, from 2003–2006, as shown by data from high resolution LIDAR surveys.

References

Boon, J.D, Byrne, R.J. (1981), On basin hypsometry and the morphodynamic response of coastal inlet system, *Marine Geology*, 40, 27–48.

Dronkers, J. (1986), Tidal asymmetry and estuarine morphology, *Netherlands Journal of Sea Research*, 20, 117–131.

Friedrichs, C.T., Aubrey, D.G. (1988), Non-linear tidal distortion in shallow well-mixed estuaries: a synthesis, *Estuarine, Coastal and Shelf Science*, 27(5), 521–546.

Speer, P.E., Aubrey, D.G. (1985), A study of non-linear tidal propagation in shallow inlet/estuarine systems, part II: theory, *Estuarine, Coastal and Shelf Science*, 21, 207–224.

Wang, Z.B., Jeuken, M.C.J.L., Gerritsen, H., de Vriend, H.J., Kornman, B.A. (2002), Morphology and asymmetry of the vertical tide in the Westerschelde estuary, *Continental Shelf Research*, 22, 2599-2609.

Numerical modeling of the wind influence on the morphodynamic evolution of a subtropical estuary

MARCOS E.C. BERNARDES[1], ELISA H.L. FERNANDES[2], WILIAN C. MARQUES[2], IGOR O. MONTEIRO[2], LAURO J. CALLIARI[2], NICOLLE DEUSSFELD[3], ANDREAS MALCHEREK[3]

1. Natural Resources Institute, Federal University of Itajubá-MG, Brazil
   email: marcos.bernardes@gmail.com

2. Laboratório de Oceanografia Física, Fundação Universidade Federal do Rio Grande, Caixa Postal 474, CEP 96200-0001 Rio Grande-RS, Brazil
   email: e.fernandes@furg.br, wilian_marques@yahoo.com.br, igoromonteiro@yahoo.com.br, tsclauro@furg.br

3. Hydromechanik und Wasserbau, Universität der Bundeswehr München, 85577 Neubiberg, Germany
   email: nicolle@deussfeld.de, andreas.malcherek@unibw-muenchen.de

Keywords: sediment transport, port, Telemac, SediMorph; Patos Lagoon, Brazil

ABSTRACT

Understanding the morphological evolution of coastal areas is of utmost importance for their management. This paper addresses the morphodynamic evolution of the Patos Lagoon, Rio Grande do Sul, Brazil through numerical modeling. This coastal lagoon is located at the southernmost part of Brazil. Its estuary shelters one of the most important harbors in the country. The modeling structure consists of the hydrodynamic module Telemac-2D (©EDF – Laboratoire National d'Hydraulique et Environnement, France) and the morphological module SediMorph (Malcherek and BAW, Germany). A one-year long series of wind is used to force the model domain, which comprises not only the lagoon itself, but also the adjacent coastal area. The initial conditions include an idealized flat bottom of 3 m deep for the whole lagoon and an isotropic distribution of three different grain sizes, namely silt, medium sand and gravel. In order to estimate the decadal morphodynamic evolution of the area without increasing the computational cost, sediment transport estimates are scaled by a factor of ten. The results obtained agree well with the actual bathymetry of the area – especially for the estuary – and highlight the considerable wind influence on the morphodynamic evolution of the Patos Lagoon.

Introduction

Understanding the morphological evolution of coastal areas is of utmost importance for activities such as harbor dredging and urban planning. Despite the strategic location of estuaries, the comprehension of the complex morphodynamic interactions which take place in these areas remain incomplete. In order to support the local harbor authority in managing the sediment budget, this paper addresses, through numerical modeling, the morphodynamic evolution of the Patos Lagoon estuary, southern Brazil (Figure 1). It must be borne in mind that the findings described herein are qualitative, since this is the first effort to tackle the morphodynamic processes in this area. This choked lagoon is the largest in the world (Kjerfve, 1986), with an approximate length of 250 km, average depths of 5 m and watershed area around 200,000 km^2. The lagoon hydrodynamics is mainly forced by wind and freshwater (Fernandes et al., 2004; Möller et al., 1996). Its estuary shelters one of the most important harbors in the country (Rio Grande).

Methods

This study is part of a cooperation project entitled 'Sustainable Development of Brazilian Harbors', a Brazil-Germany initiative. Results described herein are based on the coupling between the hydrodynamic module Telemac-2D and the morphological module SediMorph (developed by A. Malcherek and BAW – The Federal Waterways Engineering and Research Institute, Germany) [www.baw.de/vip/abteilungen/wbk/Methoden/hnm/sedimorph/vd-sedimorph.pdf]. The combined use of

Figure 1. Patos Lagoon, southern Brazil, highlighting the estuarine area.

these modules results in a morphodynamic approach, where the interactions and feedbacks between the hydrodynamics, the sediment transport and bed evolution are updated as the simulation evolves in time. Telemac modules are based on the Navier-Stokes equations and on the finite elements technique, which allows for very robust representation of irregular bottoms of coastal areas. On the other hand, since the same mesh used in the hydrodynamics module is read by SediMorph, the computation performance is improved. The mesh covers the whole lagoon and the adjacent coastal area up to 3,600 m deep. Among the 8,974 nodes of the mesh, greater refinement is applied to the estuarine area.

The experiments described in this paper were forced only by the wind. Due to the large spatial area included in the mesh, the wind applied is variable both in time and in space. Data of the global atmospheric model Reanalysis [www.cdc.noaa.gov/cdc/reanalysis/reanalysis.shtml] (NCEP/NCAR) were interpolated onto the grid, reproducing the cold front passages over the area of interest. The year of 2005 was selected as a representative condition, with the predominance of northeastern winds. Idealized bottom conditions and grain size distribution are assumed. In order to investigate the development of bottom features, a constant depth of 3 m is applied to the whole lagoon, including its estuary, and to the adjacent coastal area close to the jetties which protect the harbor entrance. While in every node there are three different grain sizes – silt, medium sand and gravel, their relative proportion vary randomly on a node-by-node basis. Only the bed-load transport is considered. To assess the estuary response to decadal variations, a 'speeding factor' was implemented. This factor corresponds to scaling the effective sediment transport rates by ten. In other words, the results below ensemble the morphodynamic evolution of a decade, which is characterized by the estimated 2005 wind field.

Results

Due to the predominance of northeastern winds during the period of interest, continental water tends be flushed out to the ocean. The residual currents between the jetties (which constrain the communication between the lagoon and the ocean) are bidirectional, with ebb currents on the western side of the access channel and flood currents on its eastern portion (Figure 2a). The largest estimated residual speeds were expected to be in excess of 1 m s^{-1} at the tip of the western jetty. The most pronounced bottom changes of the whole system are shown in Figure 2b. At the end of the simulation, the coastal face of the western jetty tip and the sheltered portion of the eastern jetty are the most affected erosion spots (erosion of at least 2 m, given the initial depth of 3 m). Qualitatively speaking, several actual bottom features are replicated in the simulation: i) existence of a 'ditch' extending seawards from the tip of the western jetty; ii) net erosion on the western portion of the lower estuary, especially on the narrower areas, originating the access channel to Rio Grande harbor and iii) existence of shallower banks on the eastern side of the estuary. As only the bed-load transport was taken into account in this paper, it is very likely that more complex morphodynamic patterns may arise with the computation of the total sediment transport rates.

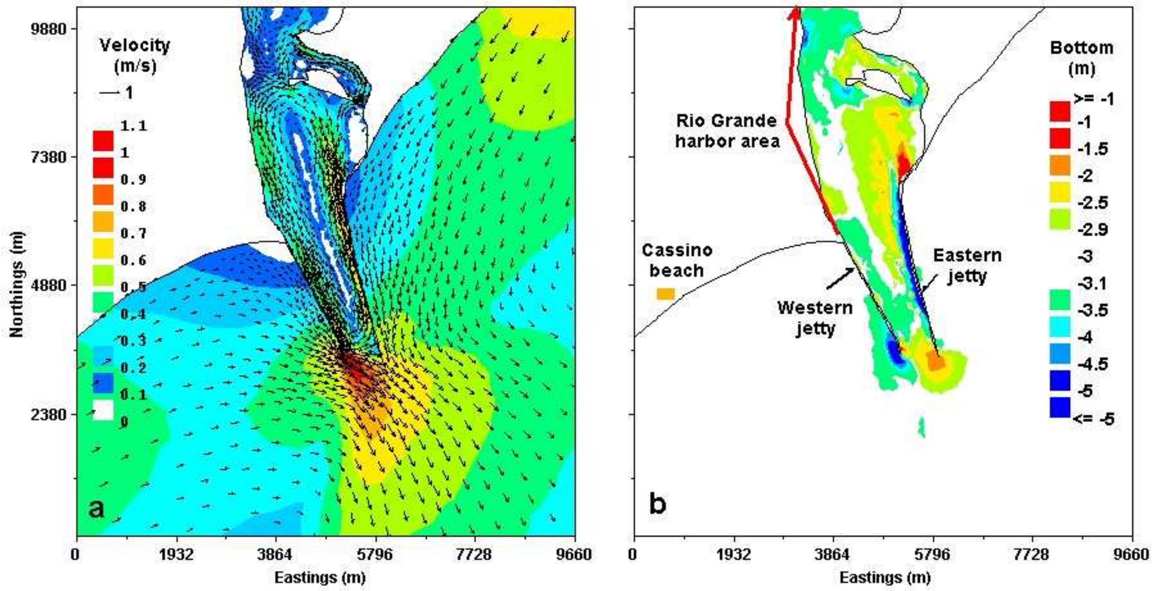

Figure 2. Close-up of the lower estuary and the nearshore area. (a) Residual currents (averaged over 1 year) showing only the areas with speeds ≥ 0.1 m s^{-1}; (b) Bottom at the end of the simulation with the removal of variations ≤ 0.1 m relative to the initial bottom depth of 3 m.

Conclusions

Through the coupling between the hydrodynamic module Telemac-2D and the morphological module SediMorph, the wind influence on the bed-load transport and on the morphodynamic evolution of the Patos Lagoon estuary was assessed. Several bottom features which are known to exist in this area were qualitatively reproduced by the model. Generally speaking, the eastern side of the estuary is dominated by residual flood currents, which tend to allow for sediment deposition in this area (exception to the inland side of the eastern jetty). On the narrower portions of the estuary, its western side is expected to be driven by ebb-directed residual currents, which seem to induce erosion processes. Further research will be based on the inclusion of i) suspended-load transport; ii) bathymetric surveys in the area in order to calibrate and validate the model results; iii) fate of different grain sizes; iv) river discharge and tidal influence and v) 3D simulations.

Acknowledgements

This research was funded by the Brazilian Research Council as part of a post-doc grant (Number 151675/2005-8).

References

Fernandes, E.H.L., Marino-Tapia, I., Dyer, K.R., Möller, O.O. (2004), The attenuation of tidal and subtidal oscillations in the Patos Lagoon estuary, *Ocean Dynamics*, 54 (3–4), 348–359.

Kjerfve, B. (1986), *Comparative oceanography of coastal lagoons*. In: Estuarine variability, Wolfe, D.A., (Ed.), Academic Press, New York, pp63–81.

Möller, O.O., Lorenzetti, J.A., Stech, J.L., Mata, M.M. (1996), The summertime circulation and dynamics of Patos Lagoon, *Continental Shelf Research*, 16, 335–351.